NASA CONTRACTOR REPORT 177326

(NASA-CR-177326) A STUDY OF THE APPLICATION OF DIFFERENTIAL TECHNIQUES TO THE GLOBAL POSITIONING SYSTEM FOR A HELICOPTER PRECISION APPROACH (Ohio Univ.) 83 p HC A05/MF A01 CSCL 17G G3/04

N85-31035

Unclas 24691

A STUDY OF THE APPLICATION OF DIFFERENTIAL TECHNIQUES TO THE GLOBAL POSITIONING SYSTEM FOR A HELICOPTER PRECISION APPROACH

DARYL L. MCCALL

CONTRACT NAG 2-231
NOVEMBER 1984

NASA

NASA CONTRACTOR REPORT

A STUDY OF THE APPLICATION OF DIFFERENTIAL TECHNIQUES TO THE GLOBAL POSITIONING SYSTEM FOR A HELICOPTER PRECISION APPROACH

DARYL L. MCCALL

NOVEMBER 1984

PREPARED FOR
AMES RESEARCH CENTER
UNDER GRANT NAG 2-231 BY
OHIO UNIVERSITY
ATHENS, OHIO

NASA
National Aeronautics and
Space Administration

Ames Research Center
Moffett Field, California 94035

A STUDY OF THE APPLICATION OF DIFFERENTIAL TECHNIQUES TO THE GLOBAL POSITIONING SYSTEM FOR A HELICOPTER PRECISION APPROACH

Table of Contents

List of Figures and Tables

List of Tables and Figures (Continued)

1.0 INTRODUCTION AND SUMMARY

This paper documents the results of a preliminary study of the application of differential techniques to the NAVSTAR Global Positioning System for the civilian helicopter environment. The results of this study will be used to assist in the specification of a differential GPS (DGPS) ground system and in the identification and evaluation of the problem areas which may inhibit the successful and timely hardware implementation of the DGPS system.

The simulated missions used a variety of receiver types; sequential/single channel, four channel, and various receiver update periods. Each receiver type was subjected to a variety of degradations of satellite range, including diffuse multipath, ionospheric delay, tropospheric delay, receiver clock error, and the Department of Defense selective availability errors. The models used to calculate these values are presented in this text.

Evaluations of the receiver types are presented by means of performance analyses of representative cases for the three different receiver modes; conventional, fixed, and differential (corrections applied to the receiver range measurements). These analyses include the discussion of position errors, the spatial correlative properties of individual range error sources, and the filtering algorithm used to smooth the position data.

The basic findings of this study are:

1) Differential GPS does show significant potential for providing a precision approach capability, particularly with respect to lateral guidance.

2) This potential may be increased by the application of some type of filtering to the range measurement of the fixed mode receiver. The high frequency effects of the diffuse multipath can produce less accurate range corrections, and the removal of these errors may boost the accuracy of DGPS to include guidance in altitude.

3) If an uplink rate of 12 seconds or greater is to be implemented in the DGPS ground system, good DGPS user positional accuracies should be obtainable with a slower (2.4 sec update period), sequential/single channel receiver implemented in the ground system.

4) The DGPS differential mode receiver should have a position fix filtering algorithm capable of tracking accelerative dynamics. The alpha-beta tracking filter's performance is, at best, marginal when subjected to levels of acceleration experienced during the execution of an approach turn maneuver.

2.0 BACKGROUND

2.1 Global Positioning System (GPS)

The Global Positioning System (GPS) is a worldwide, all-weather navigation system currently under development by the Department of Defense. The baseline space segment configuration will consist of 18 satellites equally spaced in six orbits. The orbits will be uniformly distributed about the earth, each inclined 55° with respect to the spin axis of the earth. This baseline system is scheduled to begin deployment in January, 1986 [1].

GPS will offer two systems, the Precise Positioning System (PPS) which implements the P-code and the Standard Positioning System (SPS) which will use the C/A-code. Preliminary studies have shown that the PPS will provide fixes with an accuracy of 18.1 meters (2 drms) horizontally and 29.7 meters (2 sigma) vertically [2]. In the interest of national security, the PPS will only be be available for DOD applications and those users authorized by the DOD. The SPS has been shown to have the potential to offer an accuracy of 43.6 meters (1 sigma) horizontally and 23.8 meters (1 sigma) vertically [3]. This accuracy will, for reasons of security, be purposely degraded such that available accuracy will be 100 meters (2 drms) horizontally [4]. The DOD will review the practicality of increasing the accuracy of the SPS annually.

The P-code will be transmitted on two frequencies, L1 = 1575.42 MHz and L2 = 1227.6 MHz. The C/A-code will be transmitted on the L1 frequency only. Receivers with the ability to track both carriers will have the capability to determine the phase/delay and carrier/advance effects of the atmosphere. Other receivers will have a significantly more inaccurate determination of the atmospheric effects by means of a model provided in the GPS navigation message data. Either the two frequency measurements or the model calculations will be used to correct the time delay of the GPS signals.

The user can determine position in three dimensions and receiver clock error by measuring the time of propagation of four GPS signals from four different satellites which provide good geometry. The ideal geometry would consist of one satellite at zenith and three satellites close to the horizon, each of the latter uniformly spaced by 120° in azimuth. Because the effects of the atmosphere are significantly amplified when a satellite is positioned near the horizon, a mask angle of 5-10° is usually implemented.

The user may compute his position and clock error by tracking fewer than 4 satellites if he has redundant position information available, such as knowledge of altitude, differential LORAN-C position fix, etc., or the user may only track three satellites to compute three dimensions of position if his receiver possesses an extremely stable frequency standard.

The General Aviation user, with degraded C/A-code compounded by areas of poor geometry and satellite outages, will be limited to the

enroute and, perhaps, the non-precision approach environment. Differential techniques can be employed to reduce the effects of poor geometry and expand the possibility of using differential GPS (DGPS) during a precision approach.

2.2 . Differential GPS

Differential GPS is a technique whereby the certainty of a GPS user's position is improved by providing, to the user, knowledge as to either position error or the errors induced in range measurements. Several methods have been discussed by others [5, 6] as how these corrections may be implemented, however only two methods have drawn significant attention [7]; the uplink method and the uplink method by pseudolite.

2.2.1 The Differential GPS Uplink

The basic components of a DGPS uplink ground unit consist of a GPS receiver, a central processor, and a telemetry unit with the antenna of the GPS receiver placed at a precisely known location (see figure 2.2.1.1). The DGPS ground system's processor is programmed with the coordinates of the receiver's antenna. The central processor is interfaced to the GPS receiver in such a manner that it can obtain the satellite data block information stored in the receiver as well as time/Sat ID-tagged range/range rate information.

With the knowledge of GPS system time, derived either from the satellite range data or by an external standard, the central processor can determine the true range from the receiver's antenna to any particular GPS satellite. The difference between the processor's calculated range and the receiver's measured range is the range correction provided to the DGPS user(s) in the local area via a one-way data telemetry uplink. Similarly, calculations and measurements can be made to provide the user with a range-rate or Doppler correction.

The DGPS user would have a similar breakdown of basic components consisting of a GPS receiver, a central processor, and a telemetry receiver. Once the correction has been received, the central processor would then apply them to the user's measured ranges and then proceed to compute a position fix which is significantly more accurate than those using conventional GPS. It should be noted that the user's processor would be less sophisicated than the DGPS ground system's processor. If commercially produced, the user's central processor would probably be shared with the GPS receiver.

The corrections could also take the form of position coordinate corrections. The application of position coordinate corrections to a conventional GPS position fix would only provide consistently improved results if the correction and the conventional position fix were derived from the identical selection of satellites. The application of corrections to a position fix, both of which were calculated from separate sets of satellites, would produce meaningless results.

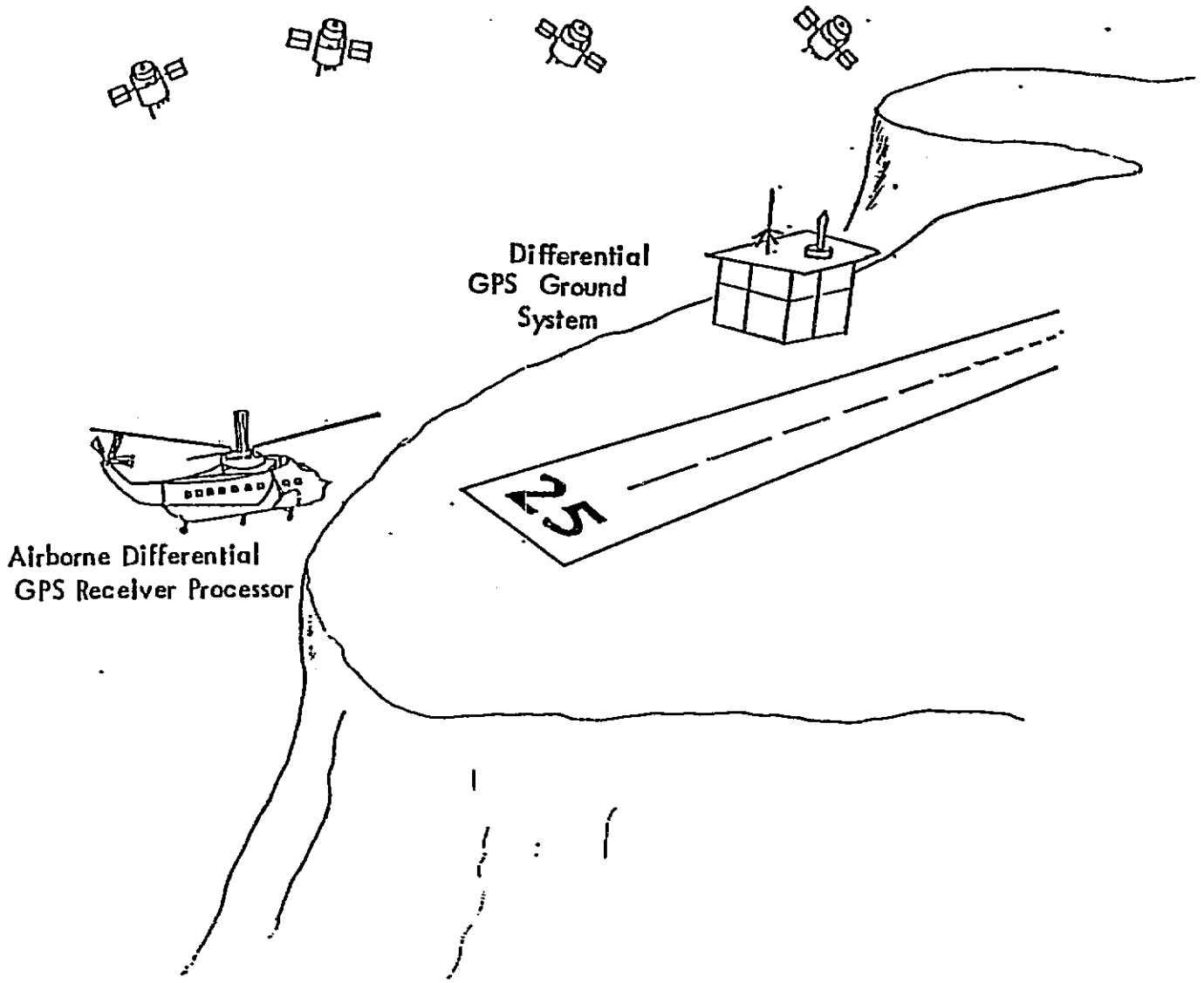

Figure 2.2.1.1 Differential GPS Uplink

2.2.2 The Differential GPS Uplink Using a Pseudolite

This method is very similar to the DGPS uplink, however the distinct advantage to this method comes from the use of a pseudolite (see figure 2.2.2.1). A pseudolite is a static, ground-based NAVSTAR transmitter. Its signal format would be identical to that of the space-based satellites, however the data content of the pseudolite would be somewhat different. Instead of several complex emphemeris constants, its position data would consist of three earth centered coordinates. The data message would also contain the DGPS corrections calculated at the pseudolite. These corrections would be derived using the techniques described in the uplink method.

The major advantage to the pseudolite uplink comes in the way of improved geometry due to having a satellite beneath the user. The pseudolite decreases the effects of the residual range errors in the DGPS range measurements and tends to provide an overall improvement to the altitude calculation when using either GPS or DGPS.

One problem with the pseudolite uplink is in coverage. The uplink method without pseudolites could employ the use of transmission frequencies with enough ground wave to service 100 miles or more over the horizon. Because the pseudolite will transmit at the NAVSTAR frequencies, there will be no ground wave, therefore all receptions of the differential information will be done within line-of-sight of the pseudolite. The coverage of the pseudolite can not be expanded by merely increasing its transmission power; to do so would risk saturating the RF front-ends of the all of the GPS receivers in the immediate area and either degrade or jam the user's receiving capabilities.

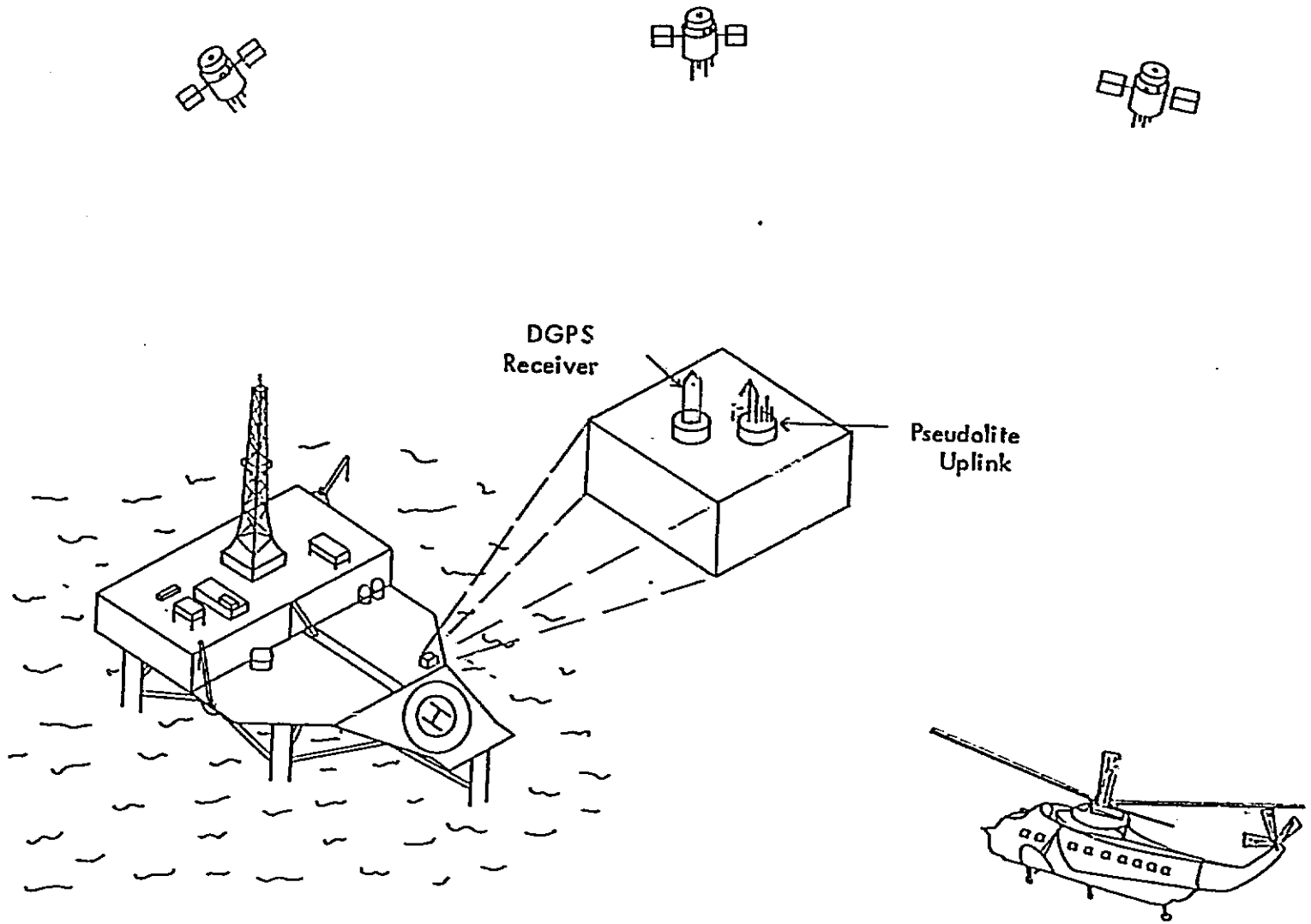

Figure 2.2.2.1 Differential GPS Pseudolite Uplink

3.0 THE DIFFERENTIAL GPS SIMULATION

The following is a discussion of the operation of the computer simulation used to derive the results in this paper.

3.1 18 Satellite Configuration [8]

The simulation uses 18 satellites distributed equally into six circular orbits about the earth (see figure 3.1.1). Each orbit is inclined 55° with respect to the spin axis of the earth. Each satellite has an earth centered radius of 14,568 nautical miles and thus the orbital period of each satellite is approximately 12 hours.

The orbits are sequentially phased 40° in such a way that if a satellite is directly above the equator, the plane adjacent to the east will have a satellite 40° ahead and the plane adjacent to the west will have a satellite 40° lagging (see figure 3.1.2). Table 3.1.1 shows the longitudes of the ascending nodes and the angles of right ascension for each satellite used. The angles of right ascension, between each orbital plane, are evenly spaced 60° apart.

3.2 DGPS User Flight Path

The user dynamics used in this simulation were modeled after those generally encountered in the GA helicopter terminal/approach environment. The mission contains six legs, each of which can contain the following characteristics:

* straight, level, constant velocity paths
* constant heading, constant velocity, constant ascent/descent paths (descent/ascent speeds varying from -300 fpm to 750 fpm).
* various turns, including a teardrop maneuver
* several different speeds (89-120 knots) and accelerations (-2 knots/second to 5 knots/second)

The final approach to the runway is made using the teardrop maneuver.

Figures 3.2.1 and 3.2.2 depict the ground track and altitude profile of the user. The entire scenario was similar to that used in a study of degraded GPS for non-precision approaches [9].

3.3 The Navigation Algorithms

The following text describes the position fixing algorithm used to derive user navigational information given time and four user pseudorange measurements. A brief discussion is devoted to the alpha-beta tracking filter employed to smooth the position calculations.

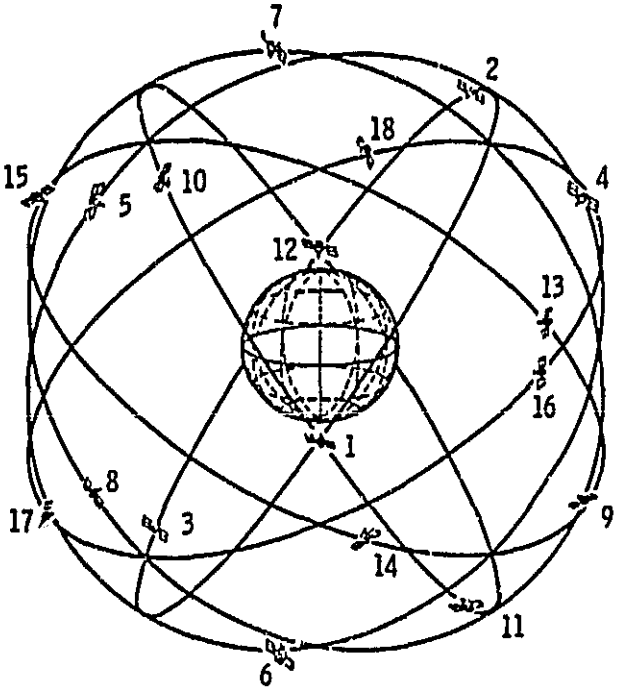

Figure 3.1.1 The Uniform 6-Plane, 18-Satellite Configuration

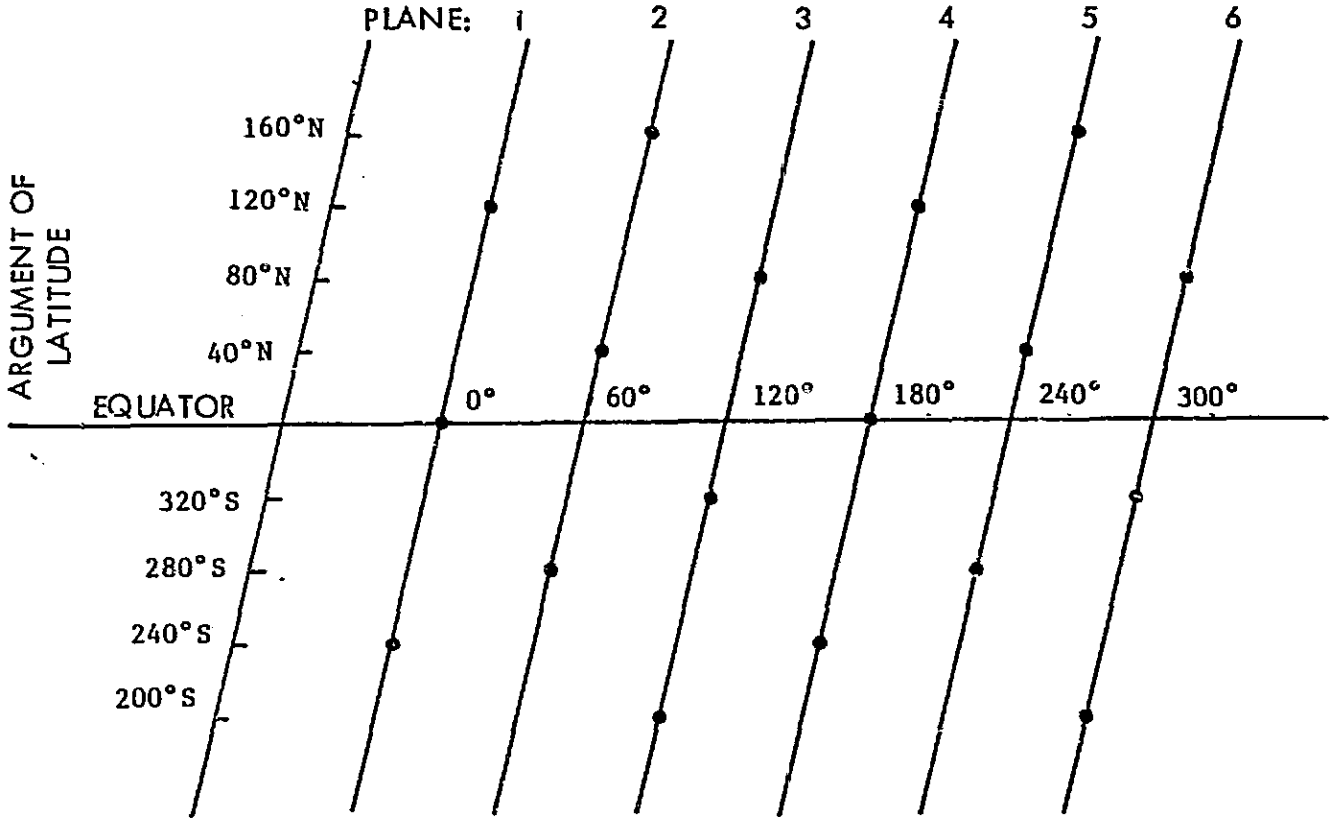

Figure 3.1.2 Phasing of the Uniform 6-Plane, 18 Satellite Configuration.

SATELLITE NUMBER	ORBIT PLANE	LONGITUDE OF THE ASCENDING NODE, DEG.		RIGHT ASCENSION OF THE ASCENDING NODE, DEG.*
1	1	0.	180.	0.
2	1	240.	60.	0.
3	1	300.	120.	0.
4	2	260.	80.	60.
5	2	320.	140.	60.
6	2	20.	200.	60.
7	3	340.	160.	120.
8	3	40.	220.	120.
9	3	100.	280.	120.
10	4	60.	240.	180.
11	4	120.	300.	180.
12	4	180.	0.	180.
13	5	140.	320.	240.
14	5	200.	20.	240.
15	5	80.	260.	240.
16	6	220.	40.	300.
17	6	280.	100.	300.
18	6	160.	340.	300.

* Referenced to astronomical coordinates of 1950.0 as of 0 hr 0 min GMT, the simulation does not allow the right ascending node to regress.

Table 3.1.1. NAVSTAR GPS Orbit Description as Implemented in the Computer Simulation, Longitude Relative to Earth and Astronomical Coordinates

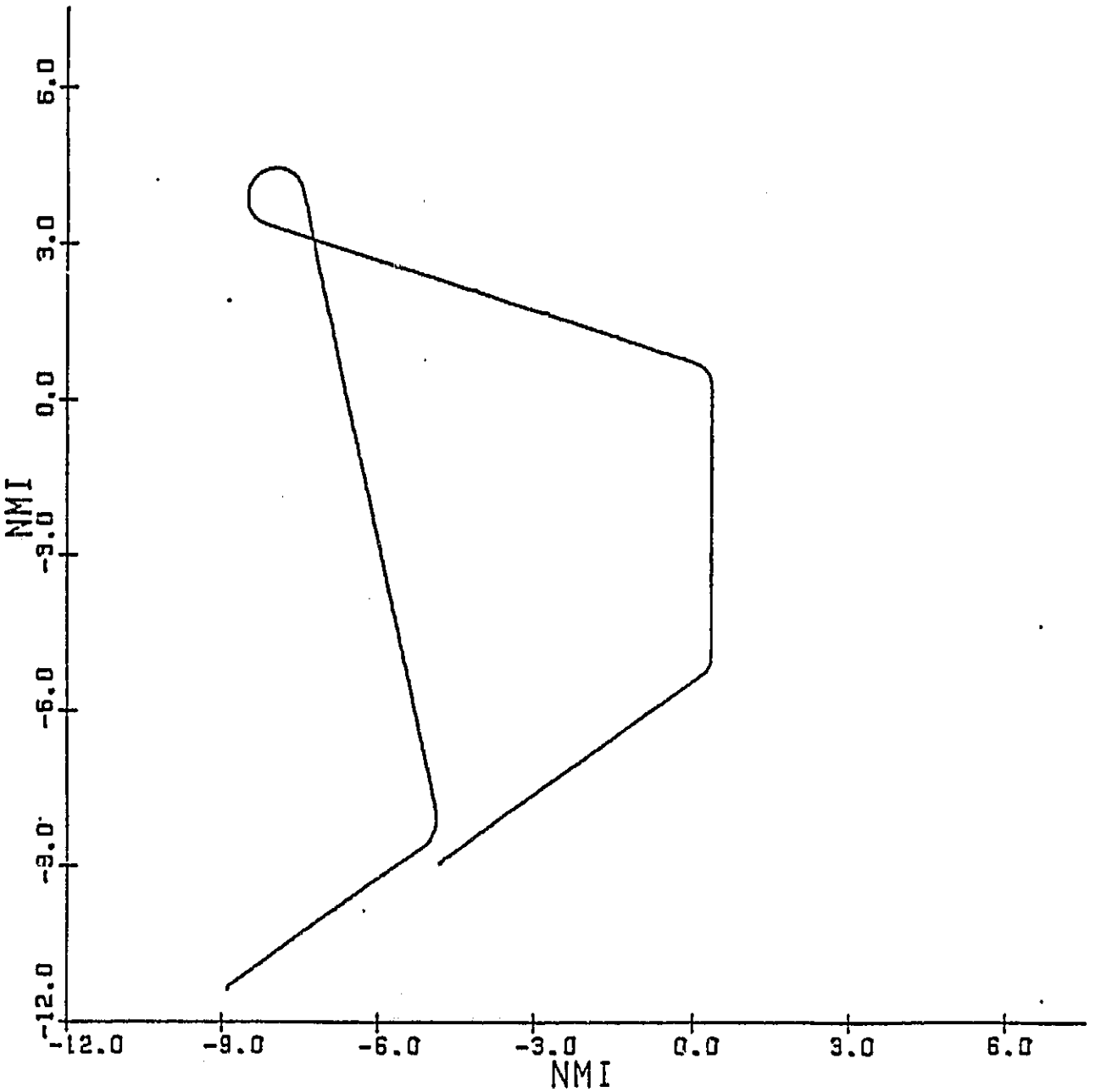

Figure 3.2.1 Teardrop Flight Path Ground Track

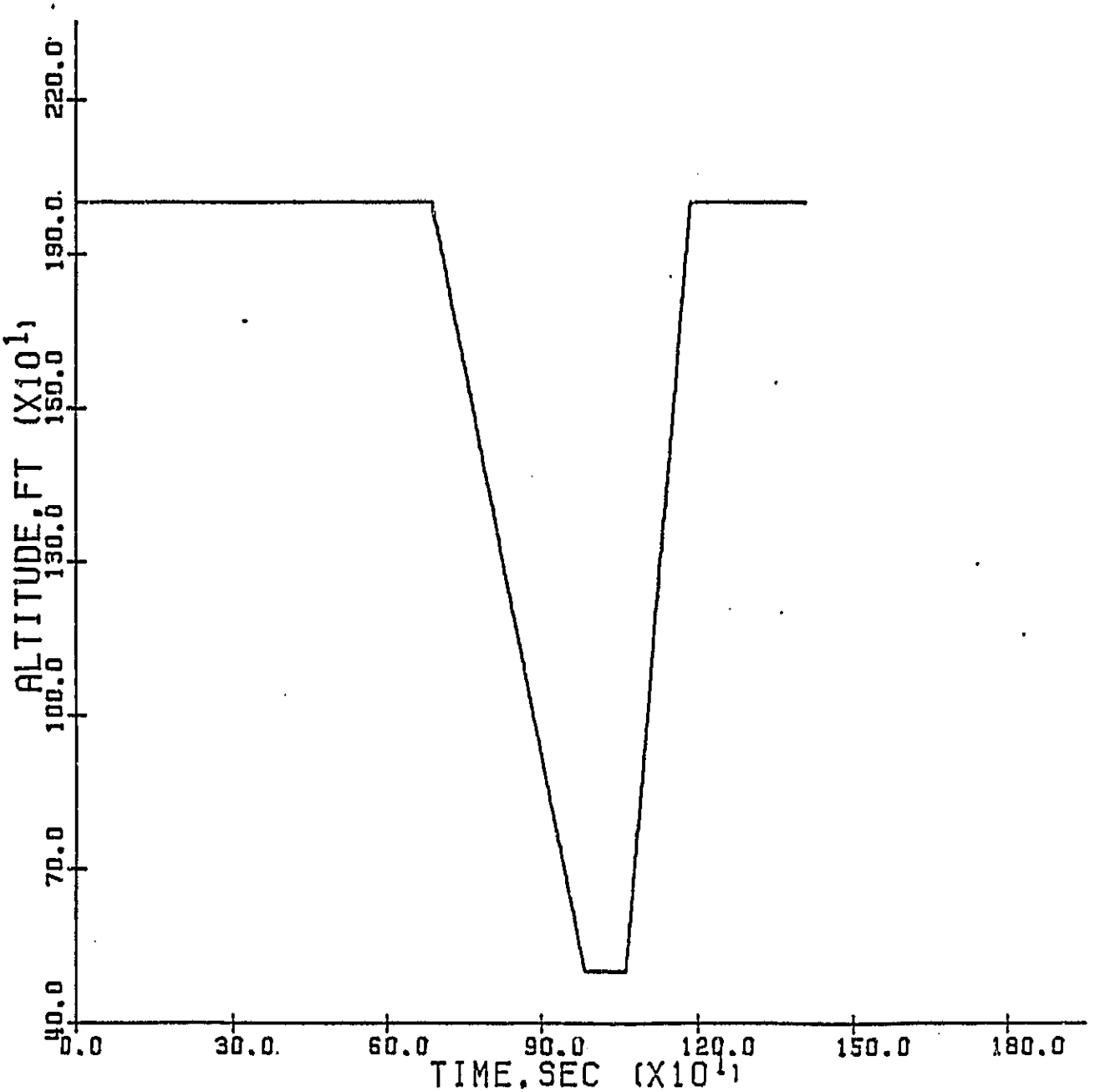

Figure 3.2.2 Teardrop Flight Path Altitude Profile

3.3.1 Position Fixing Algorithm

The following discussion is based upon the information presented by Noe and Myers [10].

The algorithm used to calculate the user's position requires the inputs of time, an estimate of the user's position and four user pseudorange measurements. To assist in the discussion of this algorithm, assume that the pseudorange is equal to the true range between the user and a satellite, plus user clock error.

The following expression relates the user's position (u_1, u_2, u_3) and receiver clock bias (b), i^{th} satellite position (x_{i1}, x_{i2}, x_{i3}) and the measured pseudorange r_i;

$$\text{Eq. 3.3.1.1} \quad \sum_{j=1}^{3}(x_{ij}-u_j)^2 = (r_i-b)^2, \text{ for } i = 1, 2, 3, 4$$

Figure 3.3.1.1 expresses graphically the Pythagorean relations used to derive the earth centered user's position.

Expanding the equation and solving for r_i, the following expression is obtained;

$$\text{Eq. 3.3.1.2} \quad r_i = \sqrt{(x_{i1}-u_1)^2 + (x_{i2}-u_2)^2 + (x_{i3}-u_3)^2} + b$$

To obtain the desired navigation algorithm, it is first necessary to Taylor series expand the pseudorange measurement r_i about the user position estimate $\overline{U}$. This results in the following equation;

$$\text{Eq. 3.3.1.3} \quad r_i = \overline{r_i} + \left(\frac{\partial r_i}{\partial U}\right)\Bigg|_{\overline{U}} \delta U + \frac{1}{2!}\left(\frac{\partial^2 r_i}{\partial U^2}\right)\Bigg|_{\overline{U}} \delta^2 U + \frac{1}{3!}\left(\frac{\partial^3 r_i}{\partial U^3}\right)\Bigg|_{\overline{U}} \delta^3 U + \ldots$$

This equation can now be linearized by deleting all of the partial derivatives of an order greater than one, giving the expression;

$$\text{Eq. 3.3.1.4} \quad r_i = \overline{r_i} + \left(\frac{\partial r_i}{\partial U}\right)\Bigg|_{\overline{U}} \delta U \quad \text{or}$$

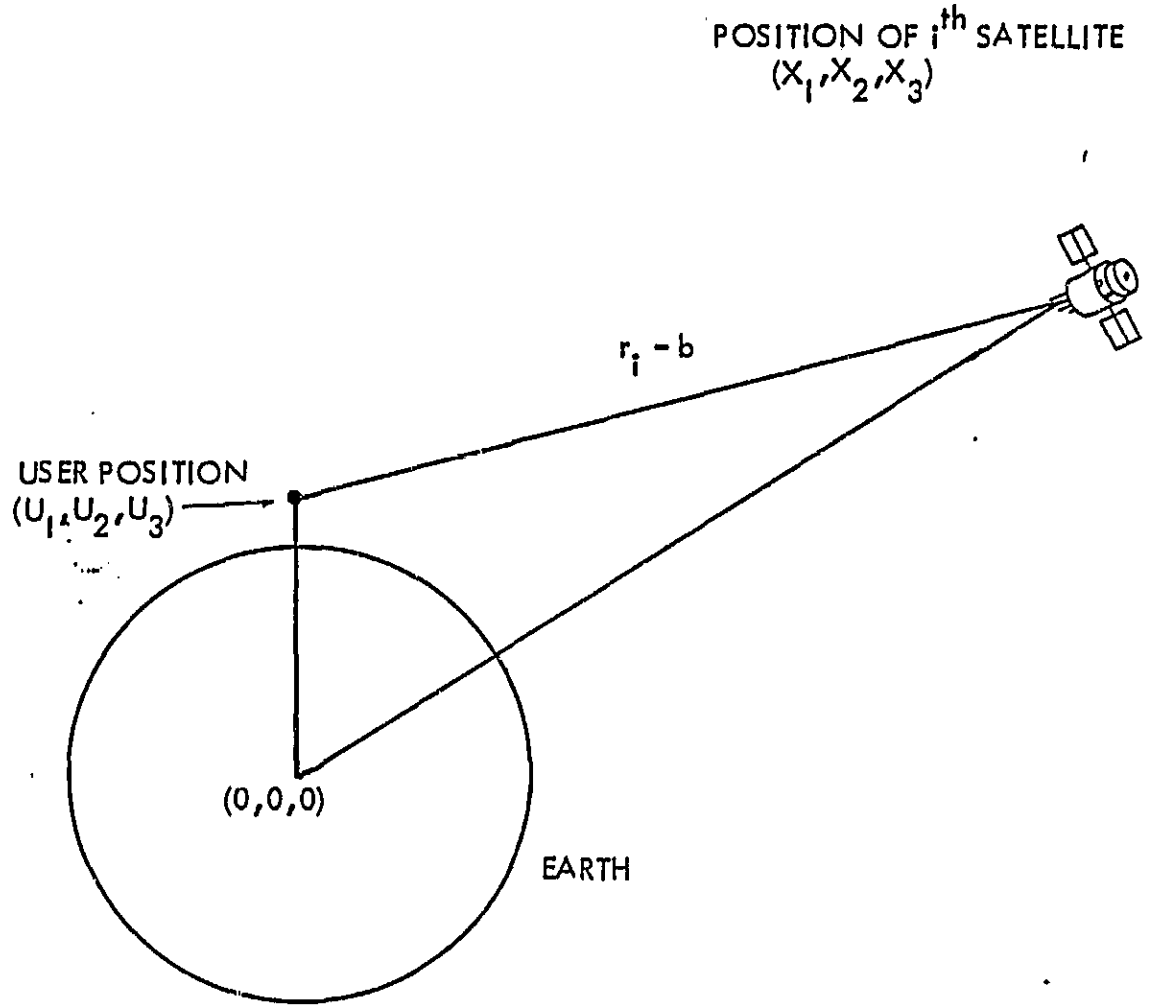

Figure 3.3.1.1 Graphic Representation of the Pythagorean Solution for Satellite Range.

Eq. 3.3.1.5 $$\delta r_i = \left[\left(\frac{\partial r_i}{\partial u_1}\right)\left(\frac{\partial r_i}{\partial u_2}\right)\left(\frac{\partial r_i}{\partial u_3}\right)\left(\frac{\partial r_i}{\partial b}\right)\right]\Bigg|_{\overline{U}} \delta U$$

Where $\delta r = r_i - \overline{r_i}$ and $\delta U = U - \overline{U}$.

Define δr as follows;

Eq. 3.3.1.6 $$\delta r_i = h_i \, \delta U$$

where h_i is the row vector of first order partial derivatives;

Eq. 3.3.1.7 $$h_i = \left[\left(\frac{\partial r_i}{\partial u_1}\right)\left(\frac{\partial r_i}{\partial u_2}\right)\left(\frac{\partial r_i}{\partial u_3}\right)\left(\frac{\partial r_i}{\partial b}\right)\right]\Bigg|_{\overline{U}}$$

Now, replace r_i in the h_i row vector with Eq. 3.3.1.2, expand the partial derivatives, substitute $r_i - b$ from Eq. 3.3.1.2, and obtain;

Eq. 3.3.1.8 $$h_i = \left[\left(\frac{u_{i1}-x_{i1}}{r_i - b}\right) \quad \left(\frac{u_2-x_{i2}}{r_i - b}\right) \quad \left(\frac{u_3-x_{i3}}{r_i - b}\right) \quad 1\right]\Bigg|_{\overline{U}}$$

This may now be expanded to four pseudorange measurements and solved for the user position vector U;

Eq. 3.3.1.9 $$\delta R = \begin{bmatrix} h_1 \\ h_2 \\ h_3 \\ h_4 \end{bmatrix} \delta U = H \delta U$$

Eq. 3.3.1.10 $$\delta U = H^{-1} \, \delta R$$

Now, given time, four pseudorange measurements, and an user position estimate, this algorithm will provide a user position and clock bias update.

3.3.2 Alpha-Beta Tracking Filter

The data output from the position fix algorithm is filtered using a simple, fixed gain alpha-beta tracking filter. This is the same filter used in the GPS non-precision approach study simulations developed for the

Department of Transportation. The following discussion is paraphrased from the documentation of that study [11].

Figure 3.3.2.1 depicts the alpha-beta filter estimation loop and its corresponding system equations. Rearranging these filter equations yields;

Eq. 3.3.2.1
$$\frac{U_p(t+T) - U_p(t)}{T} = \frac{\Delta U}{T} + V_p(t+T)$$

Eq. 3.3.2.2
$$\frac{V_p(t+T) - U_p(t)}{T} = \frac{\beta \Delta U}{T^2} .$$

where U_p is the predicted user position component, V_p is the predicted user velocity component, T is the update period, ΔU is the position update from the position fix algorithm, and alpha and beta are the filter gain constants.

These equations can be approximated by the following differential equations;

Eq. 3.3.2.3
$$\frac{dU_p}{dt} \cong \frac{\alpha \Delta U}{T} + V_p$$

Eq. 3.3.2.4
$$\frac{dU_p}{dt} \cong \frac{\beta \Delta U}{T^2}$$

and then converted to these integral equations;

Eq. 3.3.2.5
$$U_p \cong \int \frac{\alpha \Delta U}{T} + V_p \, dt$$

Eq. 3.3.2.6
$$V_p \cong \int \frac{\beta \Delta U}{T^2} \, dt$$

By means of the Laplace Transform and deriving the transfer function of this system, it is possible to obtain the characteristic equation to determine the relationship of the filter gain constants to the damping ratio of the system. A damping ratio of unity was chosen for the non-

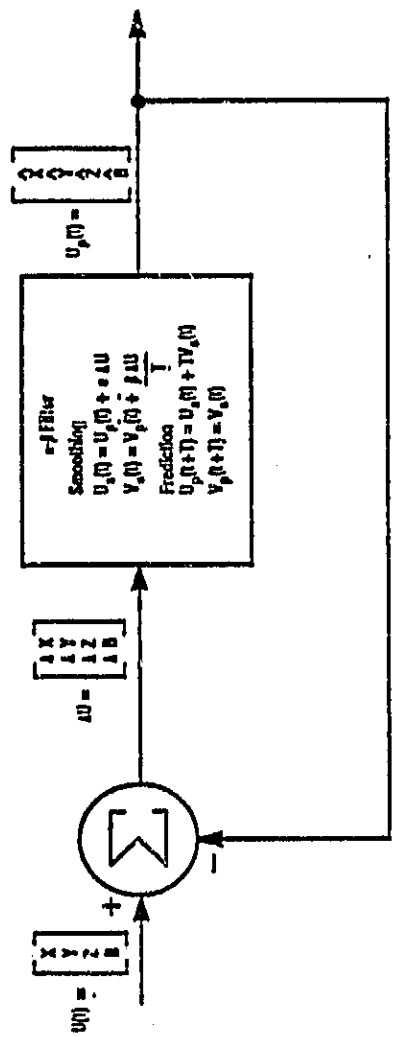

Figure 3,3,2,1 Alpha-Beta Filter Estimation Loop (Taken from Shively)

precision approach study to compromise between filter rise time, overshoot, and ringing of the transient response. This gives the relationship between alpha and beta;

Eq. 3.3.2.7 $\alpha^2 = 4\beta$

Again, using the transfer function of the system, the unit step response of the filter is found to be;

Eq. 3.3.2.8 $1 + \frac{\alpha t}{2T} e^{\frac{\alpha t}{2T}} - e^{\frac{\alpha t}{2T}}$

Now define a time constant τ_f such that at $t = 2\tau_f$, the step response is within 13.5% (e^{-2}) of the final value of the unit step response, this yields;

Eq. 3.3.2.9 $e^{-2} = e^{-\frac{\alpha\tau_f}{T}} - \frac{\alpha\tau_f}{T} e^{-\frac{\alpha\tau_f}{T}}$

This differential equation can be solved and found to have at least one real solution;

Eq. 3.3.2.10 $\tau_f \cong \frac{.72T}{\alpha}$

The values used for the DOT simulations were found by experimentation. "Reasonable performance" was achieved for alpha = .2 and beta = .01 for a dwell time of 1.2 seconds. This gave an overall time constant of $\tau_f = 4.3$ seconds. These filter gain constants were used throughout this simulation, regardless of receiver update rate. Therefore, τ_f was allowed to vary proportional to the receiver update rate, a receiver with a shorter update period filtered its position data using a filter with a faster reaction time. A receiver with an update rate of 0.3 seconds had a time constant of approximately 1.075 seconds and a receiver with an update rate of 2.4 seconds had a time constant of 8.6 seconds.

3.4 Simulation of GPS Range Errors

The following is a discussion of the error models used in this study and their derivations.

3.4.1 Multipath

Multipath can take on two basic forms of interference to GPS signals, specular and diffuse multipath. Specular multipath produces a delayed replica of the direct path GPS signal and, depending upon the media from which it is reflected, can be received at various signal levels. This degradation can be substantial if the receiver does not lock on the earliest received signal; usually this can only occur if the signal delay is greater than one pseudorandom (PRN) code chip width. Specular multipath was not included in the simulation. The diffuse multipath was modeled as described in the following text.

Diffuse multipath produces a random wide-band interference rather than inducing a large range offset. The diffuse multipath is caused by the addition of the many indirect signals, reflected mainly from the user's vehicle surface. These errors have an rms value of 1.0 to 3.0 meters for the P-code and 10.0 to 30.0 meters for the C/A-code [12].

The error values generated by the simulation by calling a zero mean gaussian distribution with a standard deviation of one and then multiplying the elements of the distribution by ten (see Eq. 3.4.1.1). This produces a sequence of random numbers with an rms value of ten, which is then scaled to the appropriate units of measure used by the simulation. A typical diffuse multipath error sequence is shown in figure 3.4.1.1.

Eq. 3.4.1.1 Multipath Error = 10.0 * N(0,1)

Where N(0,1) denotes a sequentially accessed zero mean Gaussian number sequence, with a unity standard deviation.

3.4.2 Ionospheric Range Error

The delay caused by the ionosphere is due to the free electrons encountered by the signal along the ray path between the satellite and the user. The delay encountered when a satellite is at zenith varies from about 5 nanoseconds during the evening to a peak of 35 nanoseconds during the middle of the day for the L-band frequencies. A plot of the average value of zenith propagation delay versus time, over a 24 hour period, is shown in figure 3.4.2.1.

Superimposed with the ionospheric data is a plot of the raised cosine model approximation of the ionosphere. This model was developed by Klobuchar [13] and has been incorporated into the GPS simulation to calculate the ionospheric propagation delay, at zenith, given the time and location at the point where the ray path, between the user and the satellite, pierces the bottom of the ionospheric layer. This location is called the local ionospheric point (see figure 3.4.2.2).

The local ionospheric point is calculated from the satellite's earth angles, elevation and azimuth angle as viewed from the user, and the

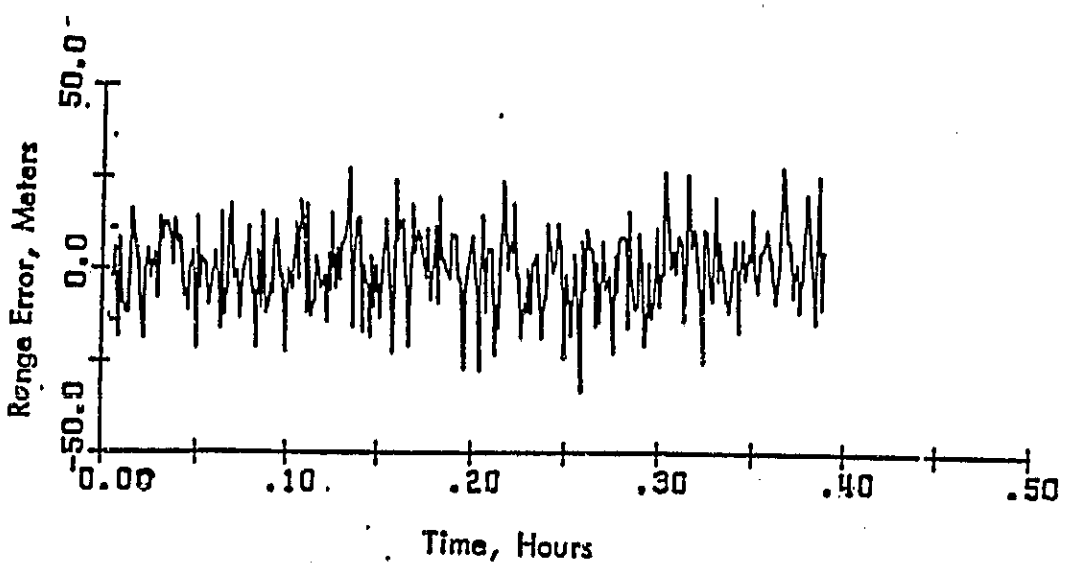

Figure 3.4.1.1 Diffuse Multipath Range Error

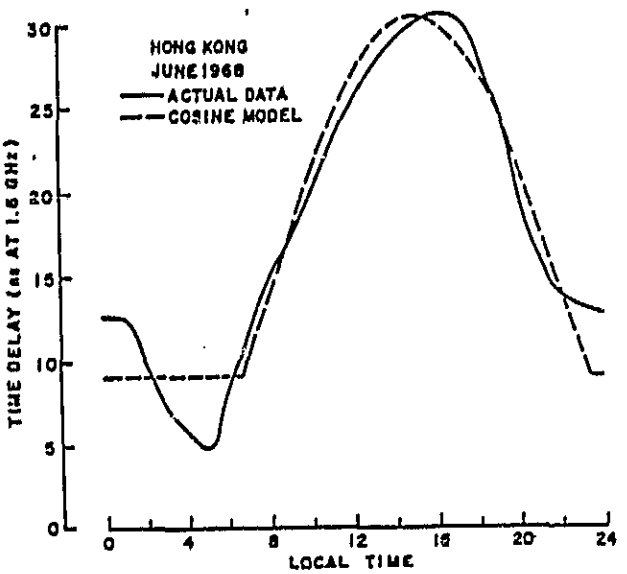

Figure 3.4.2.1 Average Monthly Value of Zenith Propagation Delay and the Raised Cosine Model (Taken from Klobuchar).

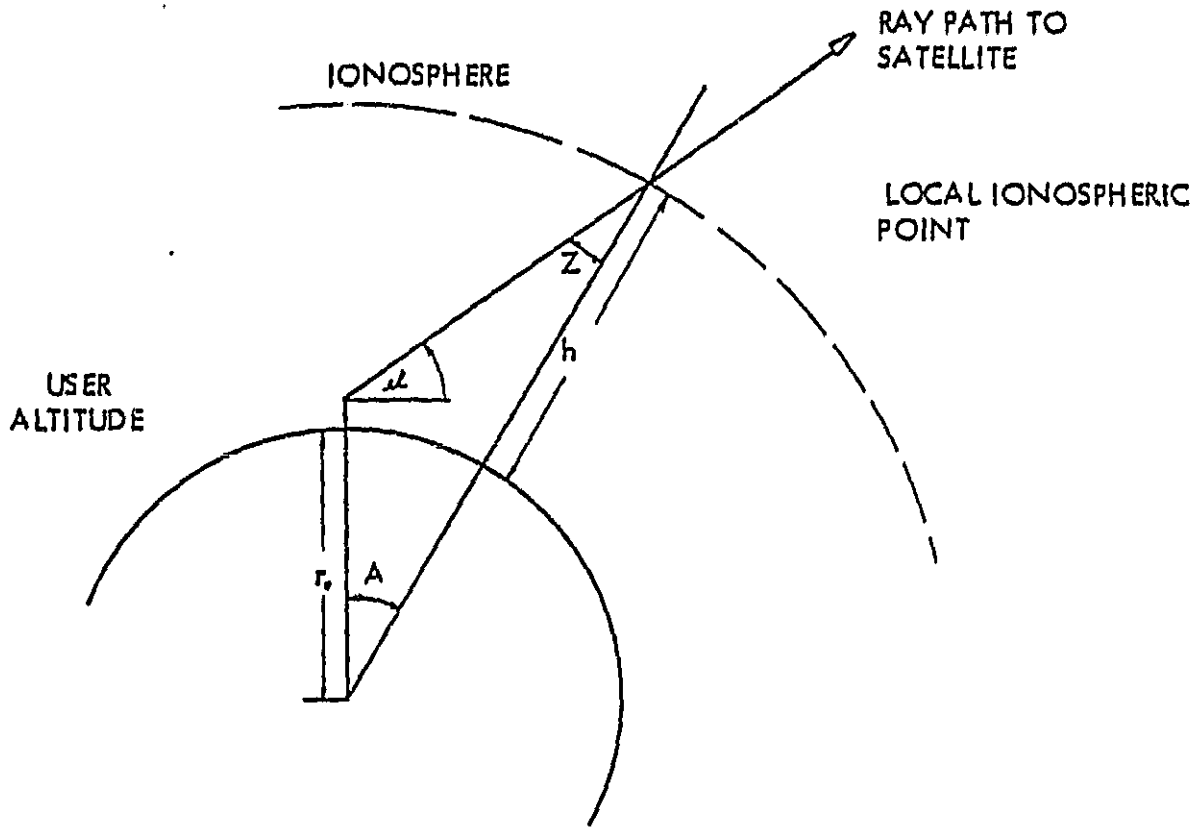

Figure 3.4.2.2 Ionospheric Range Error Model Parameters

user's location using a flat earth approximation. By applying a few simple trigonometric rules and identities to the triangle depicted in figure 3.4.2.2, the earth angle A can be found to be described by the following equation;

$$\text{Eq. 3.4.2.1} \quad A = 90^\circ - el - \arcsin\left[\frac{r_0 + alt}{r_0 + h}\left(\cos el\right)\right]$$

The location of the local ionospheric point may now be calculated using;

$$\text{Eq. 3.4.2.2} \quad \phi_I = \phi_0 + A \cos AZ$$

$$\text{Eq. 3.4.2.3} \quad \lambda_I = \lambda_0 + \frac{A \sin AZ}{\cos \phi_I}$$

Where ϕ_0 is the user's latitude, λ_0 is the user's longitude, AZ is the satellite's azimuth angle, ϕ_I is the latitude of the local ionospheric point, and λ_I is the longitude of the local ionospheric point.

Given time, in GMT hours at the user's location, and the calculated longitude of the local ionospheric point, the time at the local ionospheric point is calculated from;

$$\text{Eq. 3.4.2.5} \quad t = \frac{\lambda_I}{15} + GMT$$

Note: $t = t - 24$, if t is greater than 24 hours

Now that time is known at the local ionospheric point, the zenith propagation delay can now be computed using the raised cosine model. For values of local time at the ionospheric point between 0600 and 2200 hours, the zenith propagation delay can be represented by;

$$\text{Eq. 3.4.2.6} \quad \text{Ion Zenith Delay} = DC + A \cos\left(\frac{(t - \phi)2\pi}{P}\right)$$

Where DC = nighttime component of the zenith propagation delay, approximately 5 nanoseconds; A = the peak zenith propagation delay, 30 nanoseconds; P = period of the

cosine model, 32 hours; and t is the local time at the local ionospheric point.

For all other times, the delay will equal the nighttime component only.

Thus far, the computation of the ionospheric delay has only been concerned with a signal ray path at zenith, however rarely are there any satellites available exactly at zenith. For those ray paths not coinciding with zenith, a slant factor or obliquity factor must be calculated. The slant factor is defined as the secant of the zenith angle, Z, at the local ionospheric point. The angle Z is equal to;

Eq 3.4.2.7 $$Z = \arcsin\left[\frac{r_0 + alt}{r_0 + h}\left(\cos\ el\right)\right]$$

which, if user altitude is considered negligible, is approximately;

Eq. 3.4.2.8 $$Z = \arcsin[\ .94792\ \cos(el)\ ]$$

The slant factor, SF, is then equal to;

Eq. 3.4.2.9 $$SF = \sec[\ Z\ ]$$

The propagation delay, due to the true signal ray path, is then calculated to be a product of the zenith propagation delay and the slant factor (see EQ.3.4.2.10).

Eq. 3.4.2.10 Total Time Delay = SF * Ion Zenith Delay

Figure 3.4.2.3 shows typical ionospheric range error produced by this model.

3.4.3 Tropospheric Range Error

This particular error model was developed by Altshuler and Kalaghan [14]. The inputs required for this model included user altitude, satellite elevation angle, and the season or month of the year. The basic equation used is;

Eq. 3.4.3.1 $$\Delta R(\theta,h,N_s) = G(\theta)\ H(h) \cdot F(h,N_s)$$

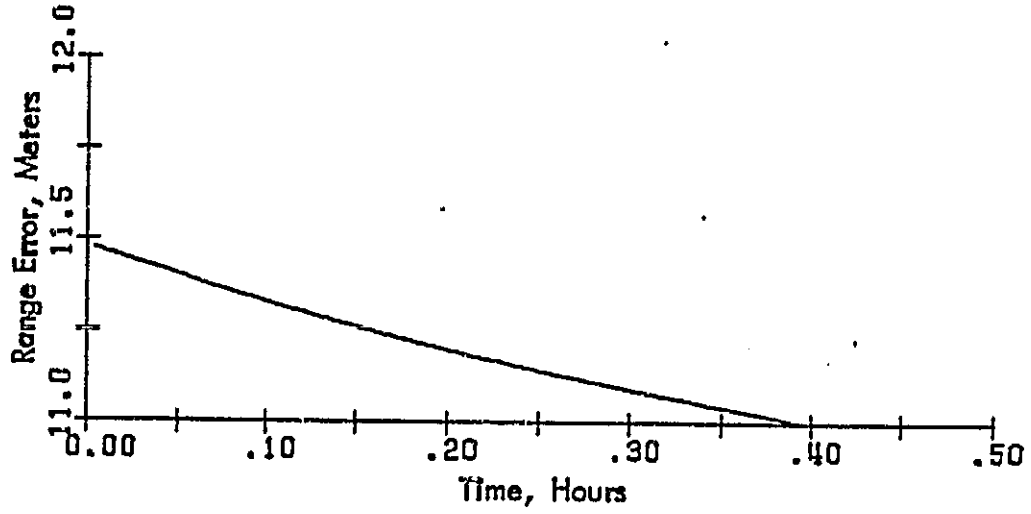

Figure 3.4.2.3 Ionospheric Range Error

Where $G(\theta)$ is a function of satellite elevation angle, $H(h)$ is a function of user altitude, and $F(h,N_s)$ is a function of user height and surface refractivity N_s.

The functions of the tropospheric range error are found from the following equations;

Eq. 3.4.3.2 $$G(\theta) = (g_0 + g_1\theta^{-1} + g_2\theta^{-2} + g_3\theta^{-3})\ [g_4 + g_6(\theta - g_5)^2]$$

Where θ, is valid only for $\theta > 5°$.

Eq. 3.4.3.3 $$H(h) = [(b_0 + b_1(h+8.6286)^{-1} + b_2(h+8.6286)^{-2} + b_3(h+8.6286)^{-3})]$$

Eq. 3.4.3.4 $$F(h,N_s) = c_0 \left[\frac{c_1}{h + c_0} + c_2(h+c_0) + c_3N_s - c_4\right] \left[1 - c_5(N_s - c_6)^2\right]$$

Eq. 3.4.3.5 $$N_s(h,L,M) = \alpha_0 + \alpha_1 h + \alpha_2 L + \alpha_3 hs^2 + \alpha_4 Ls^2 + \alpha_5 hc + \alpha_6 Lc$$

Where L is the user's latitude in degrees and;

Eq. 3.4.3.6 $$s = \sin\left(\frac{\pi}{12M}\right)$$

Eq. 3.4.3.7 $$c = \cos\left(\frac{\pi}{12M}\right)$$

Good results can be obtained by using an average global surface refractivity value of 324.8 N units and deleting the calculation of N_s.

The constants required for these equations are as follows:

$g_0 = 0.1556$	$b_0 = 0.00970$	$c_0 = 3.28084$	$\alpha_0 = 369.0300$
$g_1 = 138.8926$	$b_1 = -2.08809$	$c_1 = 6.81758$	$\alpha_1 = -.01553$
$g_2 = -105.0574$	$b_2 = 122.73592$	$c_2 = 0.30480$	$\alpha_2 = 0.92442$
$g_3 = 31.5070$	$b_3 = 703.82166$	$c_3 = 0.00423$	$\alpha_3 = 0.00160$
$g_4 = 1.000$		$c_4 = 1.33333$	$\alpha_4 = 0.19361$
$g_5 = 30.000$		$c_5 = 1.41723\text{X}10^{-6}$	$\alpha_5 = 0.00063$
$g_6 = 1.0\text{X}10^{-4}$		$c_6 = 315.00000$	$\alpha_6 = -0.05958$

Season	M Value (Month Number)
Winter	1.5
Spring	4.5
Summer	7.5
Fall	10.5

The error values are calculated for each satellite by supplying to these equations the necessary data and scaling the results to the required units for the simulation to process the range measurements. Figure 3.4.3.1 depicts the error profile generated by this model for the teardrop flight path, notice the deviation due to the change in altitude. The tropospheric error behaves in much the same manner as the ionospheric error with respect to elevation angles. The tropospheric error induced by a satellite close to the horizon may be as much as an order of magnitude greater than that exhibited by a satellite located near zenith.

3.4.4 Receiver Clock Error

The receiver clock error model used in this simulation calculates an instantaneous clock offset biased upon a starting clock offset (SO), frequency error based upon clock temperature stability (TS), and frequency drift based upon aging rate (AR) characteristics. Given SO, TS, and AR, the clock parameters are derived using the following equations;

Eq. 3.4.4.1 Freq. Error = FE = TS * DELT * C

Eq. 3.4.4.2 Freq. Drift = FD = AR/86400. * .5 * DELT**2 * C

Where 86400. scales the aging rate from days to seconds, DELT is the update period of the receiver, and C is the speed of light.

The clock bias is then calculated to be;

Eq. 3.4.4.3 Clock Bias = SO + FE * TIM + FD * TIM**2 + SS

Where TIM is the number of elapsed update rates and SS is a short term stability term derived from a gaussian random sequence of N(0,SS). SS is assigned a value of 50 nanoseconds thus gives the quassian sequence a stand deviation of 50.

Figure 3.4.4.1 shows the output of the clock error model for the following values;

SO = 1000 nanoseconds

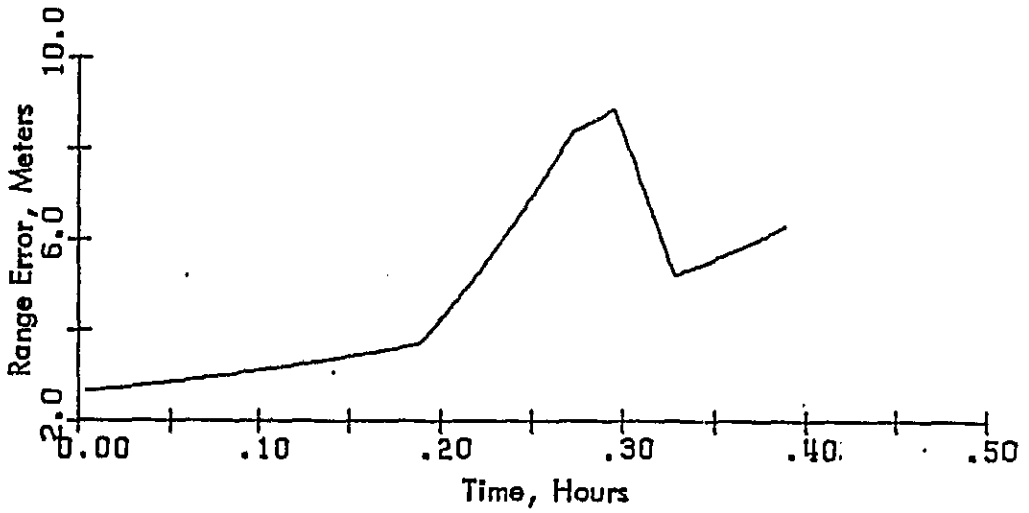

Figure 3.4.3.1 Tropospheric Range Error

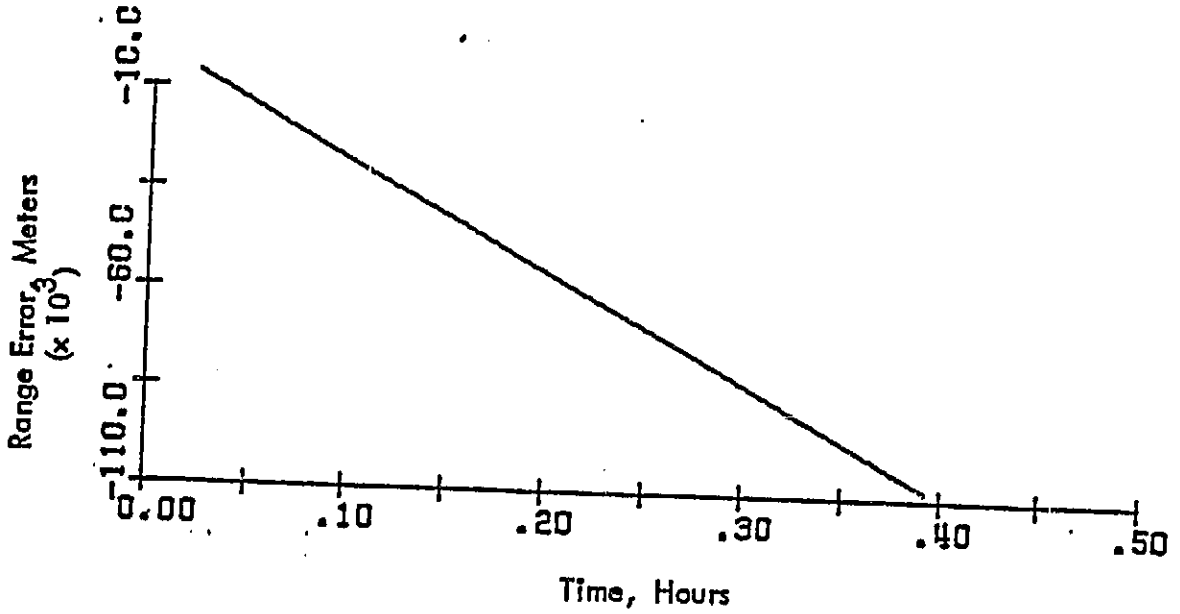

Figure 3.4.4.1 Uncorrected Range Errors Induced by an Imperfect Receiver Oscillator

TS = 5.E-07

AR = 1.0E-07

3.4.5 Selective Availability Errors

A statistical analysis has been performed by Kalafus, to determine the characteristics of the selective availability errors to be induced by the Department of Defense. These studies were performed upon unclassified samples of the SA error, given the original premise that the error was to induce a 500 meter (2d rms) horizontal position error. This has been lowered by a factor of five so now the expected horizontal position error will now be 100 meters (2d rms).

The SA model used in this study was scaled to the 100 meter criteria and maintained the dynamic characteristics found by Kalafus. These dynamics are characterized by the probability density functions, as derived by Kalafus, and are shown in figures 3.4.5.1 and 3.4.5.2.

These statistical characteristics are closely modeled by the following equation;

Eq. 3.4.5.1 SA Error(i) = SA Error(i-1) + VEL * DELT + 0.5 * ACC * DELT**2

Where VEL is a constant and ACC is a random walk generated from the summation of a gaussian random number sequence of N(0,SIGA). SIGA was assigned a value of 0.07 feet, this value was achieved through experiment.

The calculation of ACC was as follows;

Eq. 3.4.5.2 ACC = ACC + SIGA * N(0,1)

Figures 3.4.5.3 and 3.4.5.4 show the typical statistical characteristics of the SA error rate and accelerations,as computed by the model, for one satellite.

Comparing the statistics of the model and those found by Kalafus, some discrepancies can be seen. The velocity distribution does not appear entirely gaussian. However, if the model is allowed to run for longer periods of time, it is found that the distribution takes on a more, zero mean, gaussian appearance. Another discrepancy can be seen by comparing the endpoints of the distributions between those found by Kalafus and those generated by the model.

The accelerative values of the error generated by the model can take on values double those found by Kalafus, during a significant portion of the mission. Also, the velocity values generated by the model are somewhat lower than those calculated from the SA samples. The standard

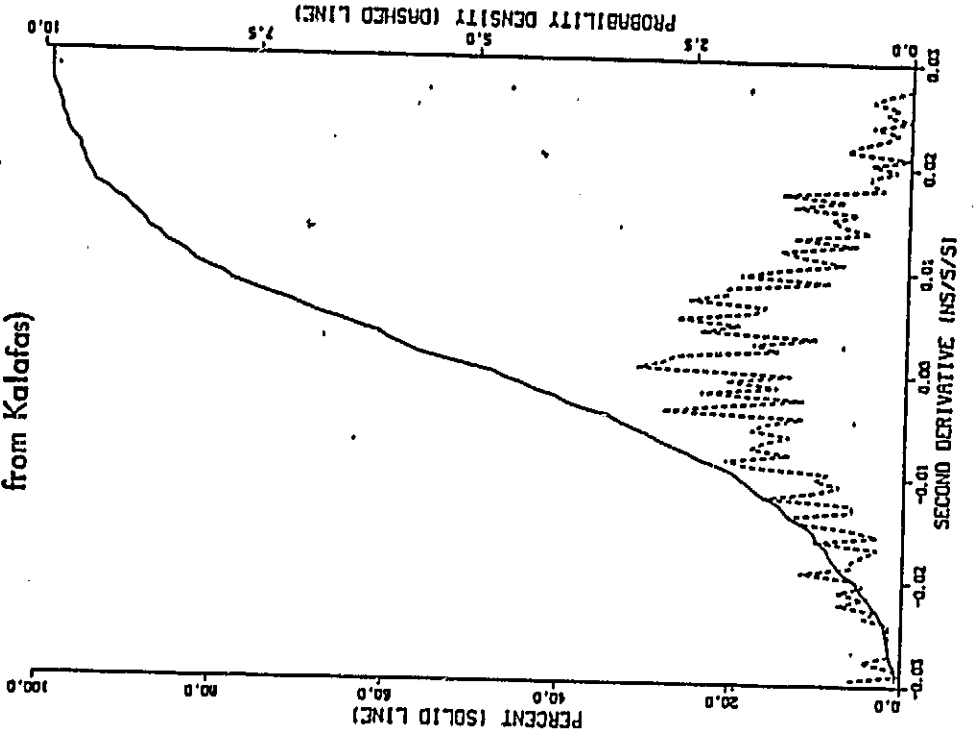

Figure 3.4.5.2 Selective Availability Second Derivative Distribution (Taken from Kalafas)

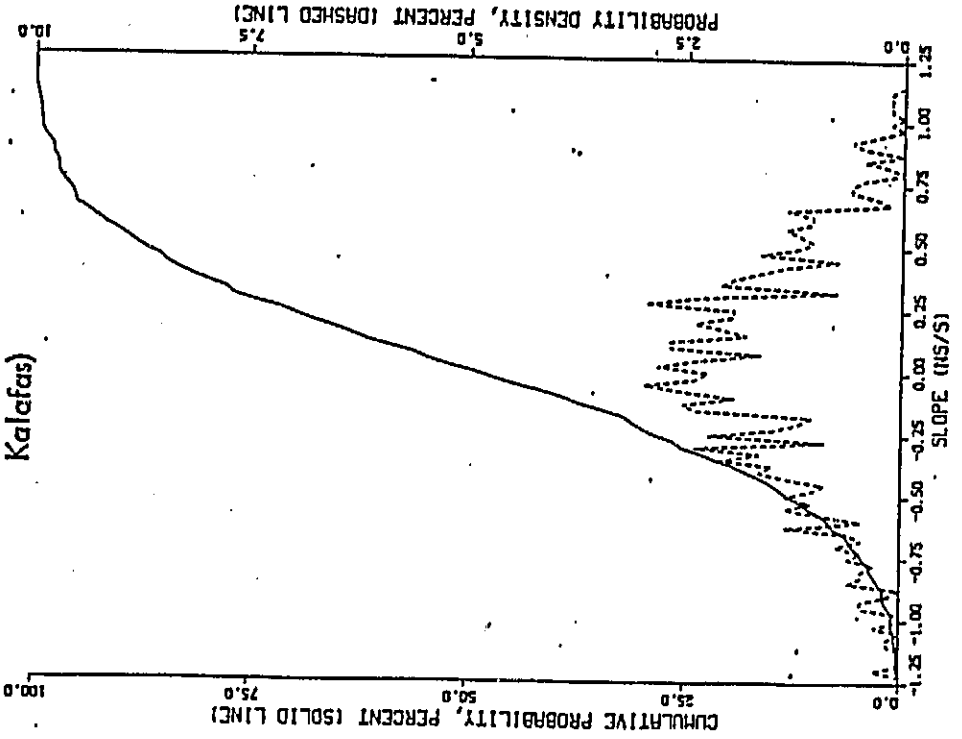

Figure 3.4.5.1 Selective Availability Rate Distribution (Taken from Kalafas)

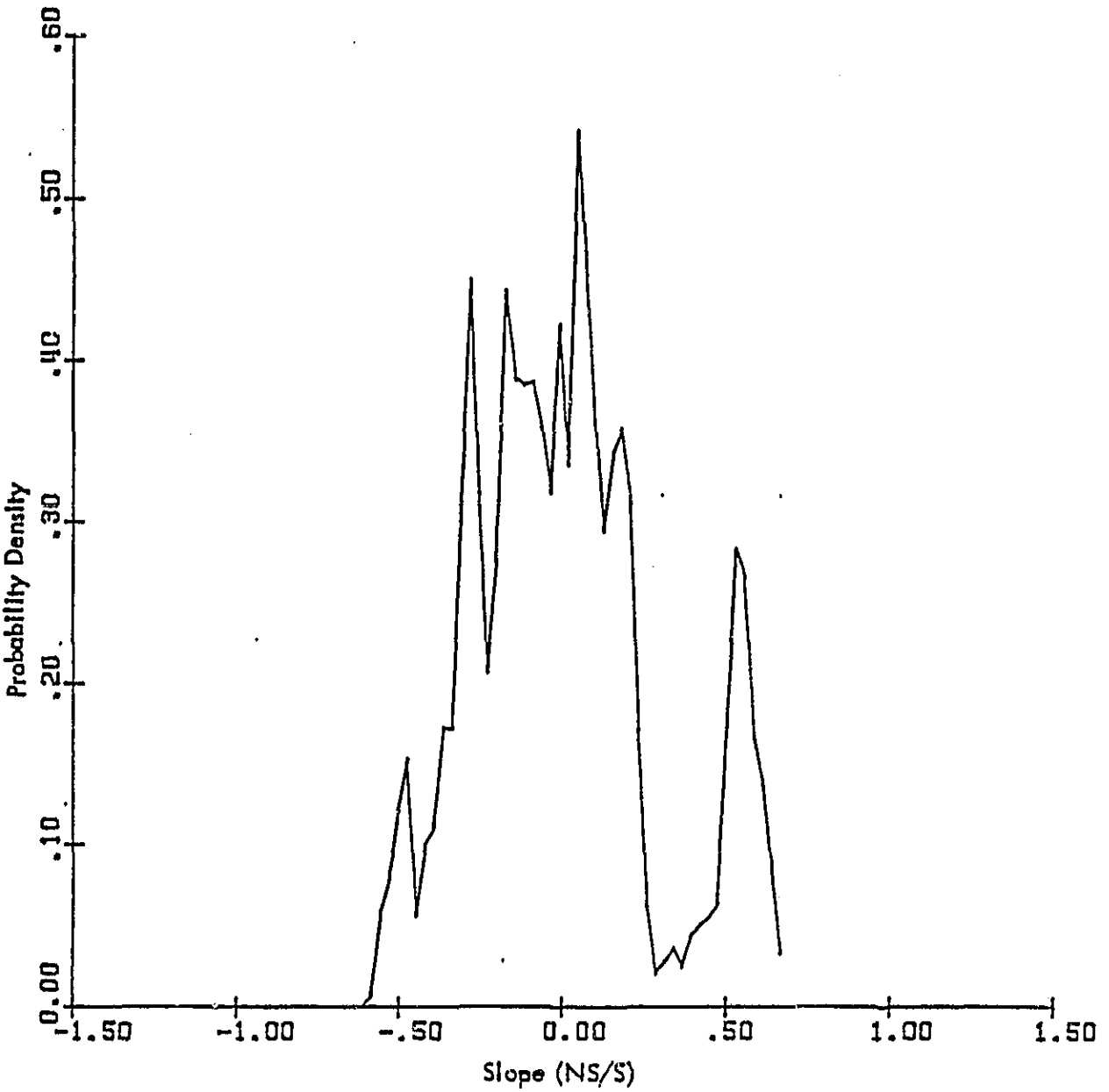

Figure 3.4.5.3 Selective Availability Model Rate Distribution

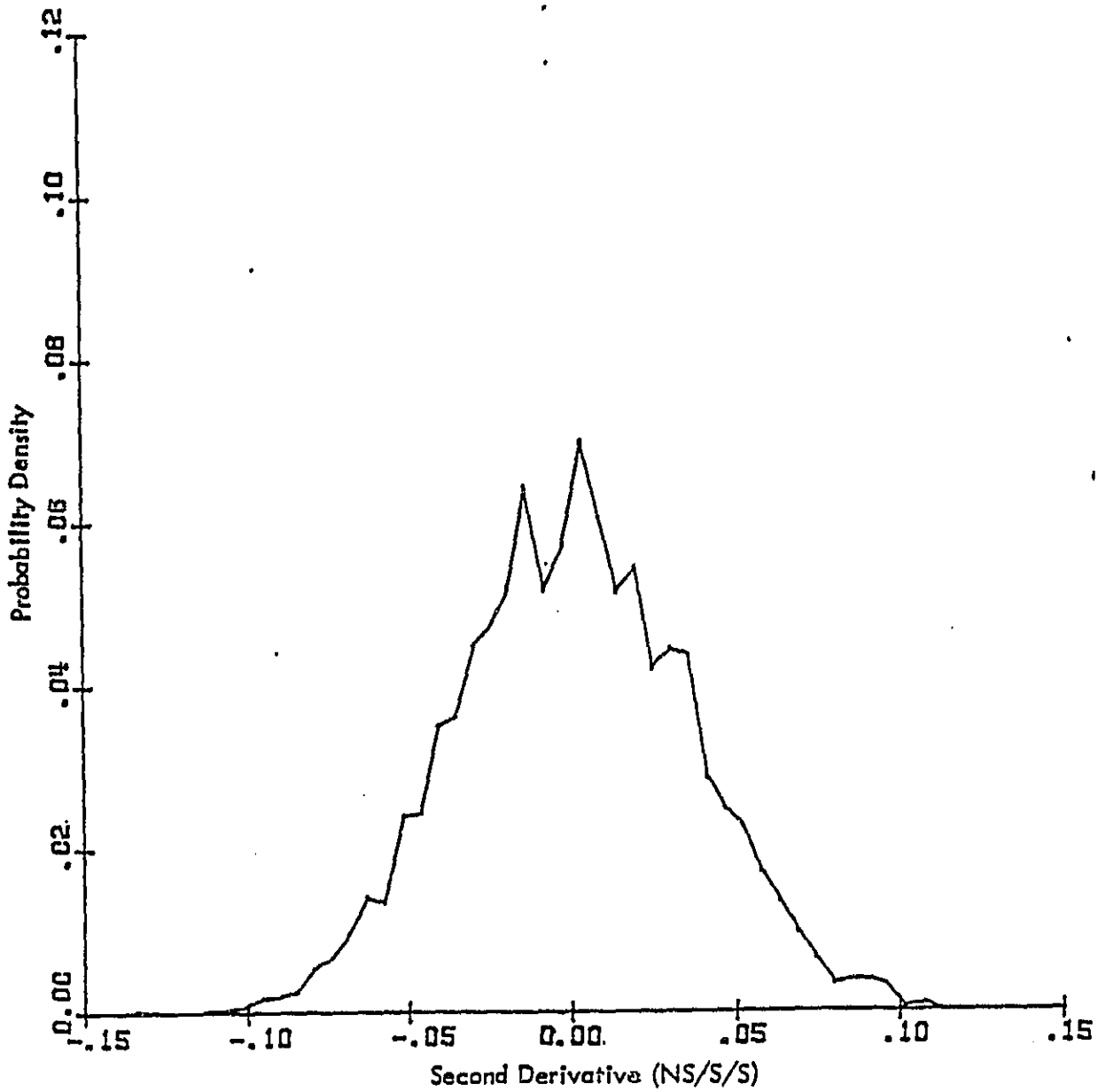

Figure 3.4.5.4 Selective Availability Model Second Derivative Distribution

deviation of the random number sequence used to generate the accelerative random walk, was scaled until the error statistics best matched those found by Kalafus. Although the accelerative values are excessive, it was felt that the velocity values were representative of those to be encountered in the field. Figure 3.4.5.5 displays the data output of this model for four satellites.

3.5 GPS Simulation Operation

Thus far, programming tools have been defined which can compute;

1) User/Receiver Position, given time

2) Satellite Position and Range to User, given time and the user's position

3) Satellite Range Error Values, given time, satellite's observed azimuth and elevation angles, and the user's position

4) Position fix and user clock error estimate based upon the best estimate of four satellite ranges

These basic tools can be used together to emulate either a sequential/single channel receiver or a four channel receiver. Each architecture is able to operate in a conventional, fixed, or differential GPS mode. These architectures were constructed to perform at 0.3, 1.2, and 2.4 second range update periods.

When operating in the conventional mode, the GPS receiver uses the range measurements to compute the receiver's position, without any corrections except for those intrinsic to operating with four satellites. The conventional mode also uses the flight path simulator to predetermine the position and velocity of the receiver.

When operating in the fixed mode, the GPS receiver collects range measurements as in the conventional mode. However, the fixed receiver and its antenna are positioned at a precisely known location, allowing the fixed receiver to compute its true range from a particular satellite at a given time. The difference between the true range and measured range is computed and provided to the differential receiver at specified uplink rate. The rate used in these studies is one correction every 12 seconds.

The differential mode incorporates many of the characteristics of the conventional mode and the application of the corrections generated by the fixed receiver. The differential receiver applies a range correction to each one of its measurements to obtain a better position fix. This correction is updated at the rate specified by the fixed receiver's uplink rate. For these experiments, the flight path and dynamics incurred during the conventional mode and the differential mode are identical.

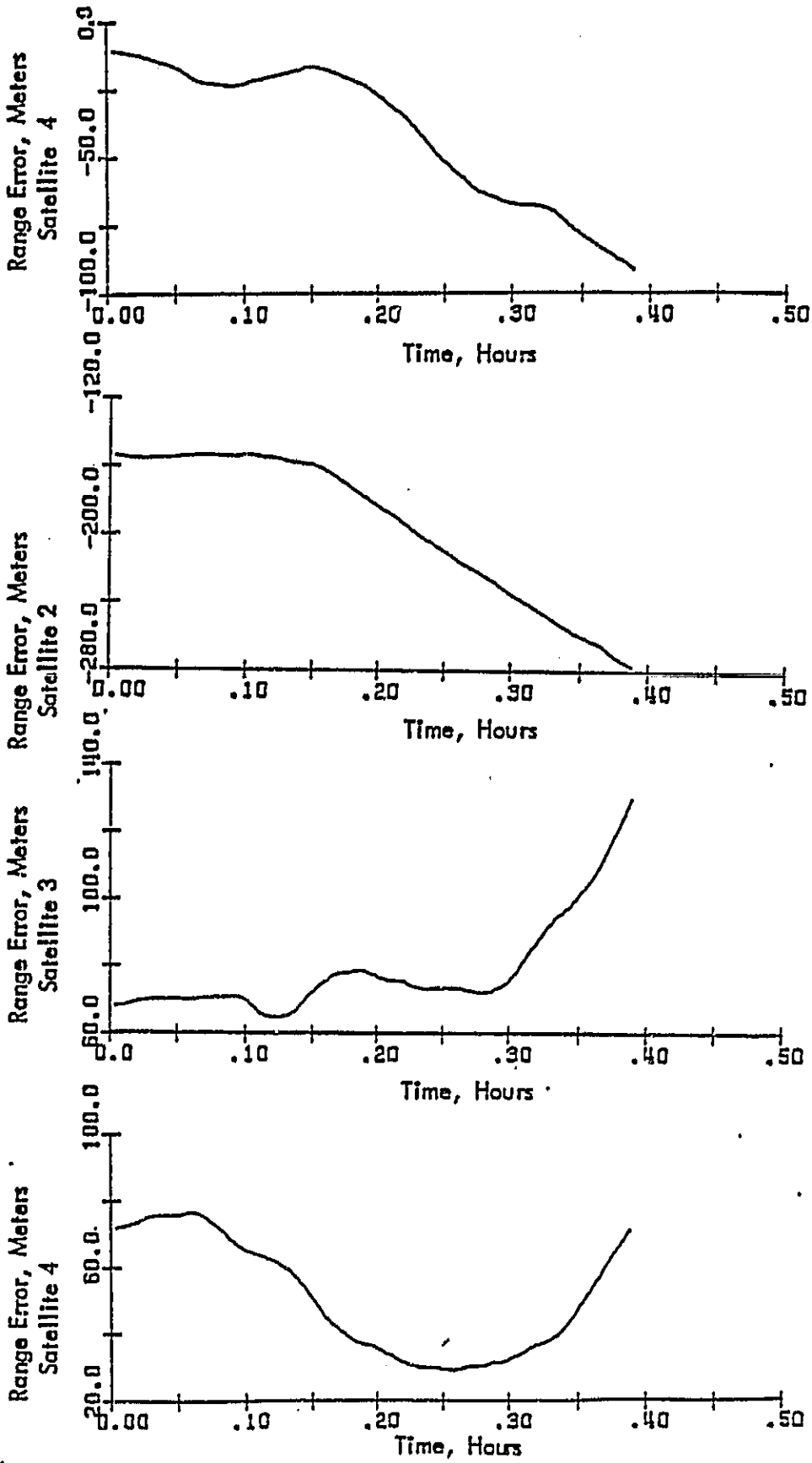

Figure 3.4.5.5 Selective Availability Range Errors

3.5.1 Sequential/Single Channel Architecture

The flowchart for the sequential/single channel receiver is shown in figure 3.5.1.1. The following text elaborates upon the program flow;

1) First the program is initialized, defining the initial time, receiver update rate, mission-end time, initial receiver position/velocity, the four satellites to be tracked and specified as KTH=one through four, initial error values, and the initialization of any program subroutines as required. the initialization defines satellite KTH=1 to be the first satellite tracked.

2) Next the true position of the receiver is determined. This position is determined by the flight path generator, given time.

3) With the knowledge of the receiver's position and time, the position fo the KTH satellite can be determined and the resulting range between the satellite and the receiver.

4) The programmer selected range errors are now computed for the current KTH satellite given time, receiver position, and the observed satellite azimuth and elevation angles. These errors can include diffuse multipath, ionospheric delay, tropospheric delay, receiver clock error, and a selective availability error.

5) Differential Mode — If the receiver is operating in the differential mode, the receiver obtains the most recent range correction from the fixed receiver and applies it to the most recent estimate of the corresponding range measurement.

   Fixed Mode — If the receiver is operating in the fixed mode and one uplink period has elapsed, the receiver will compute a correction for the most recent satellite measurement, and then provide the most recent corrections of all of the selected satellites to the differential receiver. The minimum number of satellites to be serviced by the fixed receiver is four.

   Conventional Mode — If operating in the conventional mode, once the necessary range and range error calculations have been made and properly combined, the program will then proceed to calculate a GPS position fix based upon the degraded range measurements.

6) A position fix is not calculated by the sequential receiver until at least four separate range measurements are available. Once four satellite ranges have been computed, a new position fix is made with every new range measurement. Therefore, the position fix calculation is made with ranges that are either instantaneous, or one, two, or three update periods old.

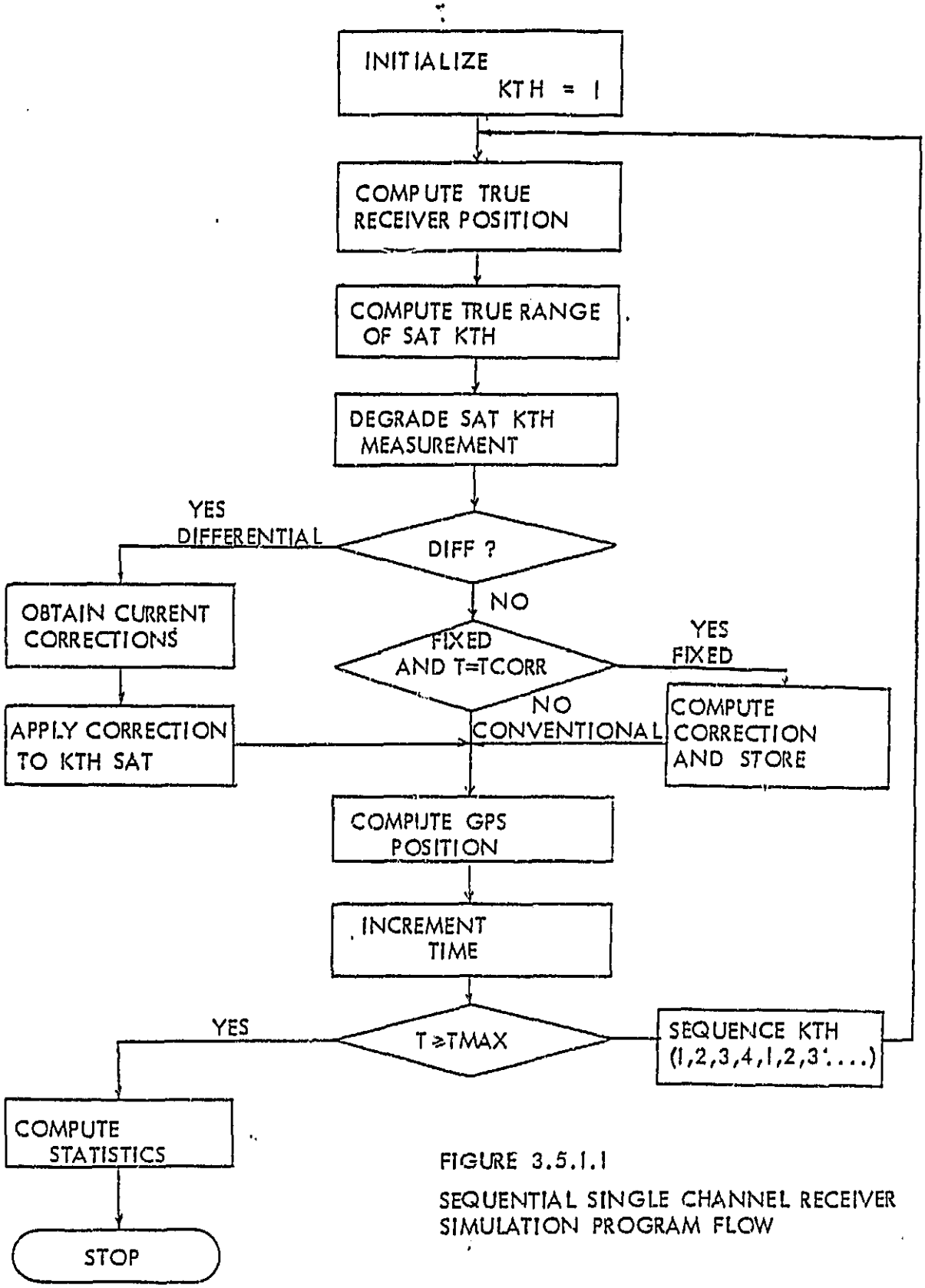

FIGURE 3.5.1.1

SEQUENTIAL SINGLE CHANNEL RECEIVER
SIMULATION PROGRAM FLOW

7) Next, time is incremented by one receiver update period.

8) If time is equal to or greater than the mission-end time, a subroutine is called to generate the statistical data and desired plot files for post program execution evaluation. Program execution is terminated after this subroutine call.

   If the mission-end time has not been reached, the value of KTH is sequenced and the process recycles beginning with step two.

3.5.2 Four Channel Architecture

The operation of the four channel set is very similar to that of the sequential/single channel receiver. The subroutines used in both programs are almost identical. The difference between the two architectures is the sequential/single channel receiver measures one satellite range each update period and the four channel receiver can measure four separate satellite ranges during the same period.

The program steps executed for the four channel receiver is shown in figure 3.5.2.1. The explanation of this flowchart is the same as the sequential/single channel receiver with the exception of the computation of satellite range and range errors. Each time the program is sequenced through the satellite position/range and satellite range error subroutines, new values for each of the four satellites are calculated. Likewise in the differential or fixed mode, either four of the latest corrections are applied or calculated at one time.

The calculation of the true receiver position, GPS position fix, time, and program statistics for both receiver types are identical.

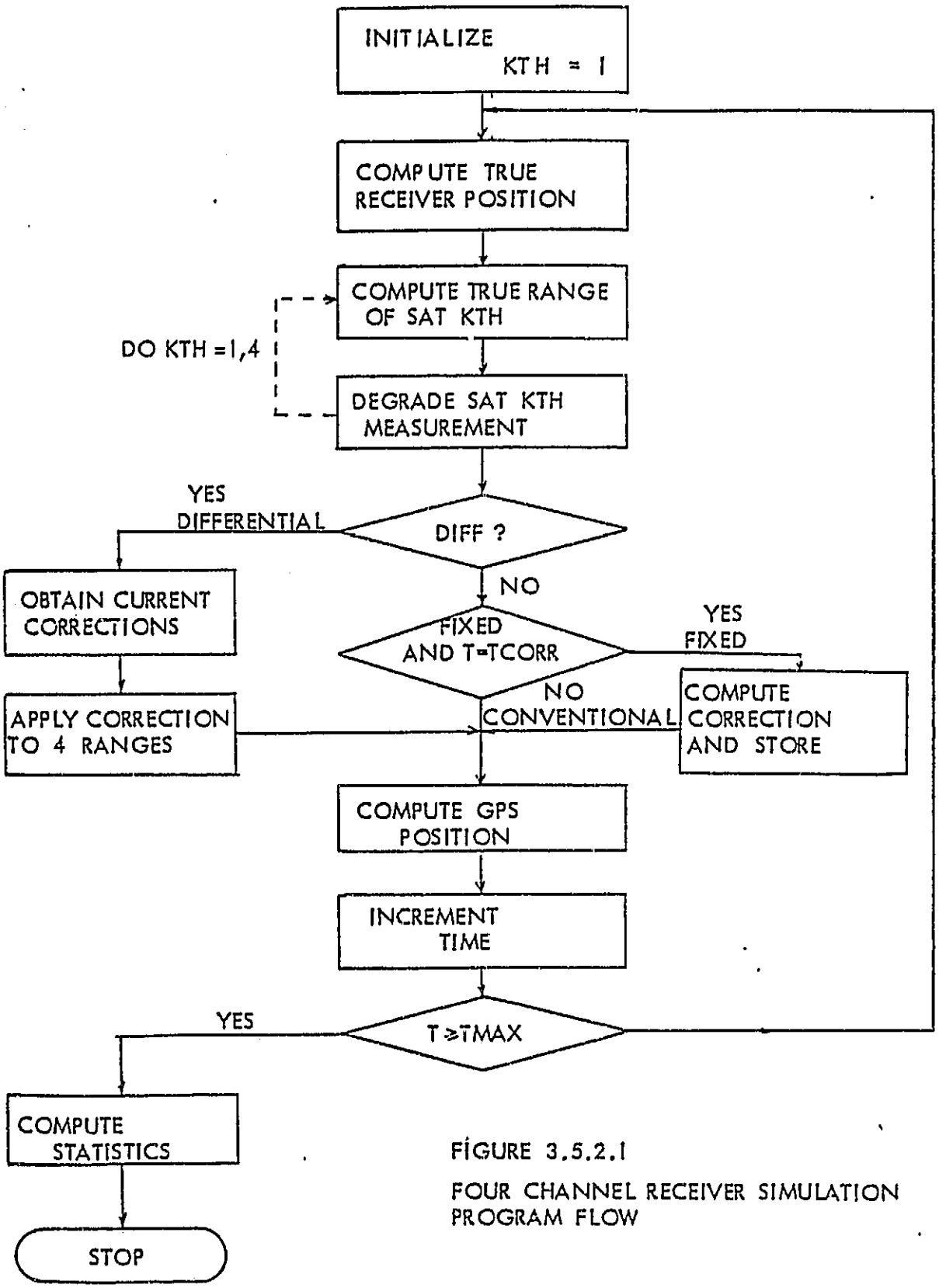

FIGURE 3.5.2.1

FOUR CHANNEL RECEIVER SIMULATION
PROGRAM FLOW

4.0 SIMULATION RESULTS

Shown in Table 4.0.1, are the basic receiver configurations used for the three different modes of operation. Two sets of data were collected for each run, one set of data was collected with the Selective Availability error evoked and the second set was run without the SA error.

The entire file of statistics generated in these experiments is not presented. This is in an attempt to lower the amount of data to be assimilated by the reader and to avoid the presentation of redundant information. Only selections of representative data and data of particular interest are shown and discussed.

4.0.1 Receiver Performance, Conventional Mode, No SA Errors

Figures 4.0.1.1, 4.0.1.2, and 4.0.1.3 show the altitude errors, three dimensional errors, and two dimensional errors encountered during the entire teardrop scenario using a sequential/single channel receiver, with an update period of 0.3 seconds, and operating in the conventional mode (run ID # C-1). Figures 4.0.1.4, 4.0.1.5, and 4.0.1.6 depict the same scenario and mode, however this receiver has four channels with an update period of 0.3 seconds (run ID # C-4).

Because the four channel receiver's measurements are more accurate, the errors induced by the alpha-beta tracking filter are amplified, particularly in figure 4.0.1.6. At times equal to approximately 0.039-0.053, 0.162-0.168, and 0.284-0.293 hours, one can see the peaks recorded in the two dimension error plots. These peaks occur during the three turns incurred during the teardrop flight path. The alpha-beta tracking filter does perform well in constant velocity dynamics. However, when submitted to the rates of velocities induced by these turns, the performance of this fixed gain filter is degraded considerably.

4.0.2 Receiver Performance, Conventional Mode, With SA Errors

Figures 4.0.2.1, 4.0.2.2, and 4.0.2.3 depict the positional errors encountered during the teardrop flight path while operating in the conventional mode, with a sequential/single channel, and an update period of 0.3 seconds with the SA error evoked (run ID # C-1). Figures 4.0.2.4, 4.0.2.5, and 4.0.2.6 depict the same type of errors for a similar receiver type with four tracking channels (run ID # C-4).

The cause for the increasing magnitudes of all of the positional errors during the second half of the mission, is evident if compared with the individual satellite SA errors shown in Figure 3.4.5.5. in Section 3.4.5. This increase corresponds with a significant increase in range error for three of the four satellites during this time frame. These errors may also be amplified by a slight increase in PDOP/GDOP. These values increase respectively from 2.44/2.67 at the beginning of the mission to the final values of 2.78/3.01 at the mission-end time.

The effects of the alpha-beta tracking errors are still noticeable in the 3D and 2D error plots, however the net effect of these errors are diluted somewhat by the large positional errors induced by the SA errors.

CONVENTIONAL MODE RECEIVER CONFIGURATIONS

RUN ID	RECEIVER TYPE	RECEIVER UPDATE PERIOD
C-1	SEQ/SINGLE CHAN.	0.3 seconds
C-2	SEQ/SINGLE CHAN.	1.2 seconds
C-3	SEQ/SINGLE CHAN.	2.4 seconds
C-4	FOUR CHANNEL	0.3 seconds
C-5	FOUR CHANNEL	1.2 seconds
C-6	FOUR CHANNEL	2.4 seconds

FIXED MODE RECEIVER CONFIGURATIONS

RUN ID	RECEIVER TYPE	RECEIVER UPDATE PERIOD
F-1	SEQ/SINGLE CHAN.	0.3 seconds
F-2	SEQ/SINGLE CHAN.	1.2 seconds
F-3	SEQ/SINGLE CHAN.	2.4 seconds
F-4	FOUR CHANNEL	0.3 seconds
F-5	FOUR CHANNEL	1.2 seconds
F-6	FOUR CHANNEL	2.4 seconds

DIFFERENTIAL MODE RECEIVER CONFIGURATIONS

RUN ID	RECEIVER TYPE	RECEIVER UPDATE PERIOD	FIXED RECEIVER MODE RUN ID
D-1	SEQ/SINGLE CHAN.	0.3 seconds	F-1
D-2	SEQ/SINGLE CHAN.	0.3 seconds	F-4
D-3	SEQ/SINGLE CHAN.	1.2 seconds	F-2
D-4	SEQ/SINGLE CHAN.	1.2 seconds	F-5
D-5	SEQ/SINGLE CHAN.	2.4 seconds	F-3
D-6	SEQ/SINGLE CHAN.	2.4 seconds	F-6
D-7	FOUR CHANNEL	0.3 seconds	F-1
D-8	FOUR CHANNEL	0.3 seconds	F-4
D-9	FOUR CHANNEL	1.2 seconds	F-2
D-10	FOUR CHANNEL	1.2 seconds	F-5
D-11	FOUR CHANNEL	2.4 seconds	F-3
D-12	FOUR CHANNEL	2.4 seconds	F-6
D-13	SEQ/SINGLE CHAN.	0.3 seconds	F-2
D-14	FOUR CHANNEL	0.3 seconds	F-2
D-15	SEQ/SINGLE CHAN.	0.3 seconds	F-5
D-16	FOUR CHANNEL	0.3 seconds	F-5
D-17	SEQ/SINGLE CHAN.	0.3 seconds	F-3
D-18	FOUR CHANNEL	0.3 seconds	F-3
D-19	SEQ/SINGLE CHAN.	0.3 seconds	F-6
D-20	FOUR CHANNEL	0.3 seconds	F-6

TABLE 4.0.1 Basic Receiver Configurations

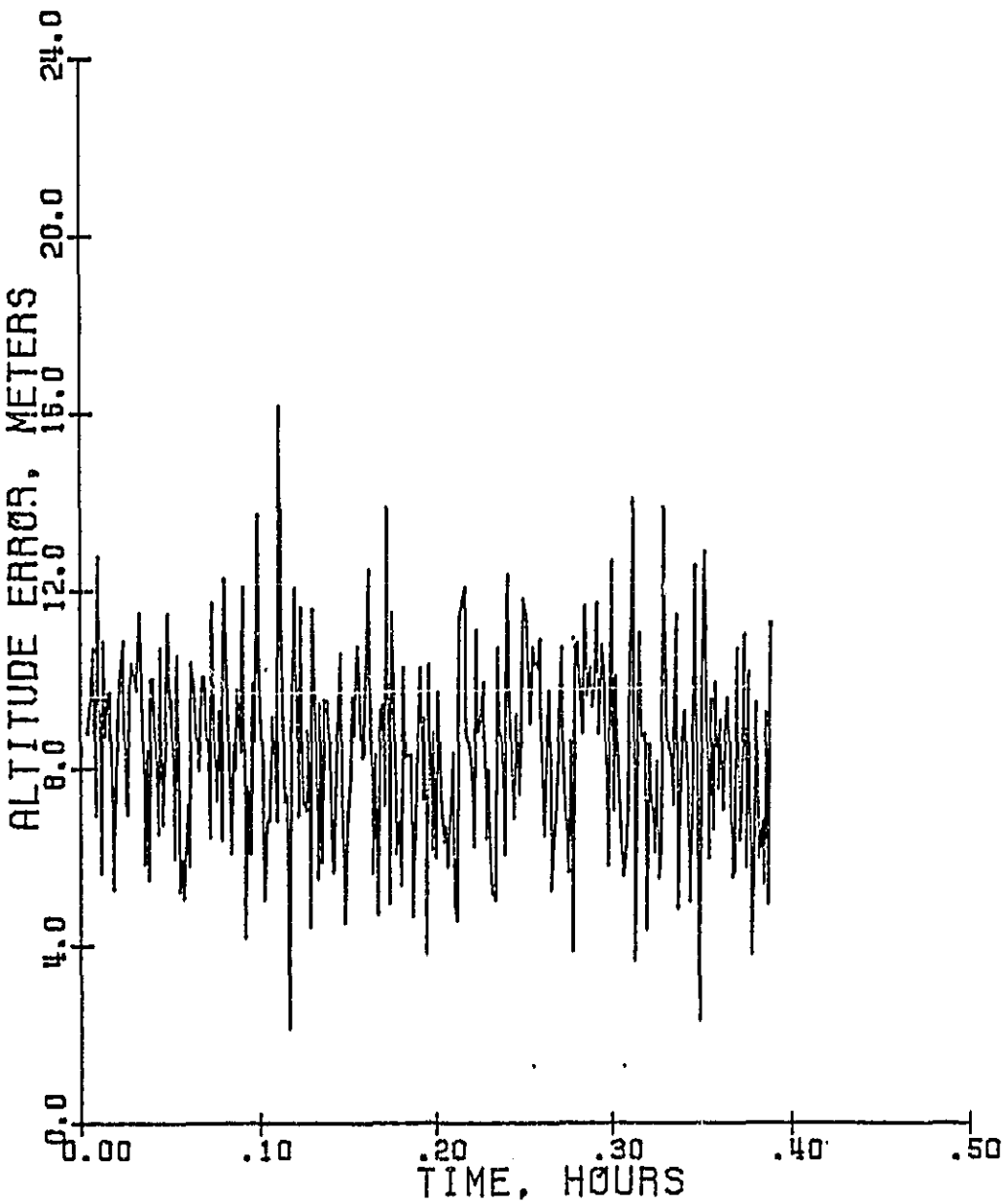

Figure 4.0.1.1 Altitude Errors, Run C-1, without SA

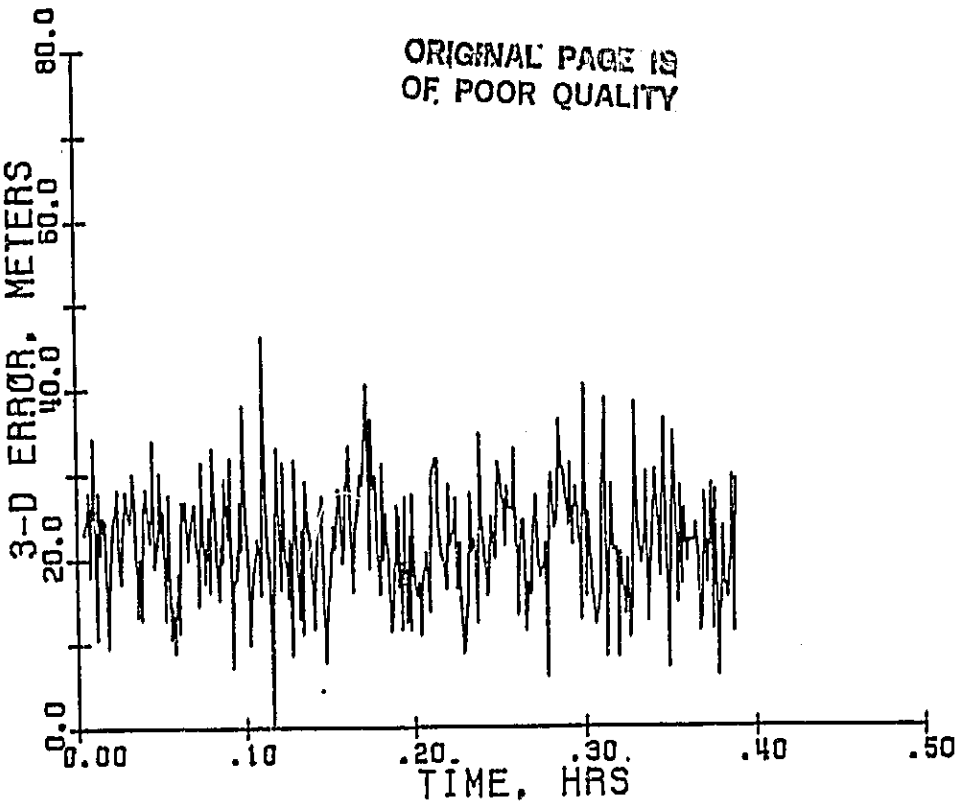

Figure 4.0.1.2 3D Position Error, Run C-1, with SA Seq/Single Chan., 0.3 sec.

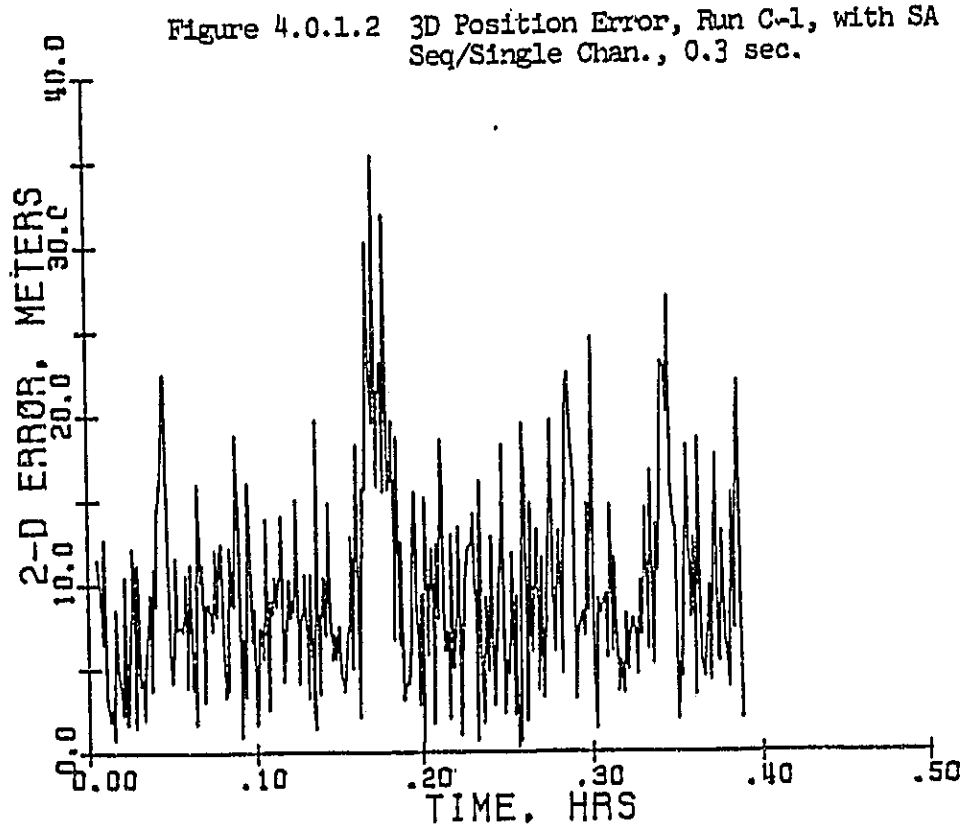

Figure 4.0.1.3 2D Position Error, Run C-1, without SA Seq/Single Chan., 0.3 sec.

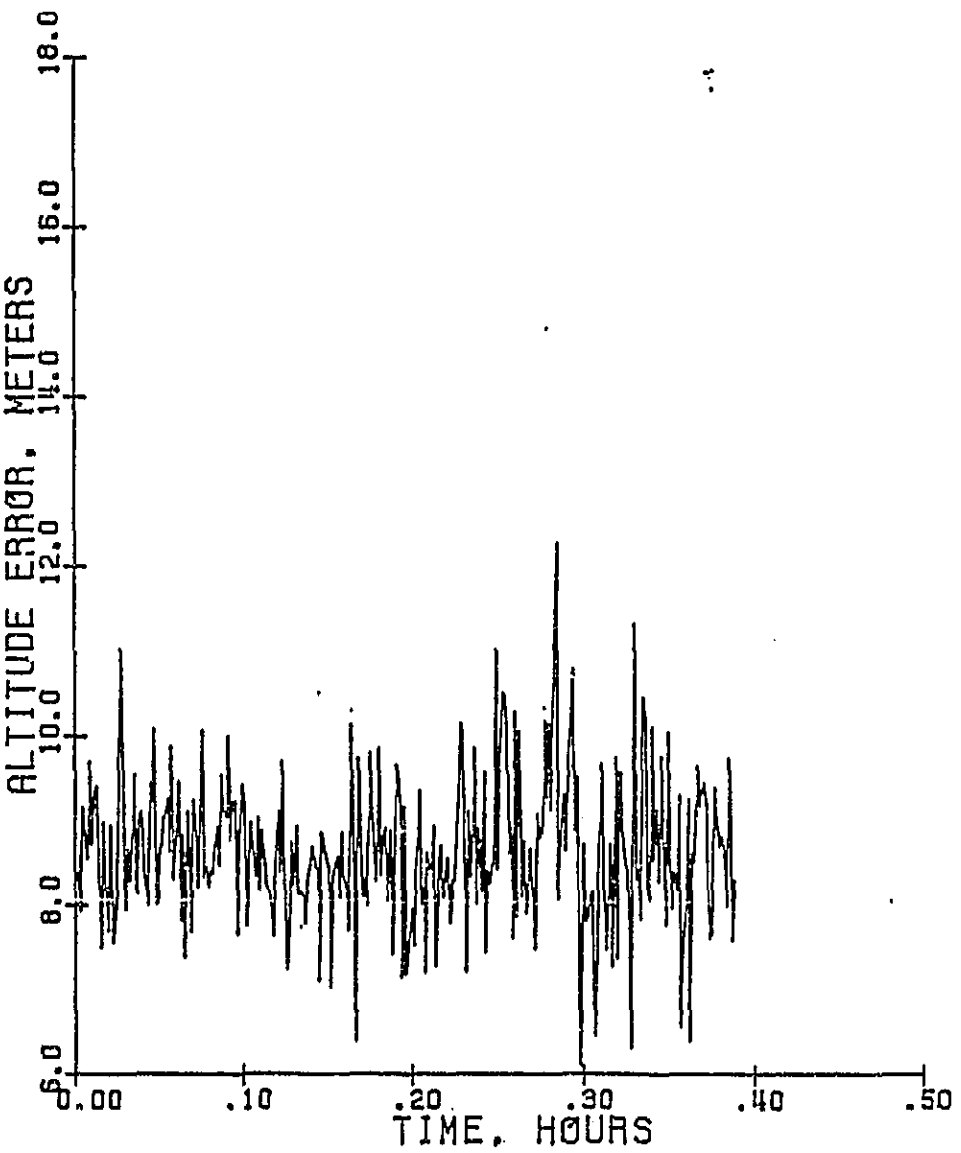

Figure 4.0.1.4 Altitude Error, Run C-4, without SA
Four Channel, 0.3 sec.

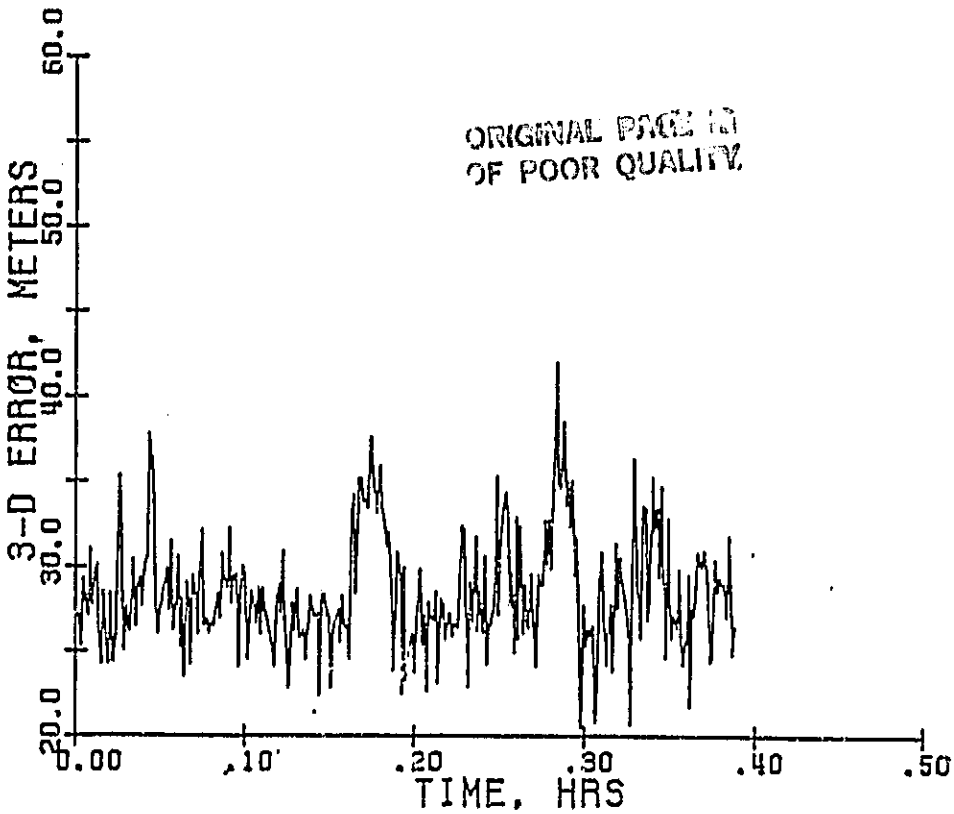

Figure 4.0.1.5 3D Position Error, Run C-4, without SA
Four Channel, 0.3 sec.

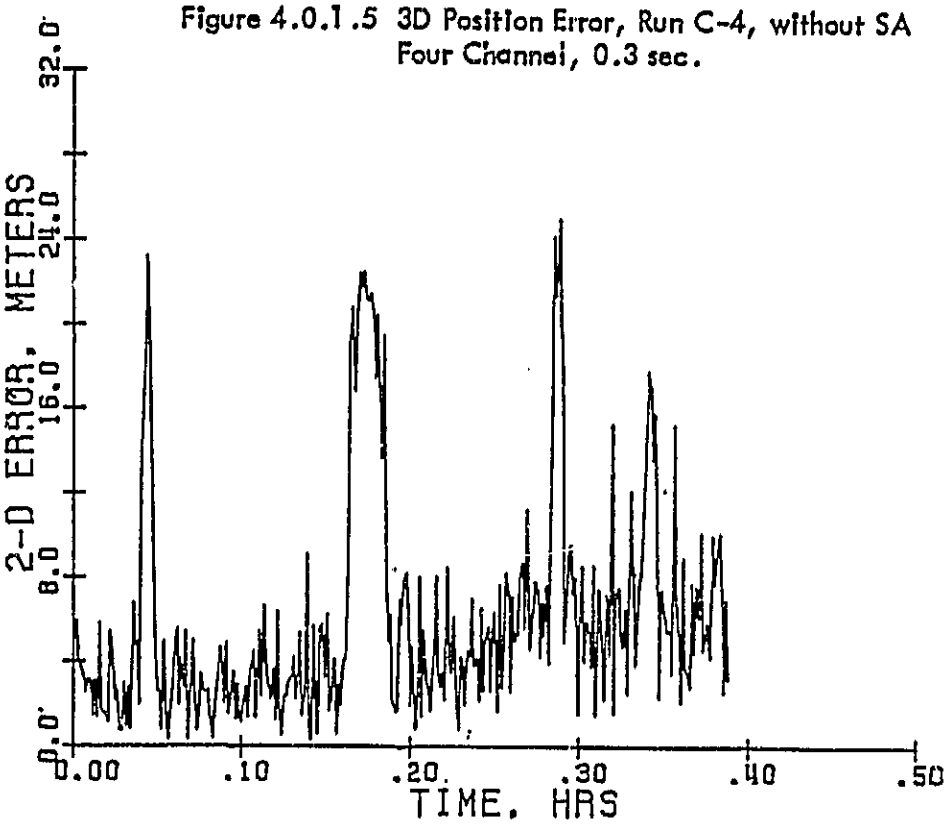

Figure 4.0.1.6 2D Position Error, Run C-4, without SA
Four Channel, 0.3 sec.

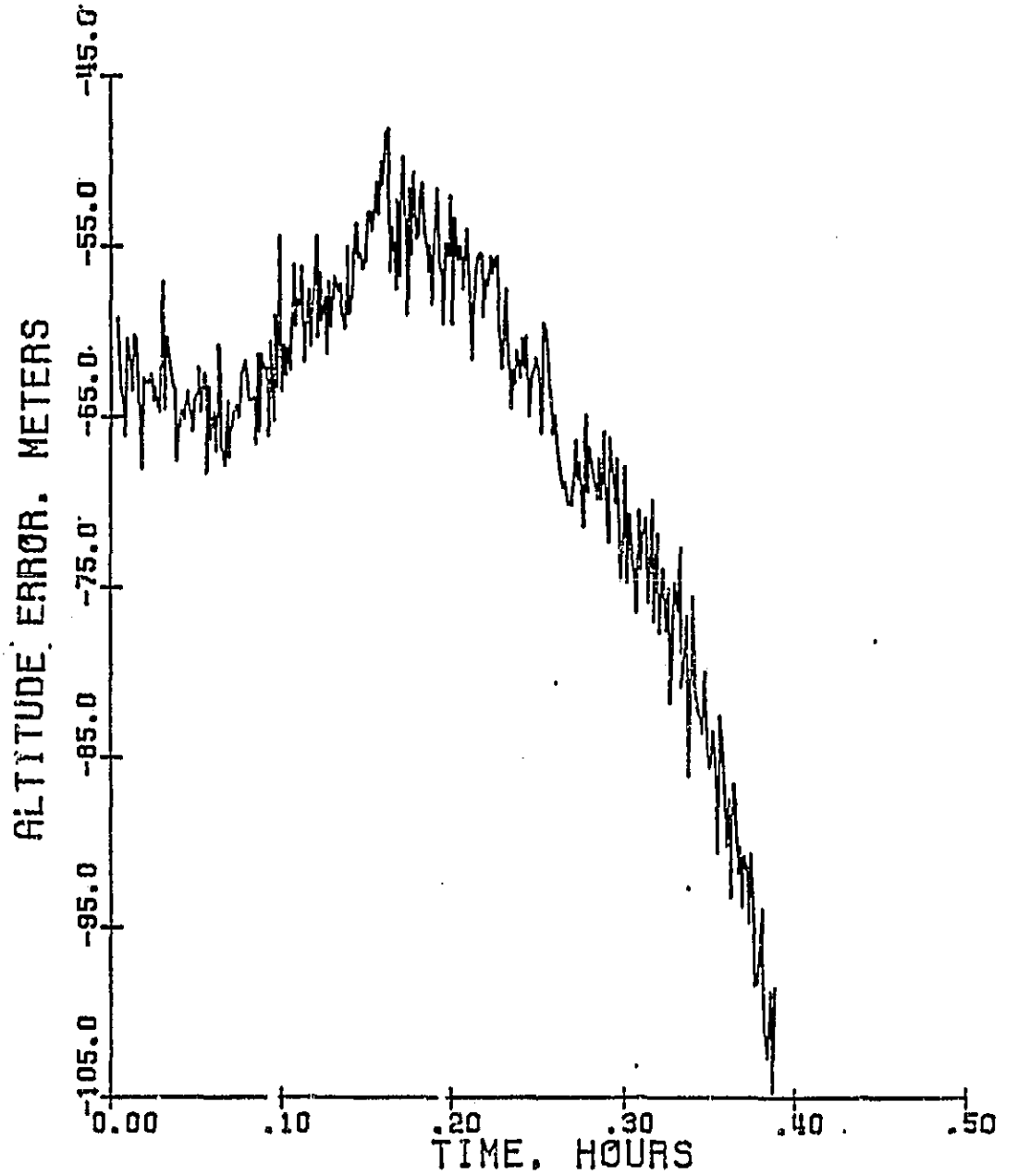

Figure 4.0.2.1 Altitude Error, Run C-1, with SA Seq/Single Chan., 0.3 sec.

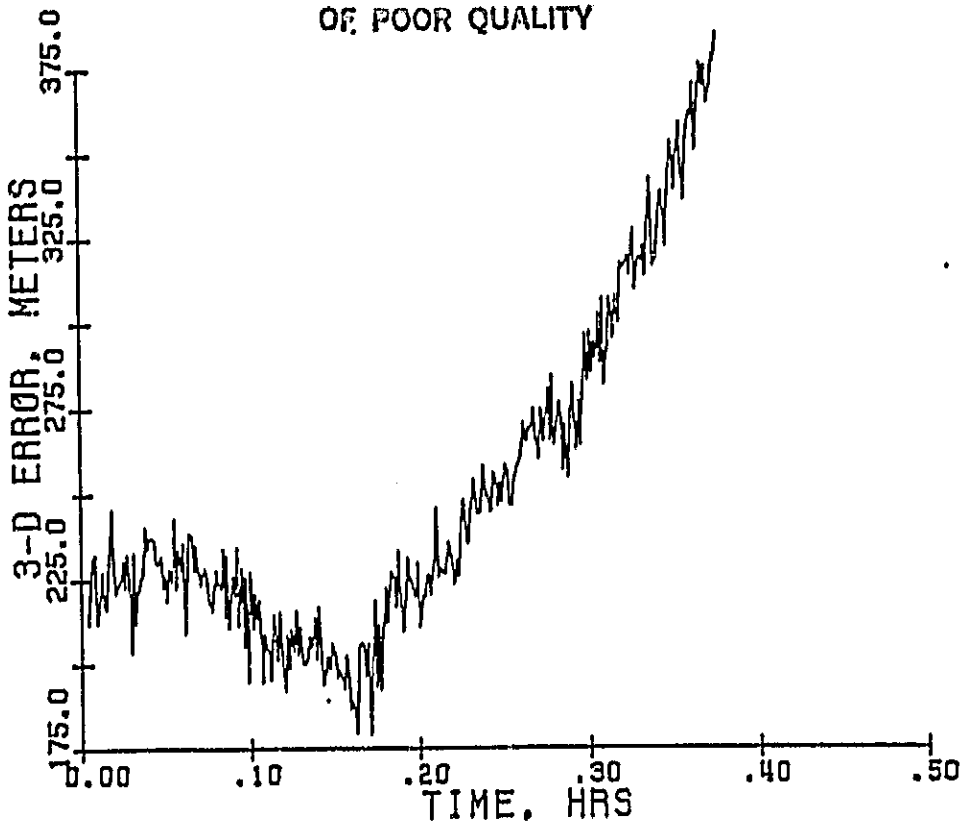

Figure 4.0.2.2 3D Position Error, Run C-1, with SA Seq/Single Chan., 0.3 sec.

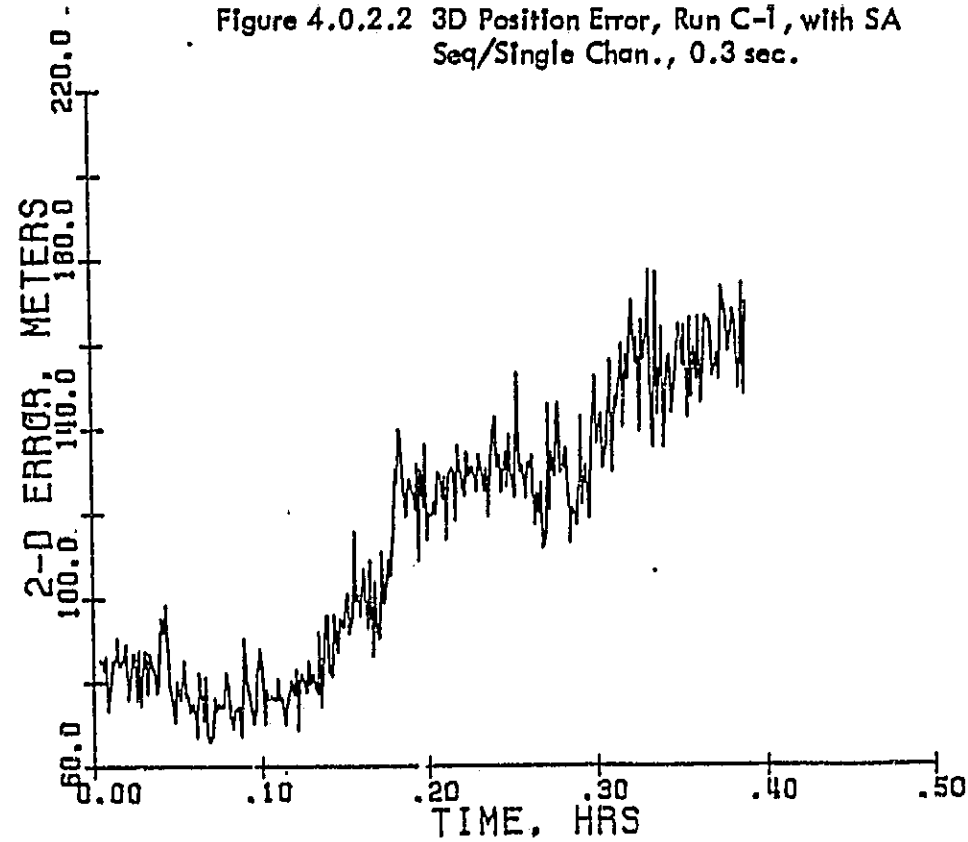

Figure 4.0.2.3 2D Position Error, Run C-1, with SA Seq/Single Chan., 0.3 sec.

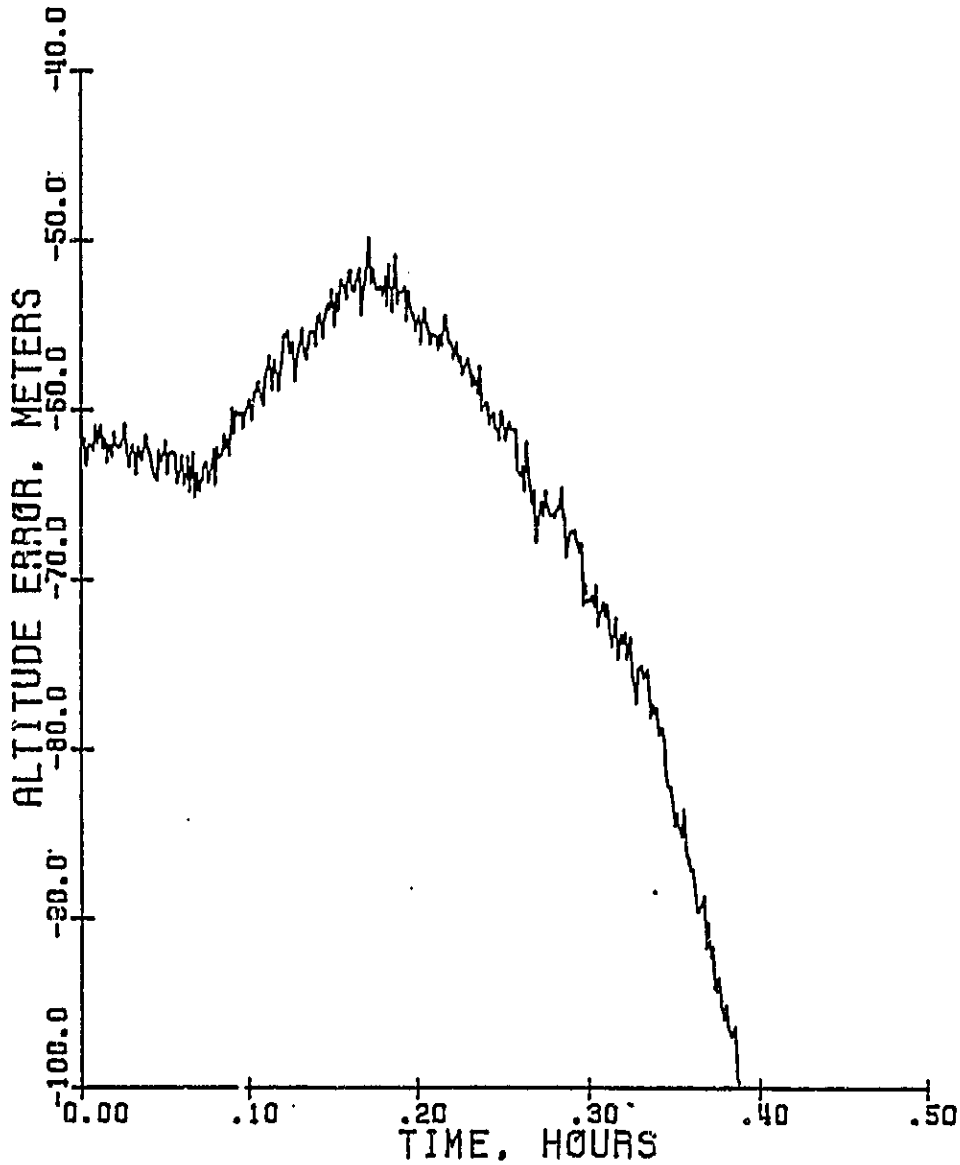

Figure 4.0.2.4 Altitude Error, Run C-4, with SA Four Channel, 0.3 sec.

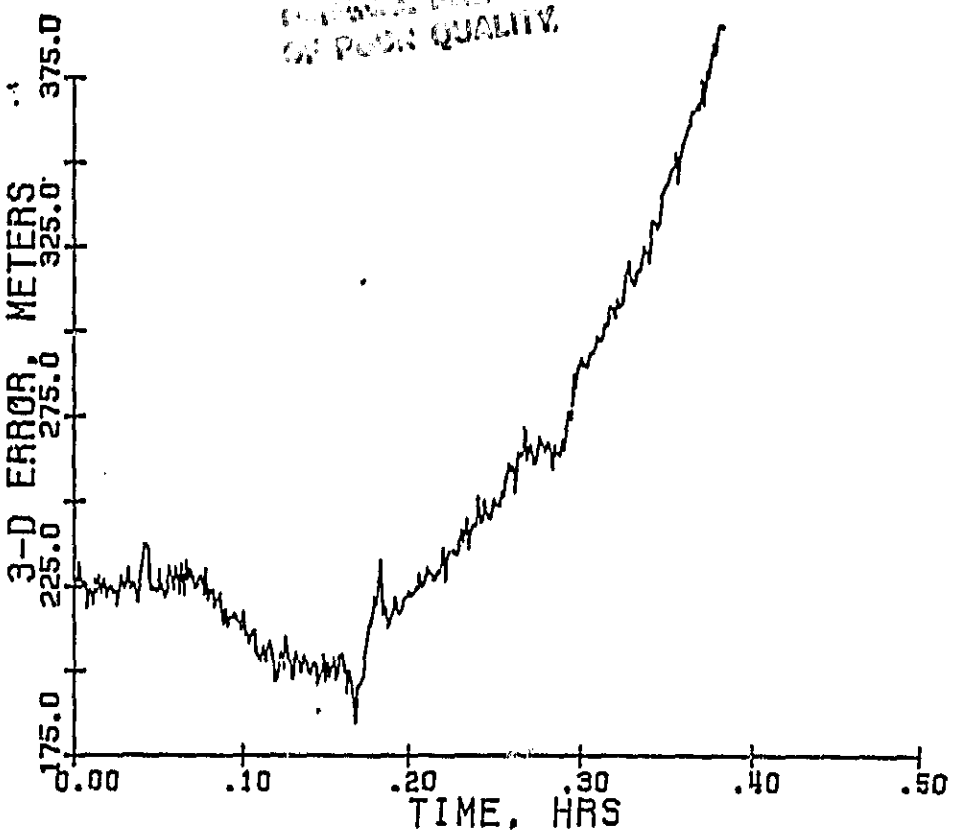

Figure 4.0.2.5 3D Position Error, Run C-4, with SA Four Channel, 0.3 sec.

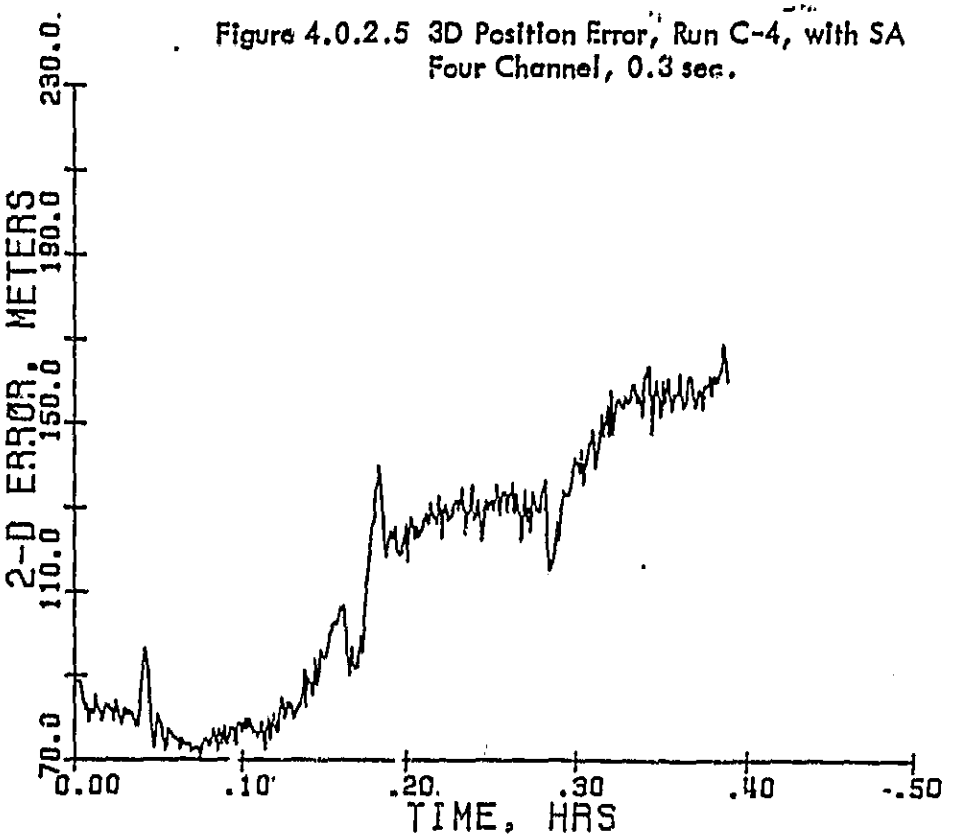

Figure 4.0.2.6 2D Position Error, Run C-4, with SA Four Channel, 0.3 sec.

4.0.3 Receiver Performance, Fixed Mode, Without SA Errors

Figures 4.0.3.1-3 and 4.0.3.4-6 depict the positional errors calculated at the fixed receiver with and without the SA error model evoked respectively. It is interesting to see that the errors induced by the alpha-beta tracking filter, as seen the dynamic cases, are no longer present.

The performance of the fixed receiver is best measured by the quality of its calculated range corrections. This comparison is rendered by the cross-correlation of the range errors experienced at the fixed receiver and those experienced at the airborne receiver for a particular satellite. The following cross correlation functions are presented in the form of plots with the computed $Rxy(\tau)$ versus the uplink period. The cross correlation coefficient is related to the uplink period due to the fact that the higher uplink periods provide under-sampled corrections and as a result produce a lower cross correlation coefficient.

4.0.3.1 Diffuse Multipath, Range Correction Effectiveness

The cross correlation of multipath errors experienced at the fixed receiver and at the airborne receiver is shown in Figure 4.0.3.1.1. This plot clearly shows, that in the case of diffuse multipath, there is no correlation between the errors experienced at the two receivers. This should be expected as the paths taken by the many indirect signals signals cannot possibly be the same for two spatially separated antenna and therefore the addition of those indirect signals should not be identical.

4.0.3.2 Atmospheric Delays, Range Correction Effectiveness

The delays induced by the ionosphere and the troposphere are very similar in that both are very correlative over relatively long periods of time. The differences lie within the diurnal dynamic properties of the ionosphere and the sensitivity of tropospheric error to receiver altitude.

Figure 4.0.3.2.1 shows the correlation between the ionospheric errors measured at the fixed receiver and those measured at the airborne receiver. The correlation between the two measurements are nearly constant over an uplink period of instantaneous corrections (uplink period = receiver update period) to a value of almost 5 minutes.

The cross correlation coefficients for the tropospheric errors are almost as well behaved as shown in Figure 4.0.3.2.2. The correlation between the two receiver measurements is fairly constant over the range from instantaneous to five minute uplink periods.

It is clear from these correlation plots that the corrections provided by the fixed receiver can produce significant improvements when applied to the range measurements at the airborne receiver.

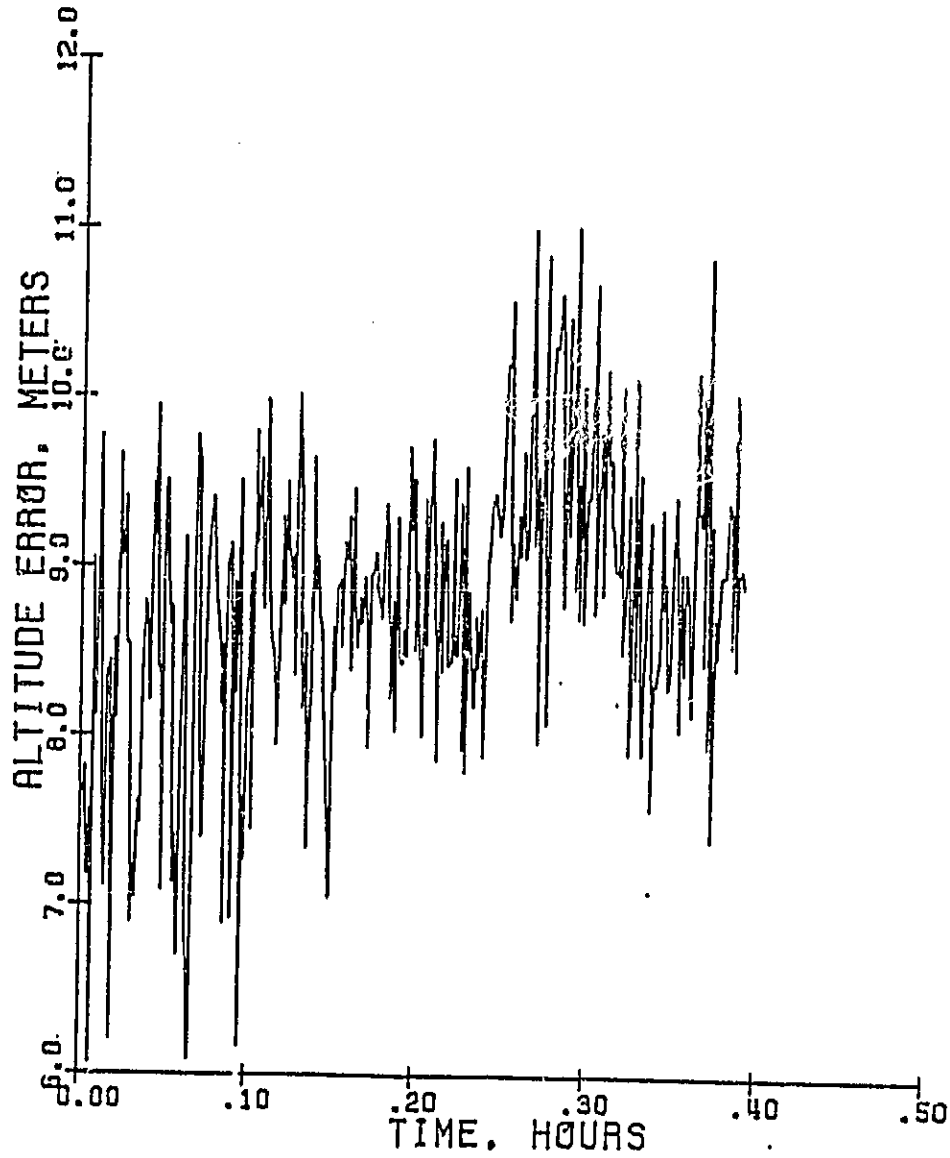

Figure 4.0.3.1 Altitude Error, Run F-4, without SA
Four Channel, 0.3 sec.

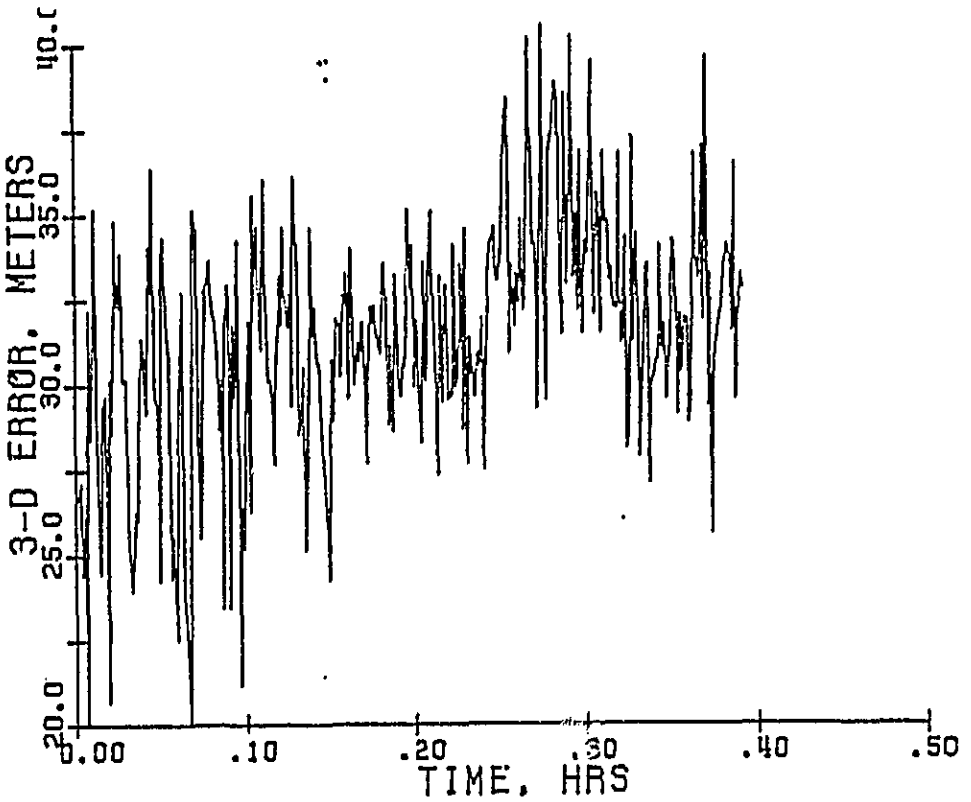

Figure 4.0.3.2 3D Position Error, Run F-4, without SA
Four Channel, 0.3 sec.

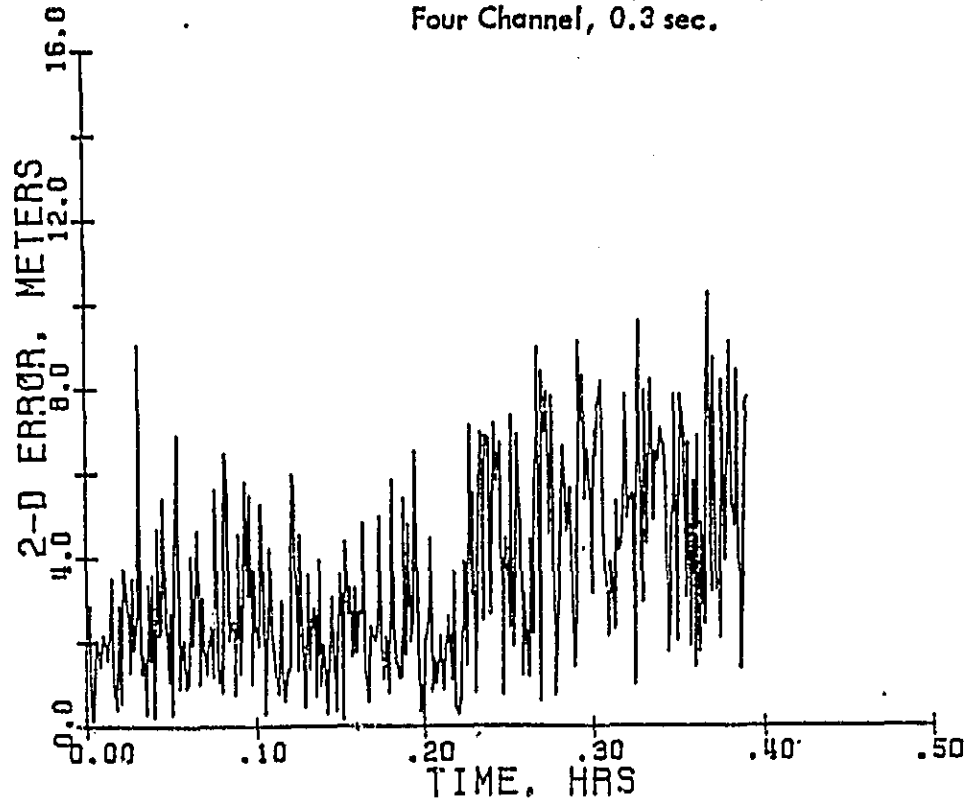

Figure 4.0.3.3 2D Position Error, Run F-4, without SA
Four Channel, 0.3 sec.

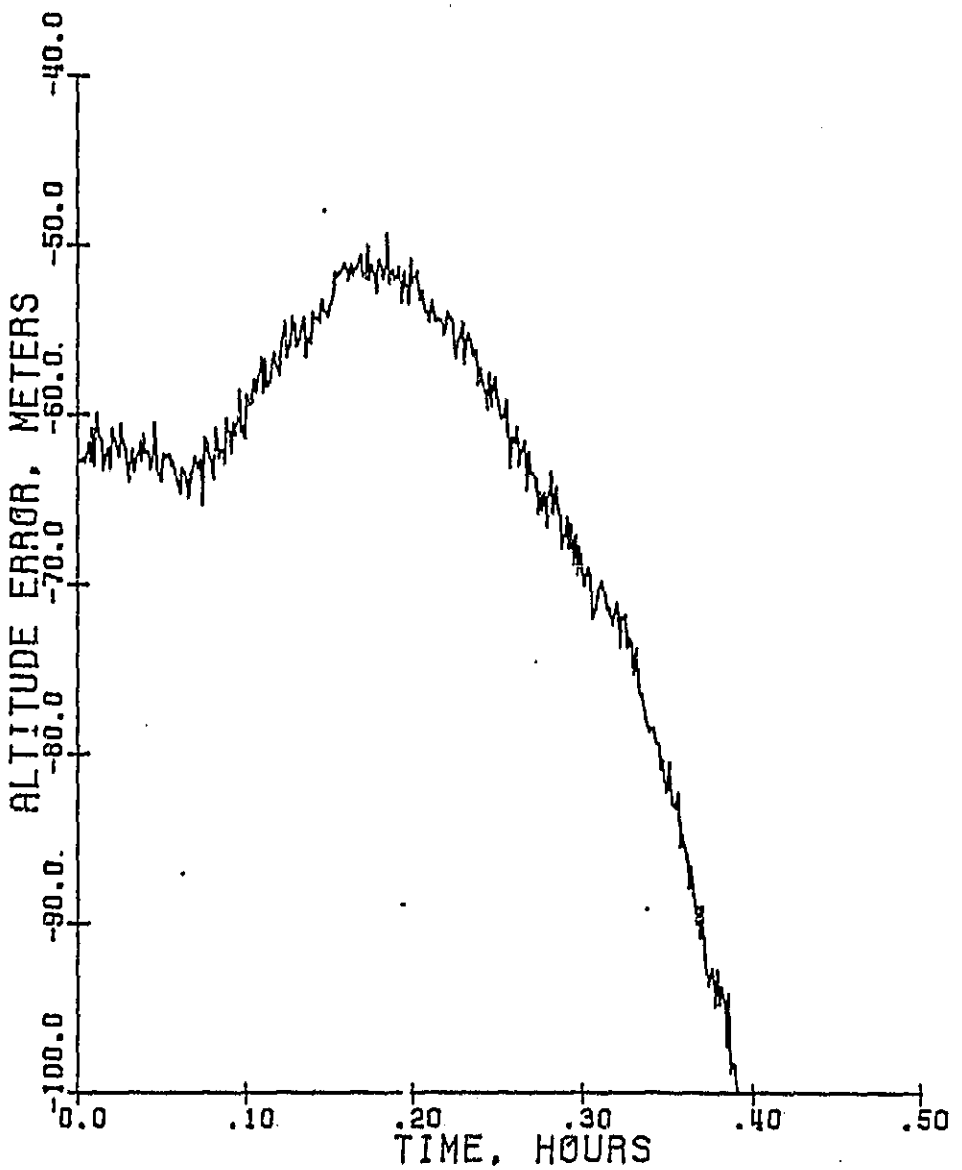

Figure 4.0.3.4 Altitude Error, Run F-4, with SA Four Channel, 0.3 sec.

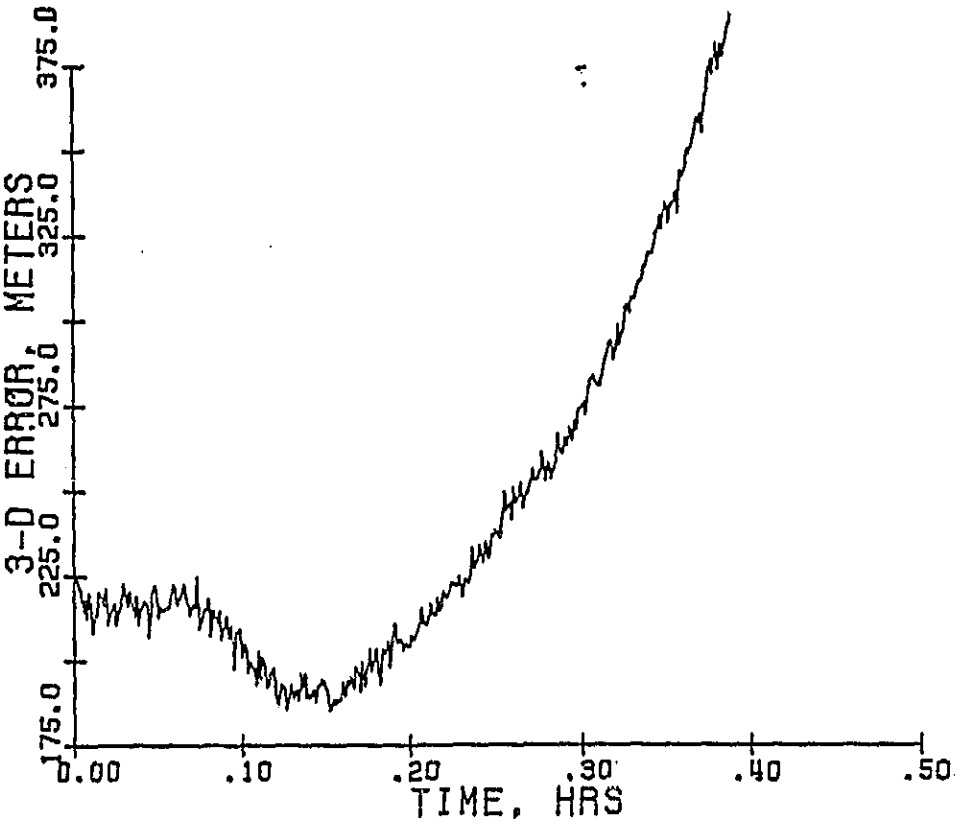

Figure 4.0.3.5 3D Position Error, Run F-4, with SA Four Channel, 0.3 sec.

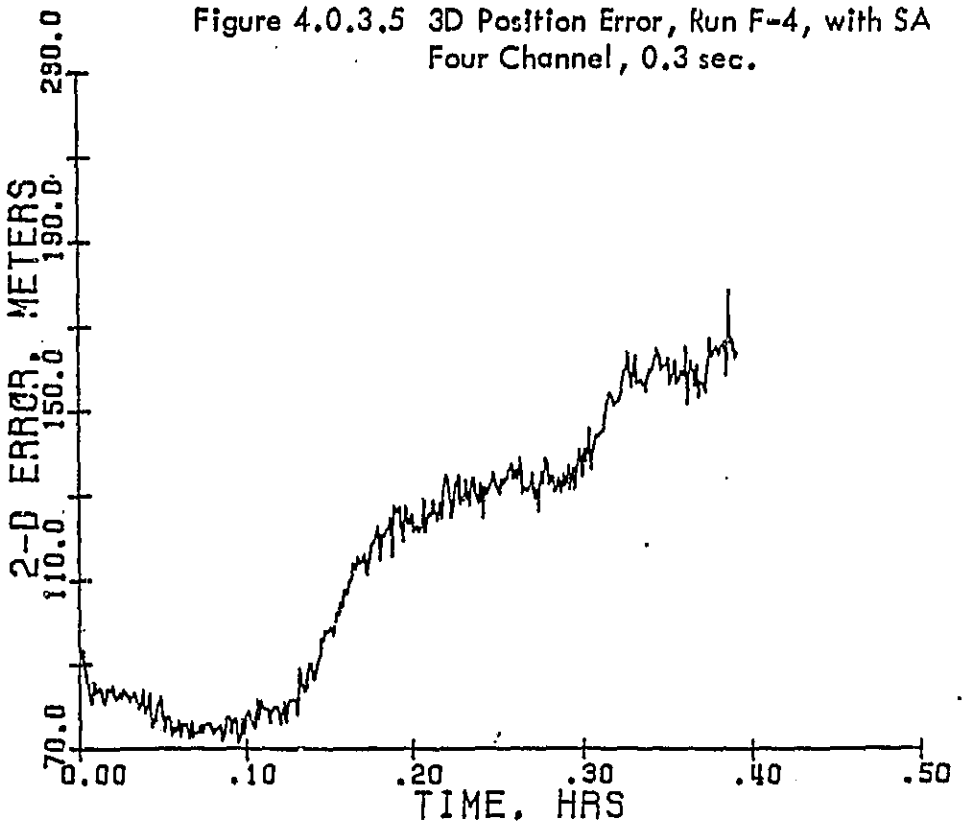

Figure 4.0.3.6 2D Position Error, Run F-4, with SA Four Channel, 0.3 sec.

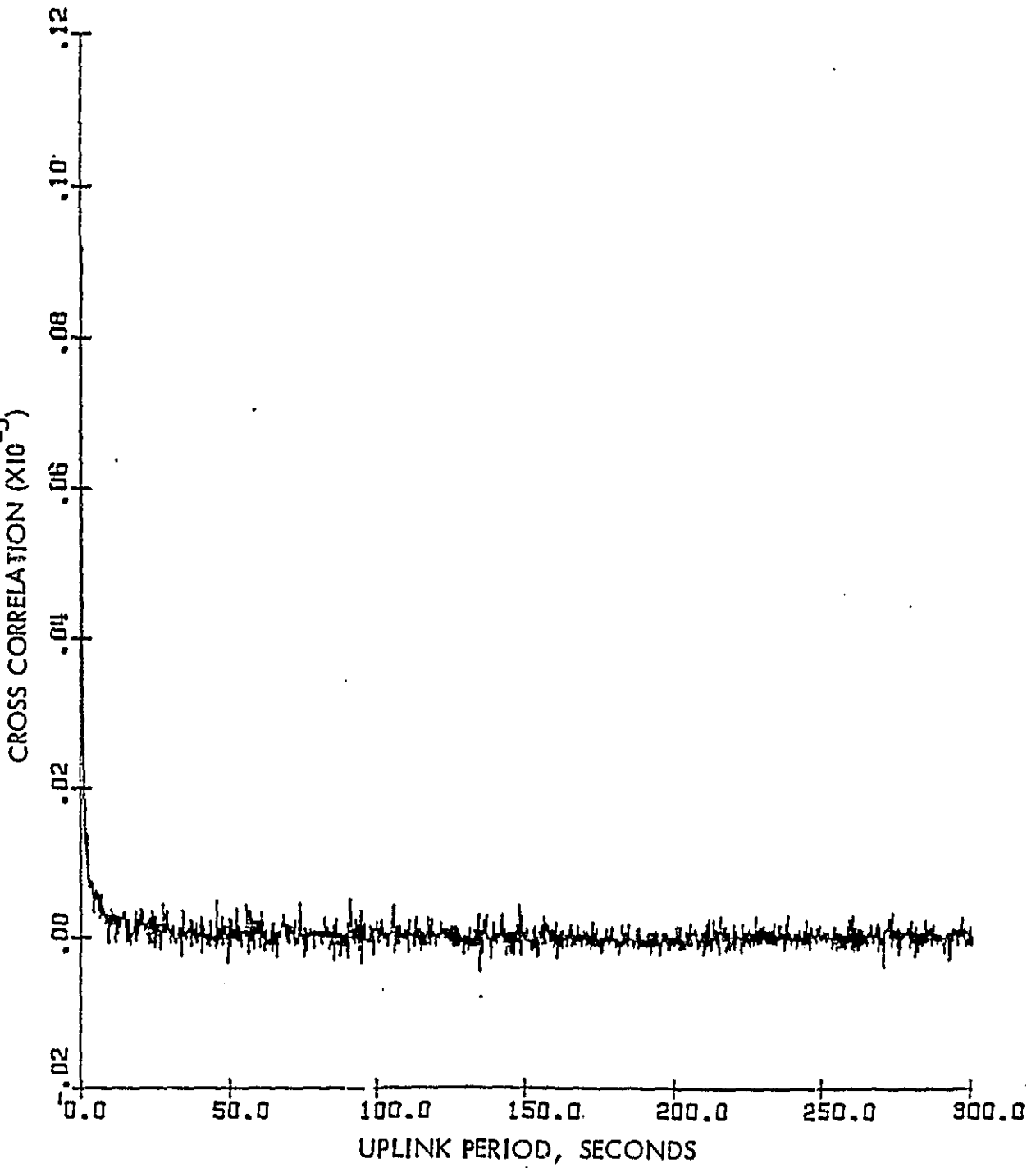

Figure 4.0.3.1.1 Cross Correlation of Multipath Error

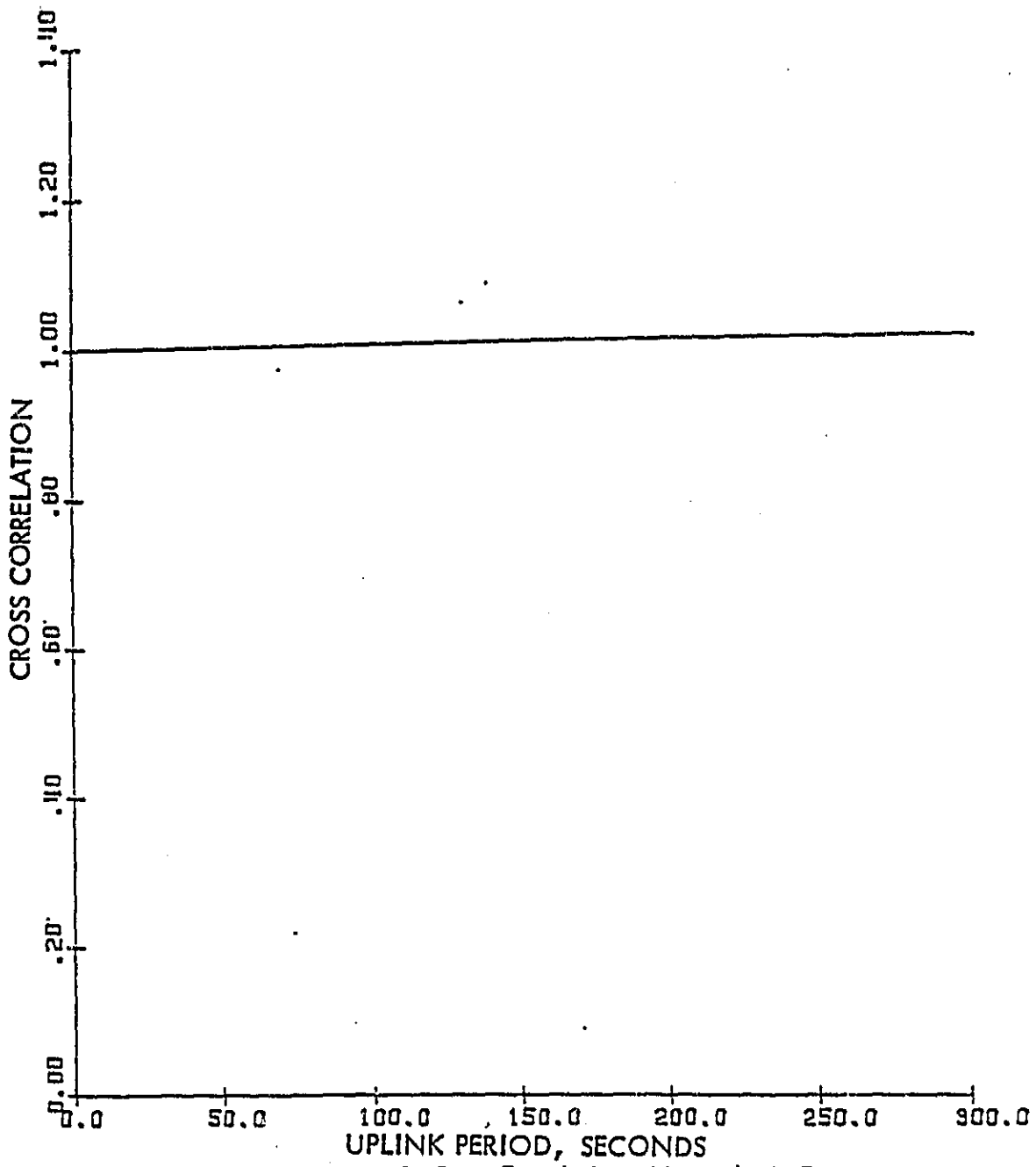

Figure 4.0.3.2.1 Cross Correlation of Ionospheric Errors

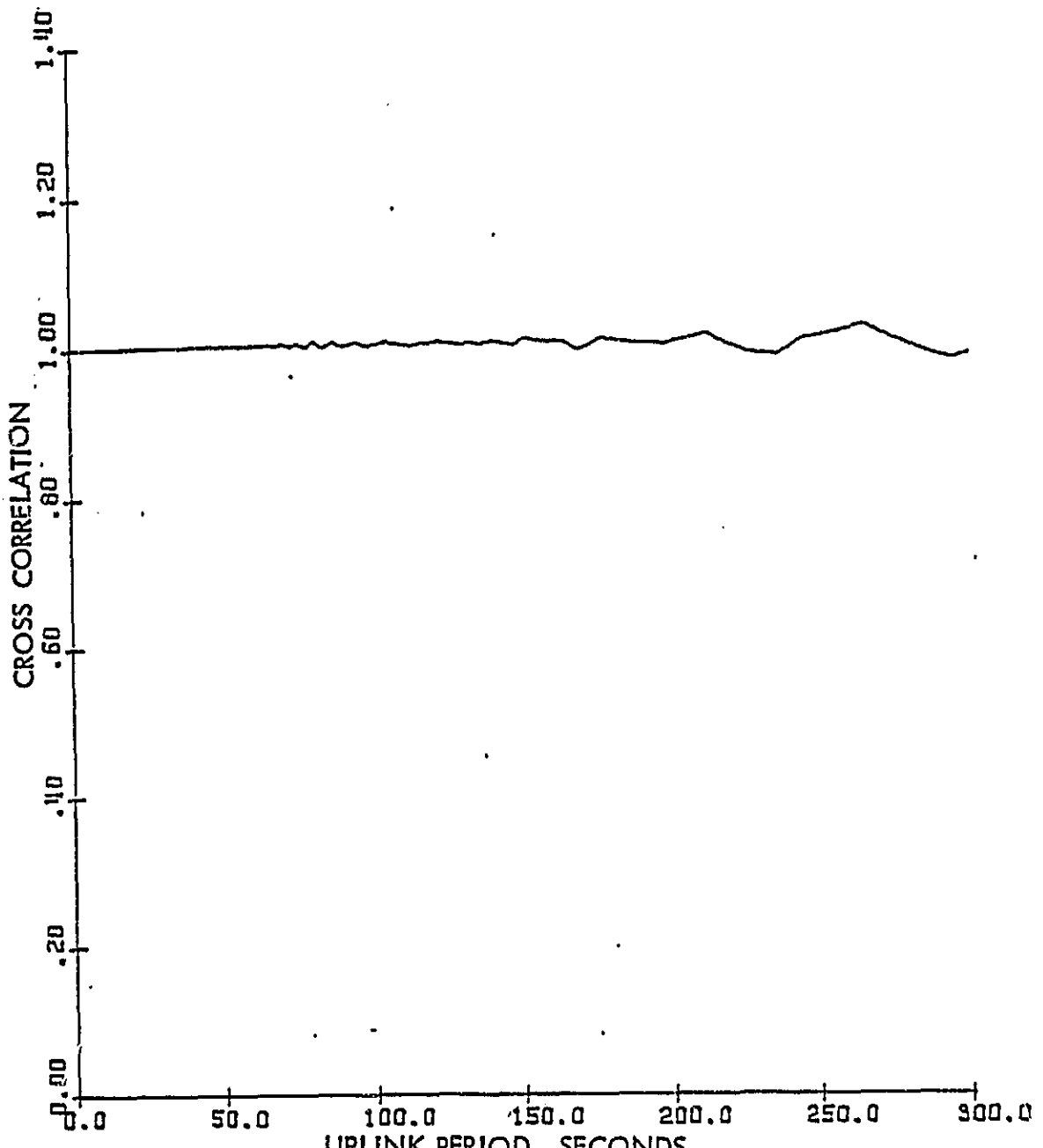

Figure 4.0.3.2.2 Cross Correlation of Tropospheric Errors

4.0.3.3 Receiver Performance, Fixed Mode, General

Although a period of 12 seconds is recommended by the RTCM Special Committee [17], these results imply that comparable improvements could be expected with higher uplink periods, given the above conditions. Figure 4.0.3.3.1 displays the correlative properties of the combined multipath and atmospheric range errors between the two receivers. This also shows that uplink periods greater than 12 seconds could provide an equally good correction. The 12 second uplink period does provide a better capability when the system is subjected to SA errors.

4.0.4 Receiver Performance, Fixed Mode, With SA Errors

The cross correlation plot of the Selective Availability errors is shown in Figure 4.0.4.1. This plot shows that the SA error is highly correlative, but does show significant decreases in correlation for higher uplink periods. The decrease in correlation appears to be linear for first 60-90 seconds and then begins to degrade with an some type of exponential decay-like function, however, continuing with the decreasing tendency displayed by the 60-90 second linear function. This phenomenon is most likely due to the fixed receiver providing under-sampled corrections at the high uplink periods (i.e., aliasing).

The effect of injecting the SA errors with the diffuse multipath, ionospheric delay, and tropospheric delay is shown in the cross correlation plot shown in Figure 4.0.4.2. As seen in the previous section, the resulting correlation plot reflects the culmination of the more negative characteristics of the error models. In this case the correlative properties are degraded by the white noise induced by the diffuse multipath and the decreasing tendency of the SA correlation function.

4.0.5 Receiver Performance, Differential Mode, Without SA Errors

The positional errors shown in Figures 4.0.5.1-3 are for a four channel, differential mode, 0.3 second update period receiver using corrections provided by a four channel, fixed mode, 0.3 second update period receiver (run ID # D-8). New corrections are provided to the differential set once every 12 seconds. These results are indicative of the statistical characteristics of the other receiver types, the differences lie mainly in alpha-beta tracking filter's inability to track turns especially for the 2.4 second update period receivers.

The overall positive effect of differential GPS can be seen in Figures 4.0.5.4 and 4.0.5.5. The plots contained in these figures are broken up into four columns of three bars each; column one contains the 3D approach results while operating in the conventional mode, column two contains the 3D positional information generated by the fixed mode receiver during the approach, column three displays the 3D positional approach information while operating in the differential mode with corrections provided by a sequential/single channel fixed receiver with a common update rate, and column four displays the 3D data from a receiver operating in the differential mode using corrections from a four channel fixed receiver with

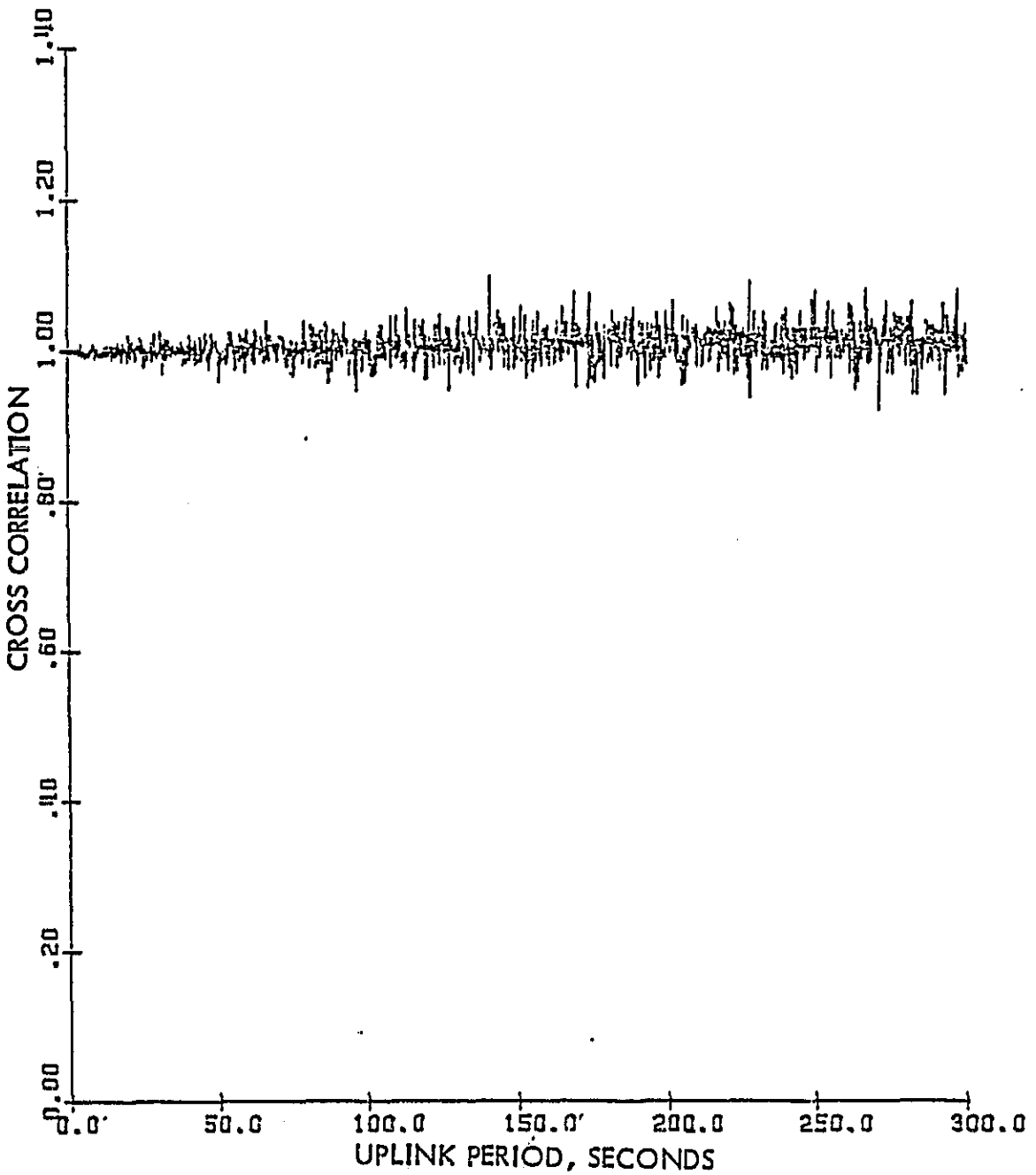

Figure 4.0.3.3.1 Cross Correlation of Combined Multipath, Ionospheric, and Tropospheric Errors.

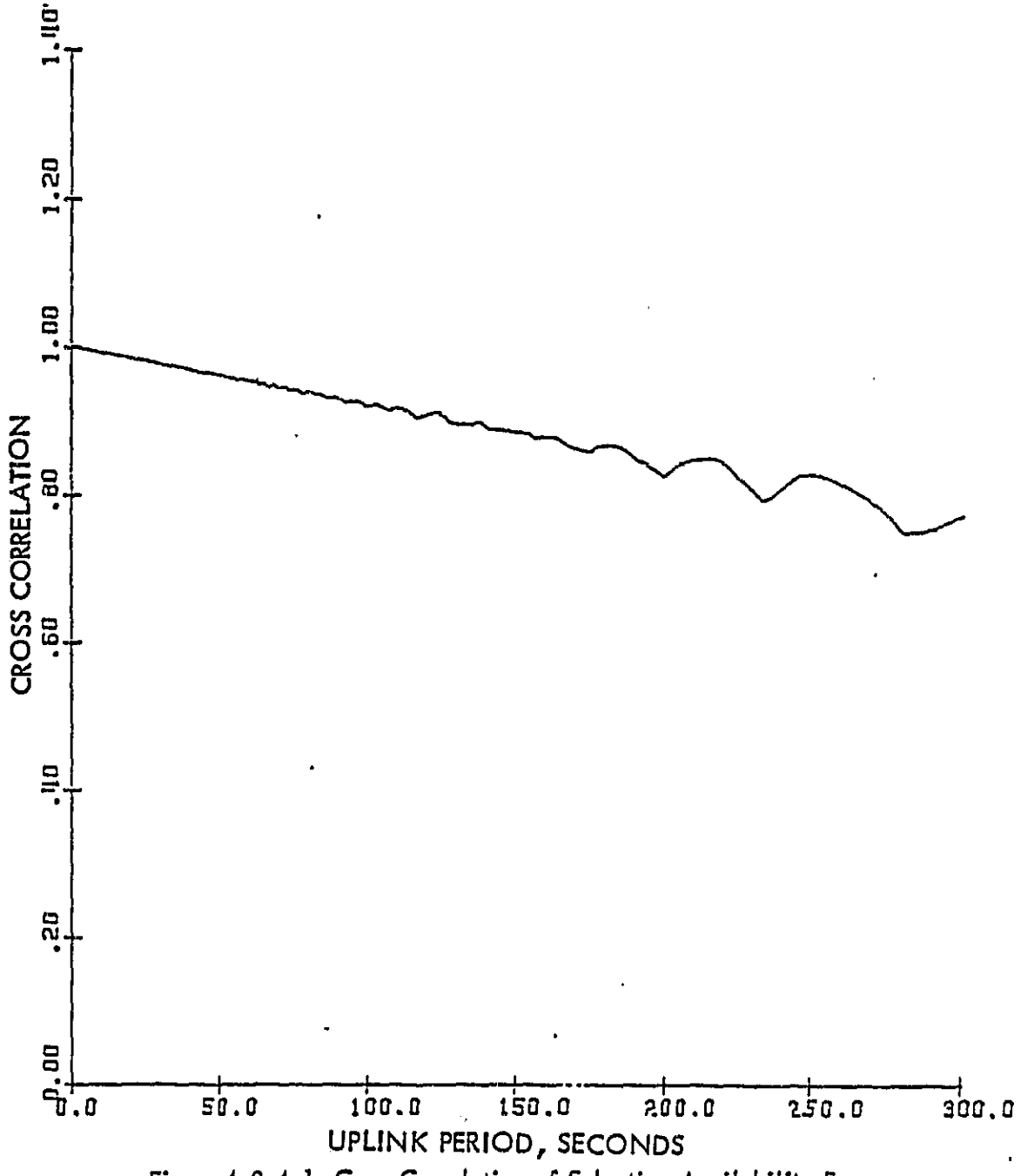

Figure 4.0.4.1 Cross Correlation of Selective Availability Errors.

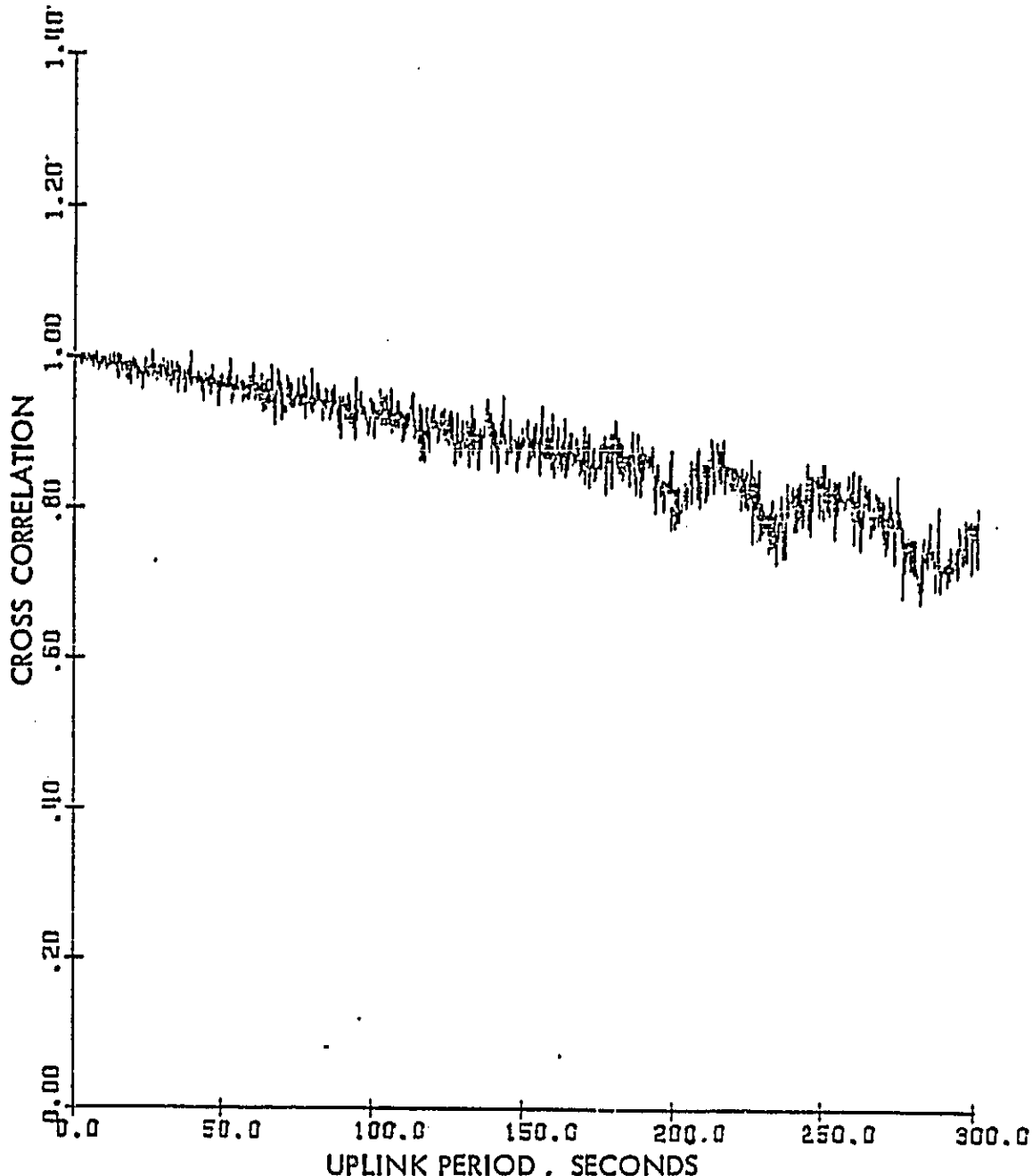

Figure 4.0.4.2 Cross Correlation of Combined Selective Availability, Multipath, Ionospheric, and Tropospheric Errors.

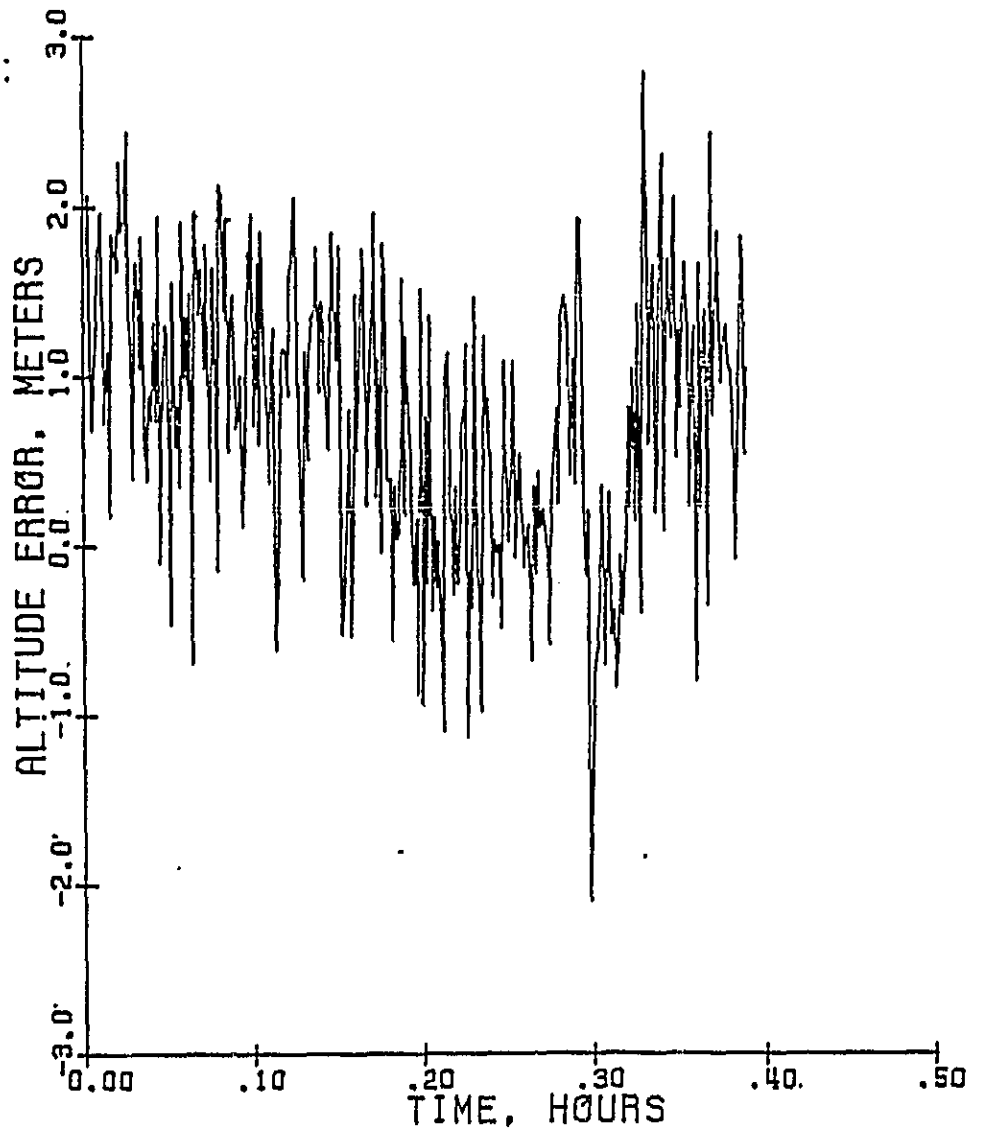

Figure 4.0.5.1 Altitude Errors, Run D-8, without SA
Four Channel, 0.3 sec.

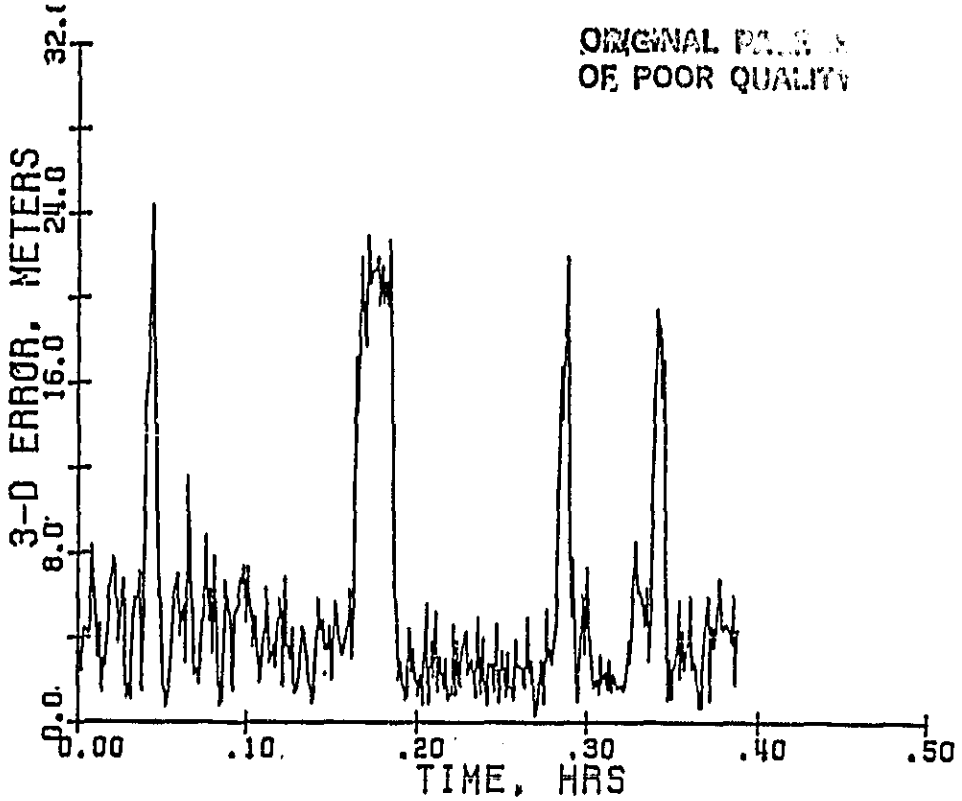

Figure 4.0.5.2 3D Position Error, Run D-8, without SA
Four Channel, 2.4 sec.

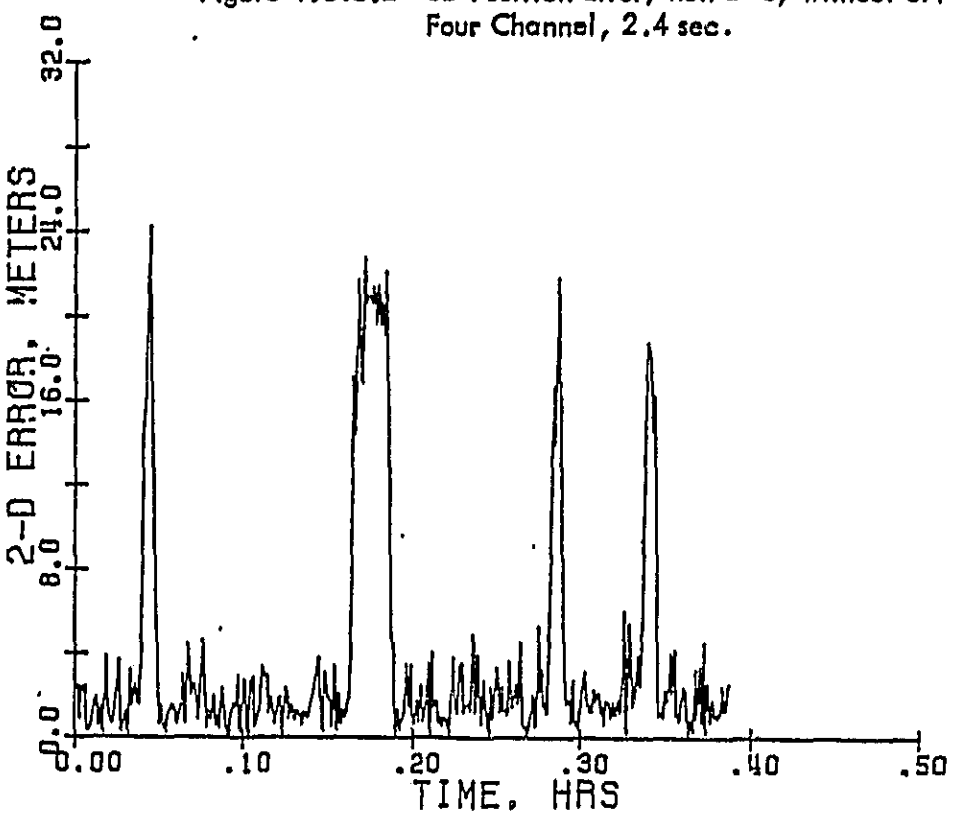

Figure 4.0.5.3 2D Position Error, Run D-8, without SA
Four Channel, 0.3 sec.

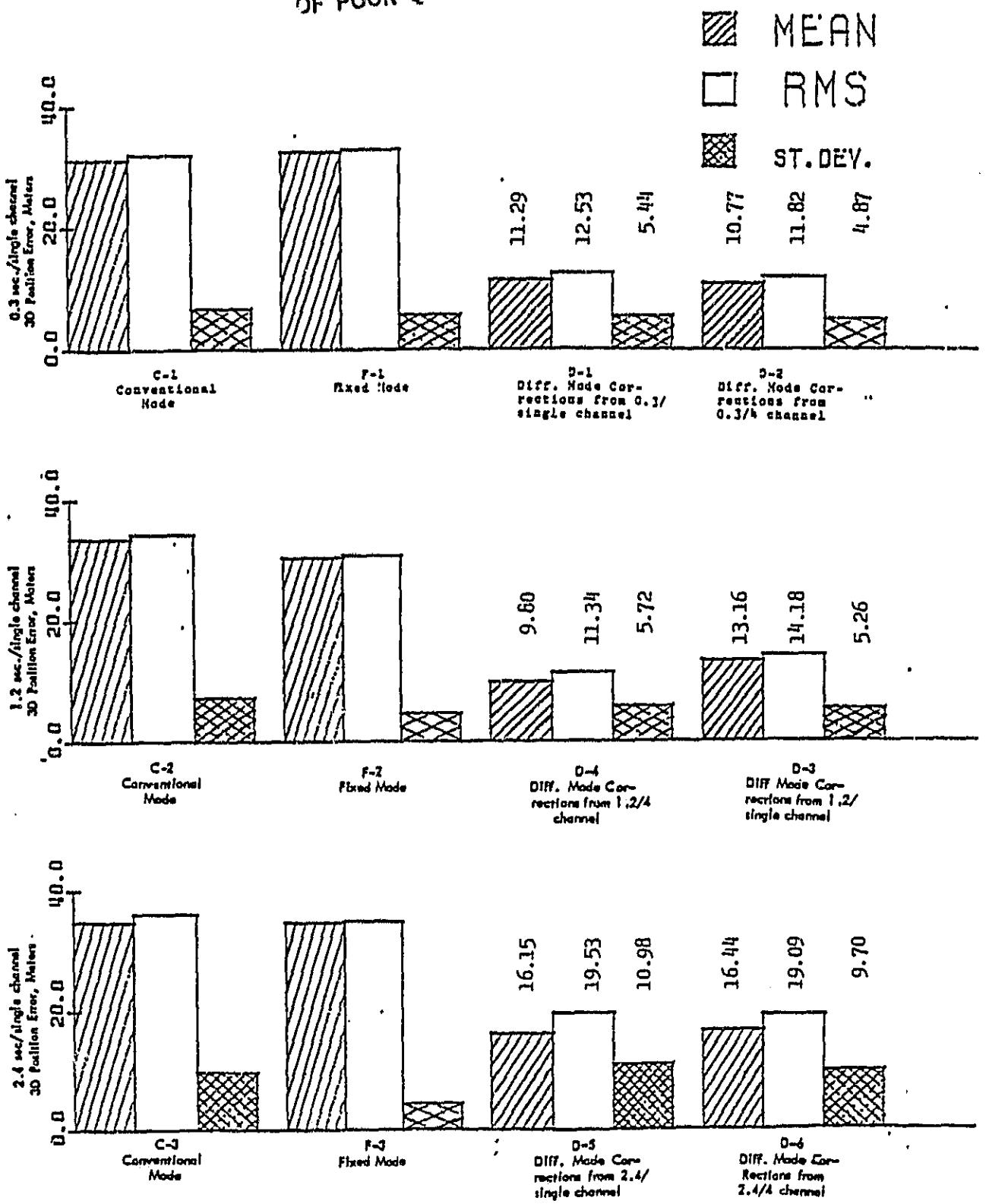

Figure 4.0.5.4 Single Channel Performance, without SA

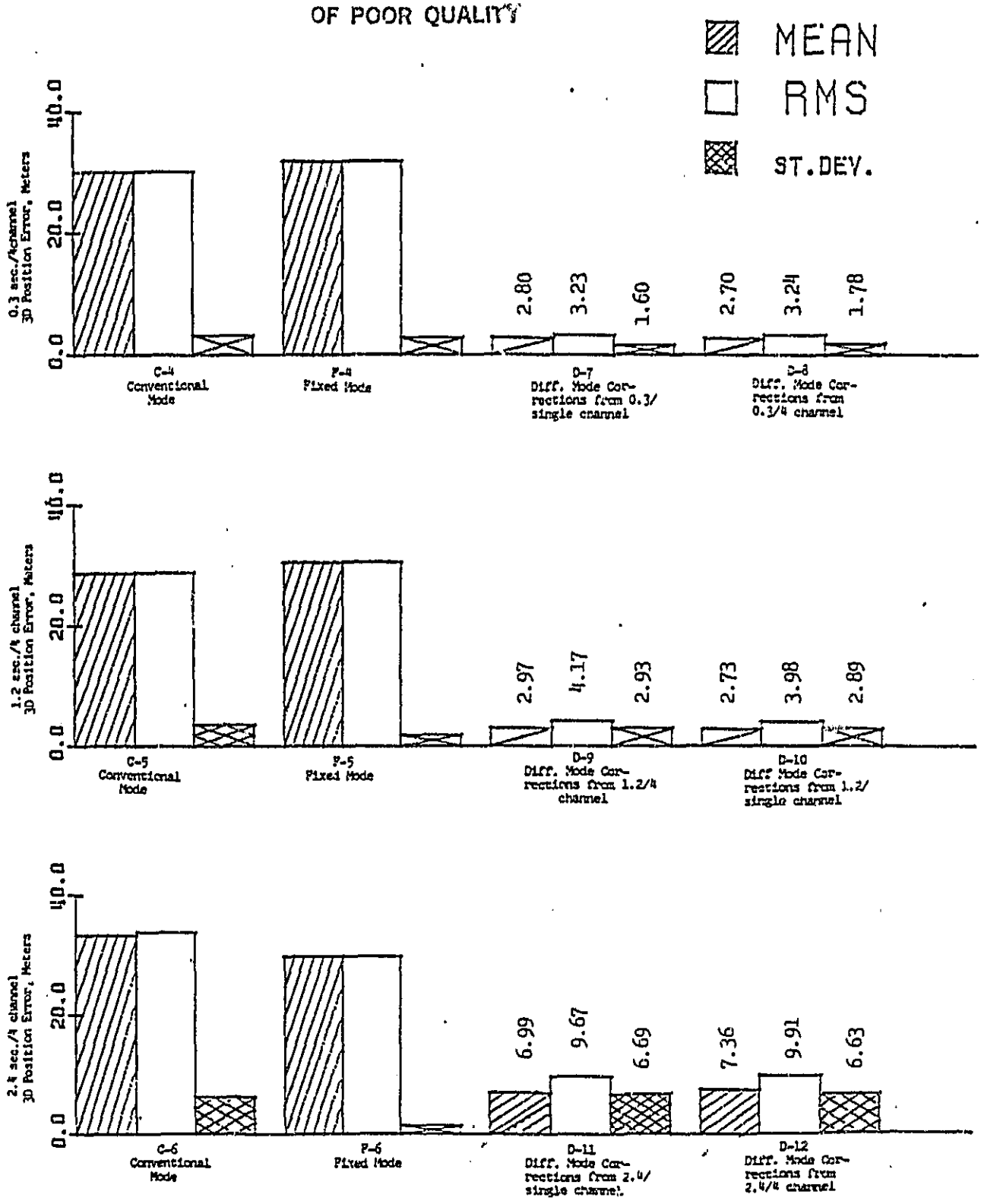

Figure 4.0.5.5 Four Channel Performance, without SA

a common update rate. Each of the columns are labeled with the appropriate receiver configuration run ID number shown in table 4.0.1 of Section 4.0 and the differential data are labeled with their respective abscissa values in meters.

The data displayed by these bar charts, and those that follow, contain the 3D positional information relevant to the approach segment of the teardrop flight path. This was done to eliminate the negative effects of the alpha-beta tracking filter. The dynamics of the approach involve constant velocities and therefore the tracking filter can perform reasonably well and provide an indication of the accuracies obtainable by using differential GPS.

The most impressive results were obtained by the 0.3 second update period, four channel, differential mode receiver. The values of one standard deviation for along-track error, cross-track error, and altitude error were equal to or less than 2.8 meters and were generally about 2 meters or less. The values for the sequential/single channel receiver were good but not nearly as impressive with a one standard deviation value for each dimension of error not exceeding 10 meters.

4.0.6 Receiver Performance, Differential Mode, With SA Errors

The data output for the four channel, 0.3 update period, differential mode receiver using a four channel, 0.3 update period, fixed mode receiver, both subjected to SA errors, is shown in Figures 4.0.6.1, 4.0.6.2, and 4.0.6.3. Again, the results are good except when the alpha-beta tracking filter is expected to track the receiver's position during turns.

Figures 4.0.6.4 and 4.0.6.5 show the same type of bar graphs as described in the previous section, except these results reflect the effects of the SA range errors. When compared with the bar graphs in Section 4.0.5, it can be seen that for an uplink period of 12 seconds, the positional accuracies obtainable with DGPS are comparable whether or not the SA errors are present. The value of standard deviation never exceeded 2.3 meters for along track (ATE), cross track (CTE), or altitude error for the four channel, 0.3 update period, differential mode receiver. The standard deviation for the ATE and altitude errors incurred by the longer update period receivers never exceeded 10.5 meters and the CTE never exceeded 15.7 meters.

The sequential/single channel, 2.4 update period, differential mode receiver was the most suseptible to the position errors due to the alphabeta filter. These prevalent deviations can be seen in Figures 4.0.6.6, 4.0.6.7, and 4.0.6.8. The large deviations, which appear in the 3D and 2D errors, directly correspond with the execution of turns in the teardrop flight path.

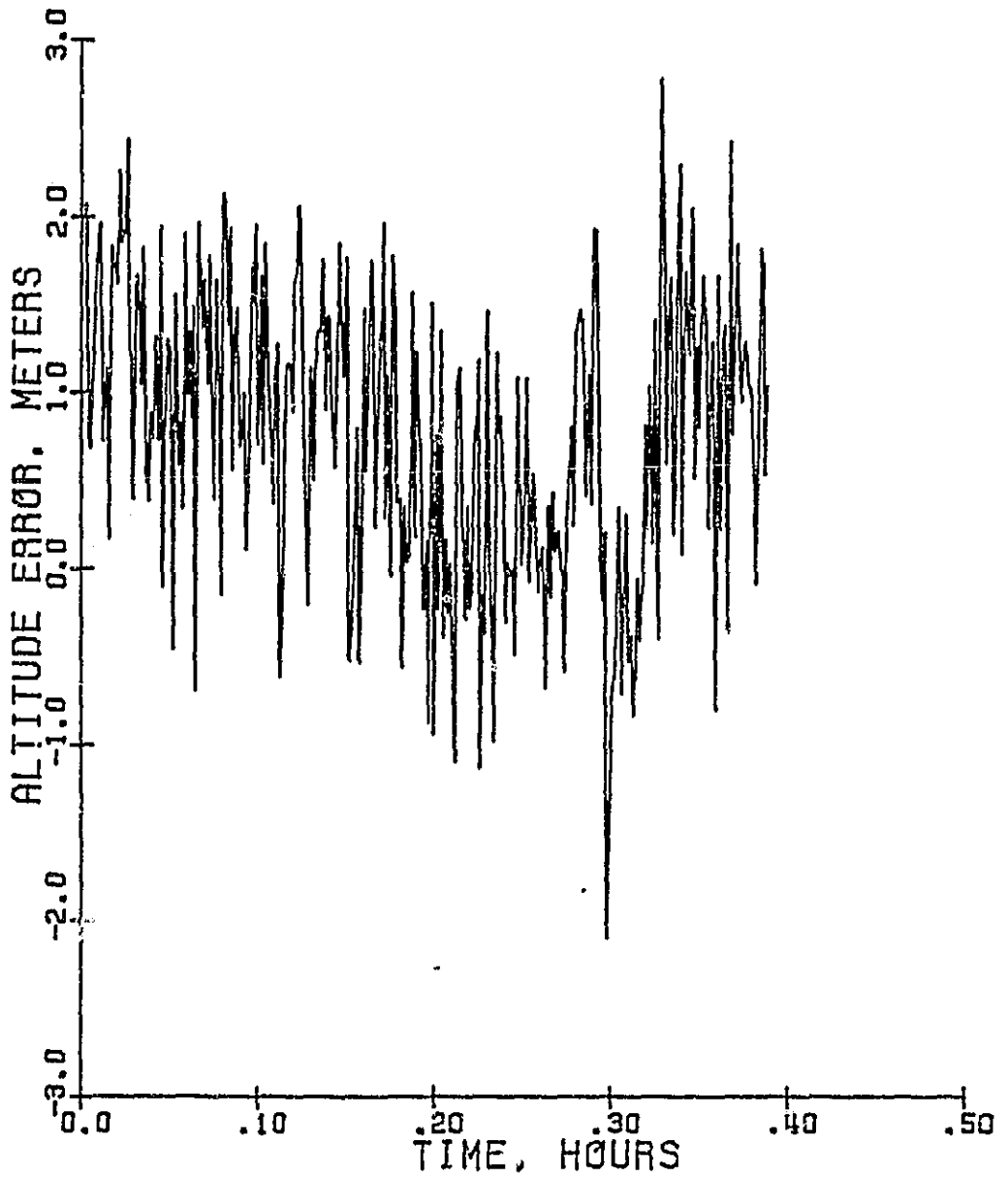

Figure 4.0.6.1. Altitude Error, Run D-8, with SA

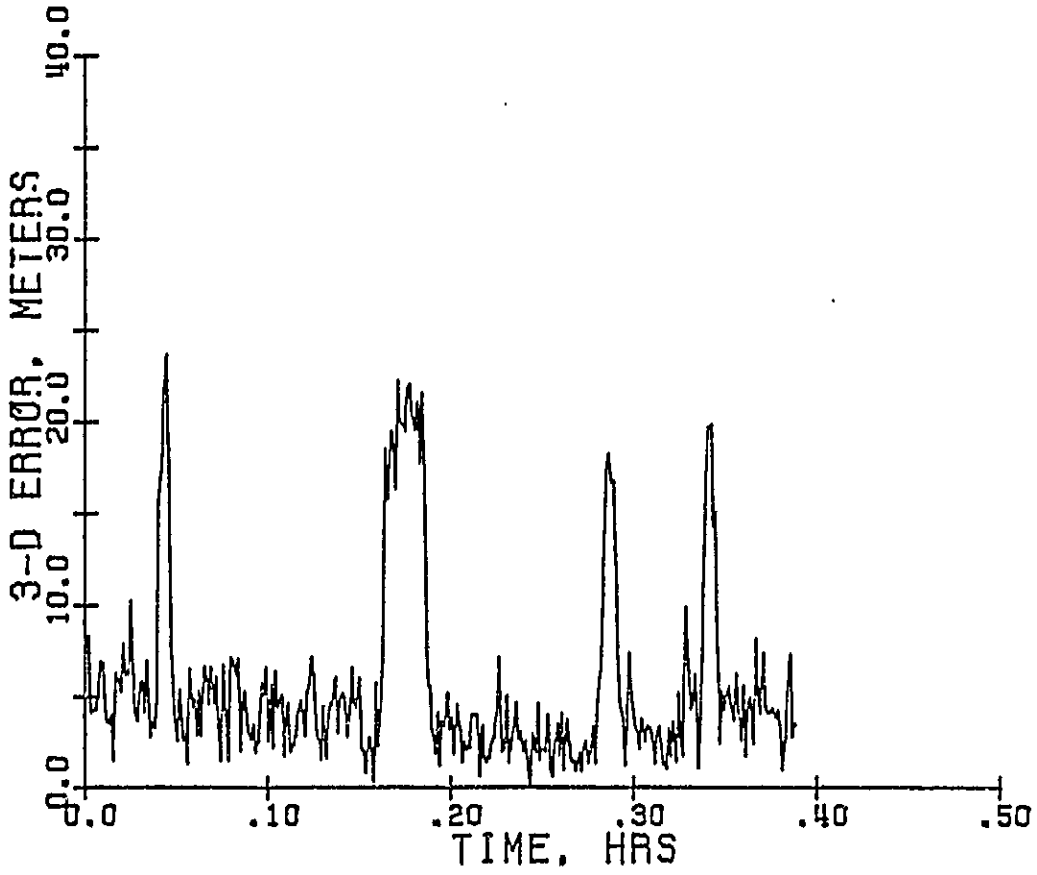

Figure 4.0.6.2 3D Position Error, Run D-8, with SA

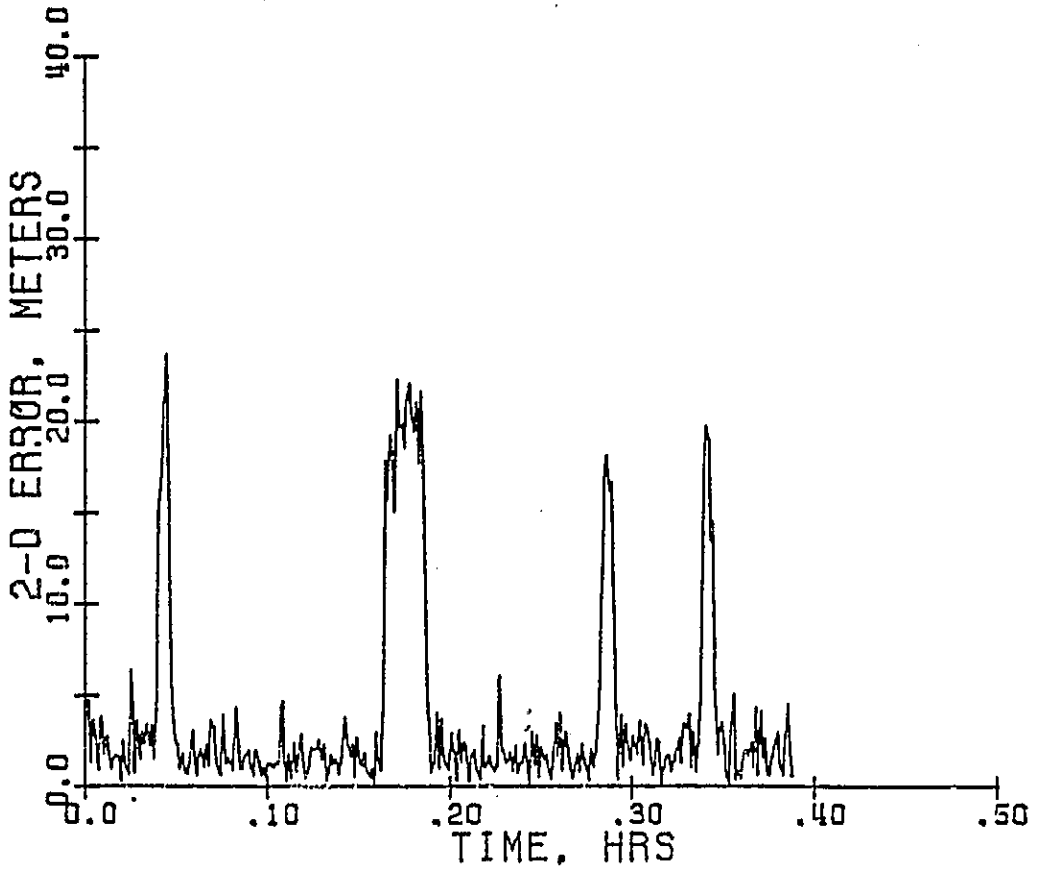

Figure 4.0.6.3 2D Position Error, Run D-8, with SA

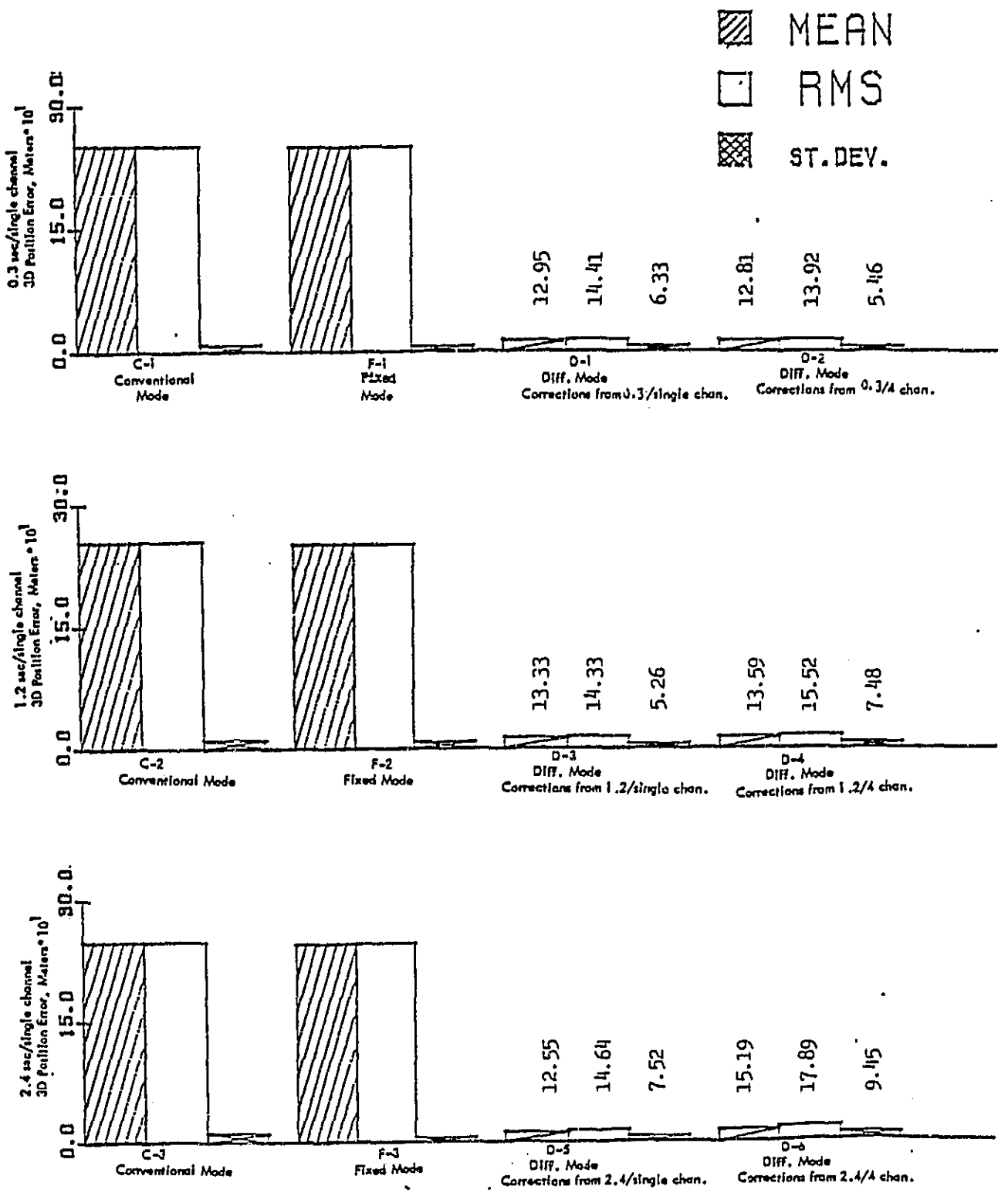

Figure 4.0.6.4 Single Channel Performance, with SA

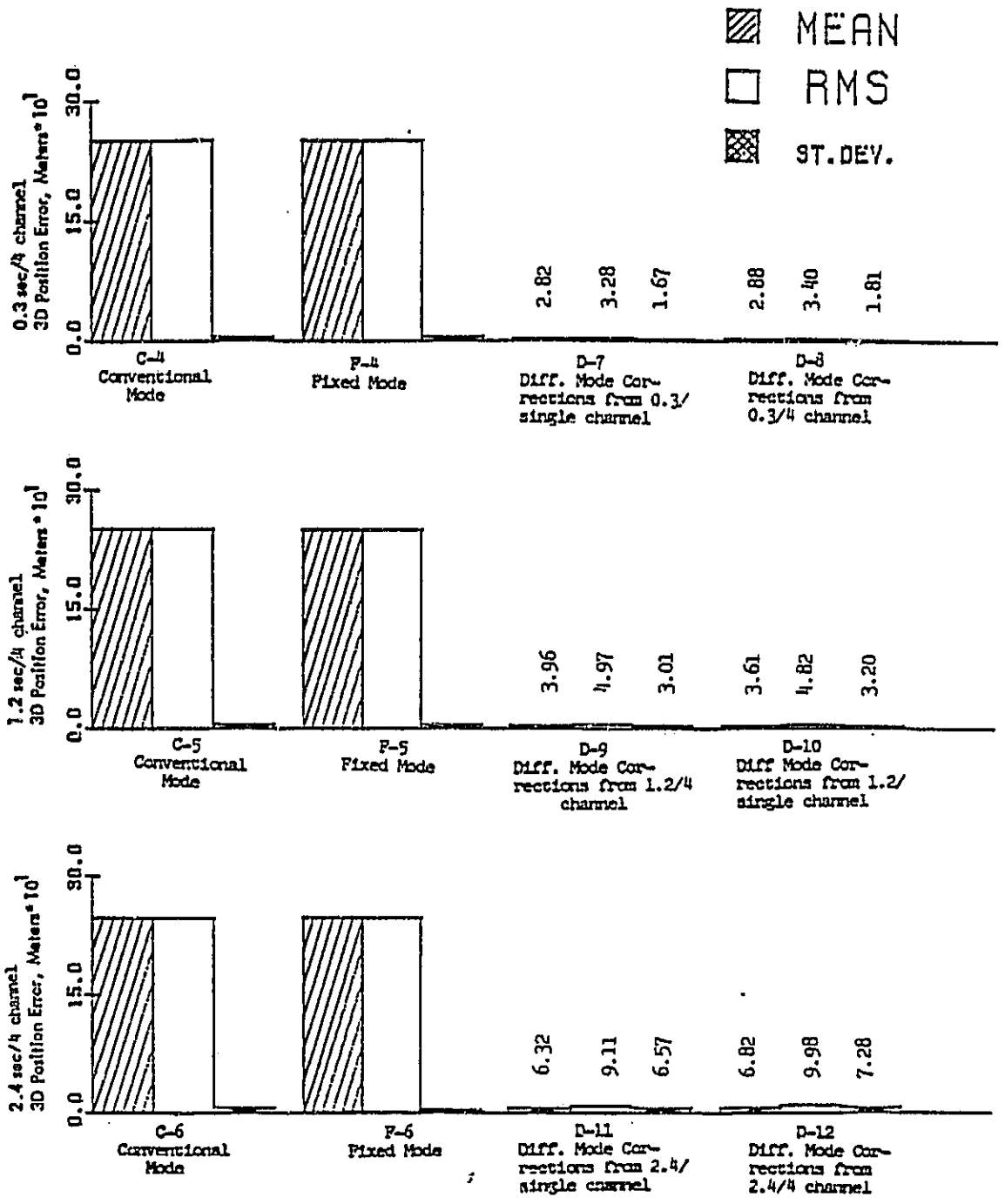

Figure 4.0.6.5 Four Channel Performance, with SA

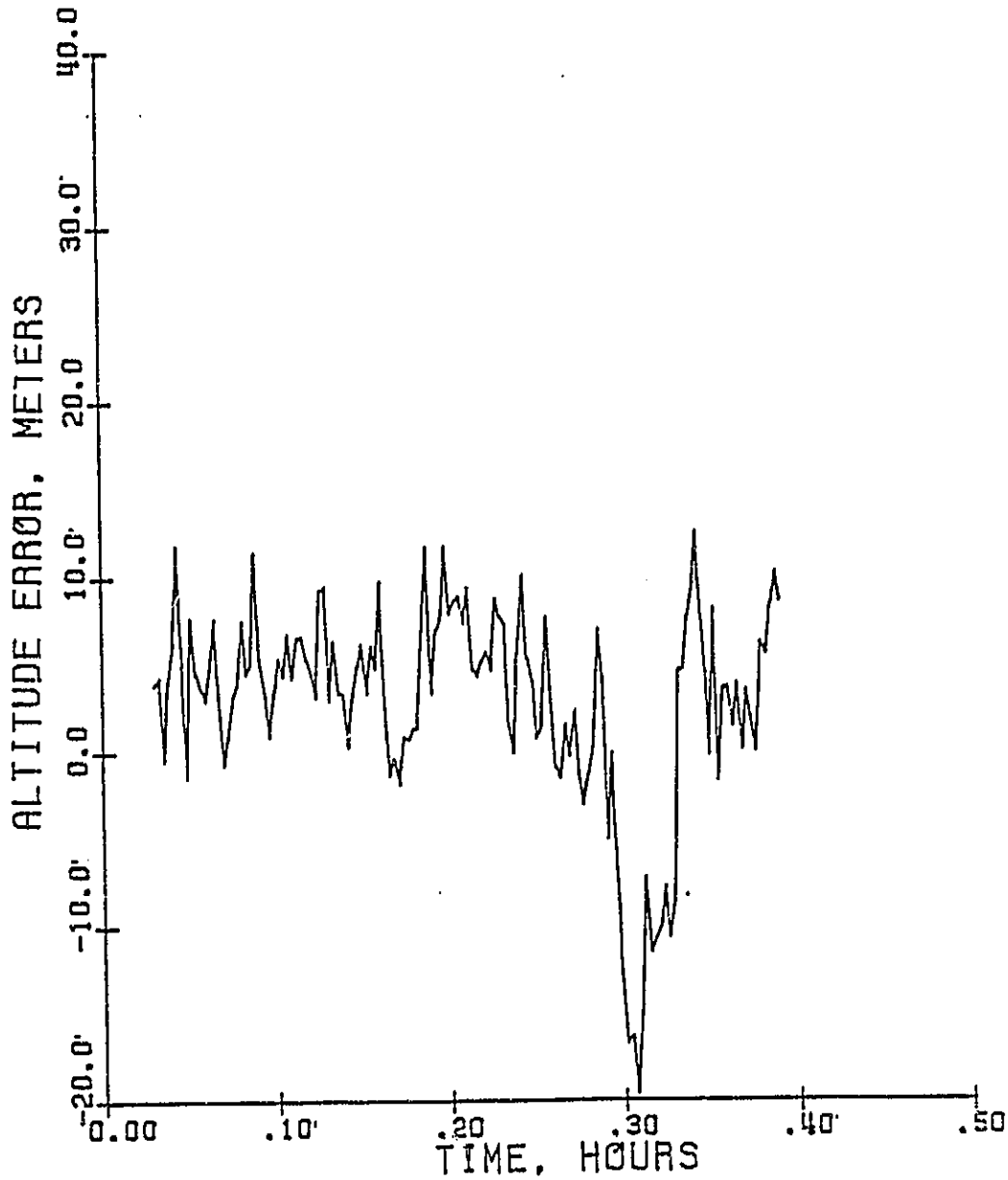

Figure 4.0.6.6 Altitude Errors, Run D-6, with SA Seq/Single Chan., 2.4 sec.

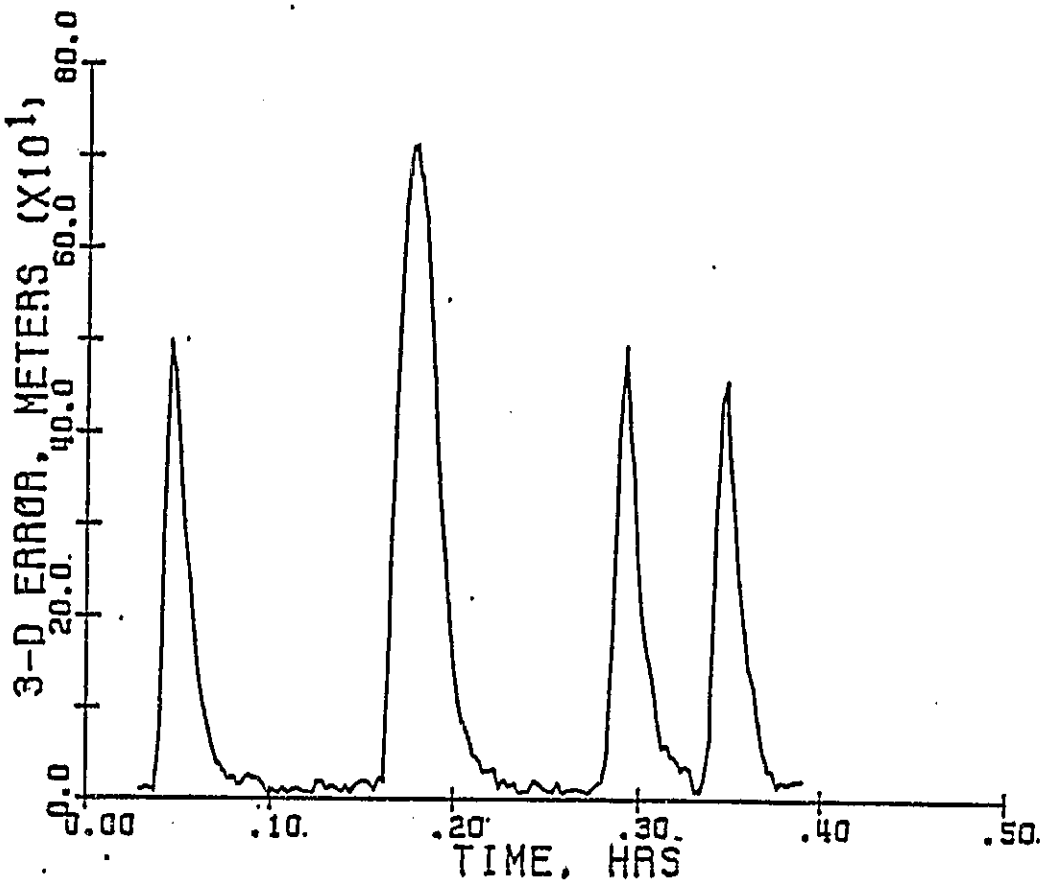

Figure 4.0.6.7 3D Position Error, Run D-6, with SA Seq/Single Chan., 2.4 sec.

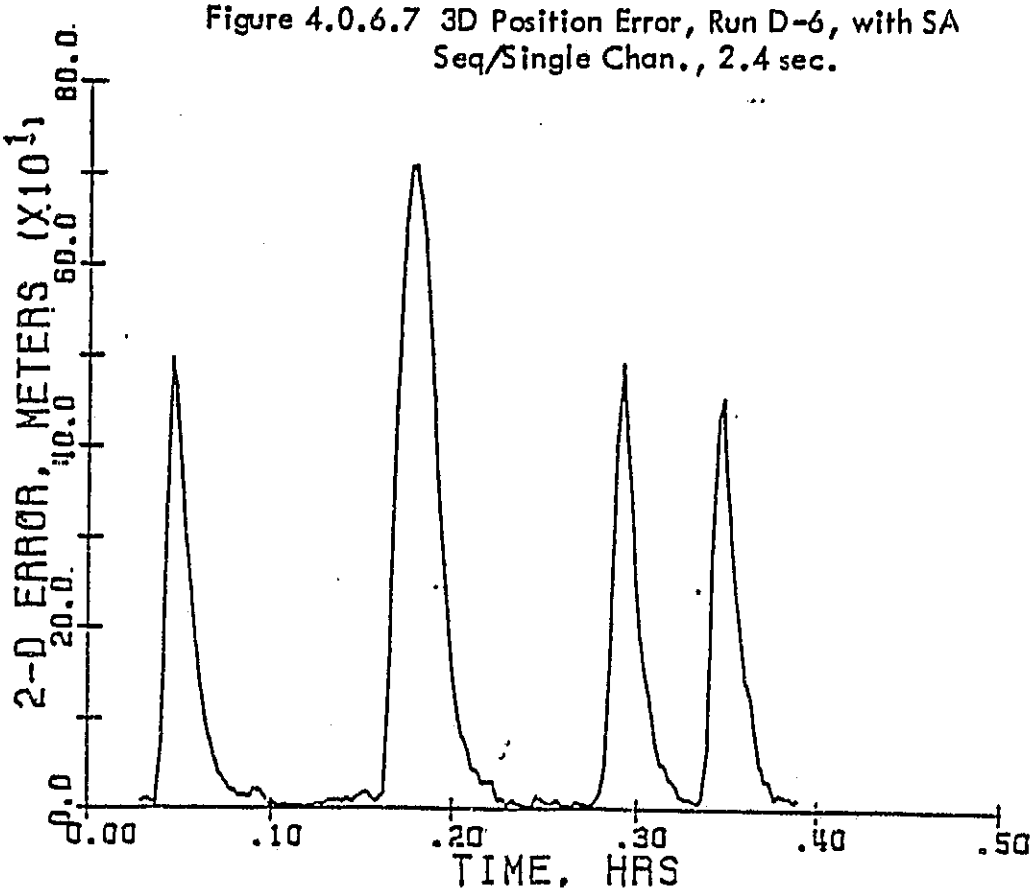

Figure 4.0.6.8 2D Position Error, Run D-6, with SA Seq/Single Chan., 2.4 sec.

4.0.7 Receiver Performance, Differential Mode, With SA Errors, Using Corrections From Different Receivers of Different Update Periods

The problems of using a receiver with an update period larger than 0.3 seconds have been presented for the dynamic case. This set of experiments were conducted to see the effects of using fixed receivers of longer update periods than that used by the airborne unit. In each case, the differential mode airborne unit was either a sequential/single channel or four channel receiver with an update period of 0.3 seconds. The fixed mode receiver varied in both channel number and update period, the period being either 1.2 seconds or 2.4 seconds.

Figure 4.0.7.1 displays the 3D position errors incurred by the 0.3 update period, differential mode receiver when using correction data provided by a fixed receiver of a slower update period. The performance of the differential mode, sequential/single channel receivers (run ID numbers D-13, D-15, D-17, and D-19) are comparable with mean error values of 11.3-13.3 meters, rms error values of 12.5-14.7, and standard deviation error values of 5.4-6.4 meters. These values correlate well with the previously discussed 0.3 update period, sequential/single channel, differential mode receivers. Likewise, the four channel, differential mode receiver errors (run ID numbers D-14, D-16, D-18, and D-20) correlated well and performed comparably to the previously mentioned 0.3 update period, four channel, differential mode receivers.

5.0 CONCLUSIONS

The simulation data shows that differential GPS does have potential to provide a precision approach capability, at least for lateral navigation. The 1982 Federal Radionavigation Plan (FRP) states the lateral accuracy of a localizer to be ± 7.6 meters at the threshold. The simulated DGPS approach data revealed accuracies of this type for the entire approach. The 2 sigma repeatable and relative lateral navigational accuracies for a Cat I approach is 9.1 meters. The 2 sigma values for the 0.3 update period, differential mode receivers came very close to this figure, the worse case exceeding it by 4.7 meters.

It also appears that, for an uplink period of 12 seconds, a sequential channel receiver with update periods slower than the Z-set (1.2 seconds) will function quite well as the fixed mode receiver. If ever produced as a part of the airway system, this characteristic alone could result in a significant savings. The slower update period and the 12 second uplink period would also reduce the computational power required for the DGPS ground system. The idle processing time gained could be spent in monitoring the integrity of the DGPS ground system and the visible NAVSTAR satellites. The DGPS ground system could serve a two fold service; 1) provide an increased accuracy to DGPS equipped users and 2) provide a net of remote monitoring systems to monitor the integrity of the entire NAVSTAR constellation.

During a constant velocity flight path the alpha-beta filter performs well and provides smoothed, well behaved data even for the longer

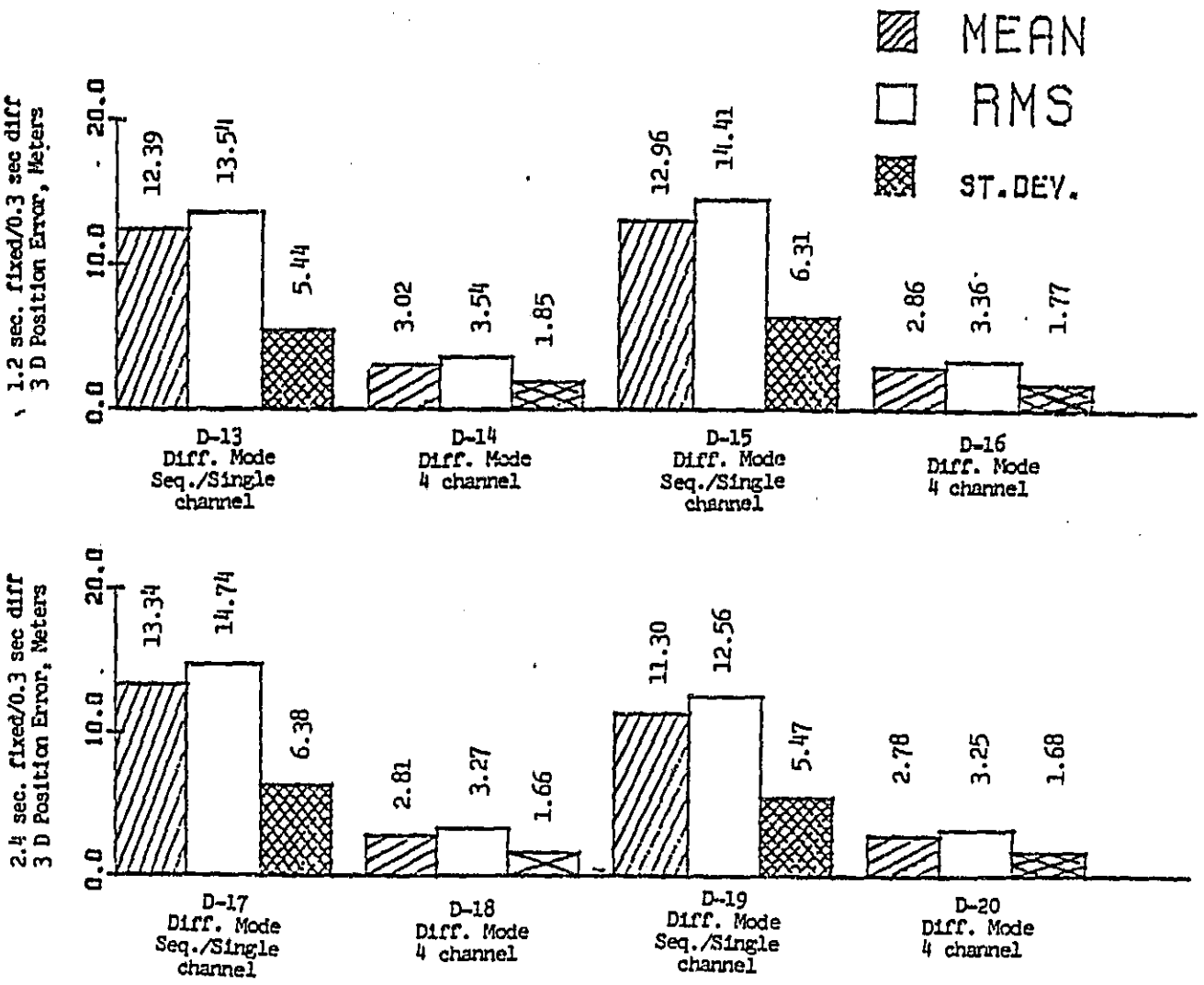

Figure 4.0.7.1 3D Position Errors of a 0.3 sec /diff. Mode Receiver, Using Corrections from either 1.2 sec. or 2.4 sec., Fixed Mode Receiver, with Selective Availability Errors.

update periods. However, if accelerative platforms are to be used, a more sophisticated filtering algorithm should be implemented. This addition alone could lower the lateral errors of the DGPS airborne unit to meet or exceed the current Cat I requirements and significantly improve the DGPS altitude guidance.

The range corrections provided to the differential receiver were not filtered by any means. The implementation of a filtering algorithm for the fixed receiver, to reduce the high frequency noise induced by the diffuse multipath, may improve the final accuracy of the airborne DGPS receiver. Considering the high correlative characteristics of the ionospheric delay, the tropospheric delay, and the Selective Availability, the highest source of range correction uncertainty is due to the white noise injected into the correction as an effect of the diffuse multipath. This may also be compounded in the hardware implementation by the noise injected by the receiver tracking loops. Considering the two sources are independent random variables, the addition of the two would serve to increase the standard deviation of the range measurement error and the resulting calculated range correction.

6.0 ACKNOWLEDGEMENTS

This work was supported under NASA Grant NAG-2-231, sponsored by NASA Ames Research Center, Moffett Field, California.

The author wishes to thank Mr. Fred Edwards, NASA/Ames Technical Monitor, for his helpful suggestions during this work; members of the Ohio University Avionics Engineering Center NASA/Ames Project: Messrs. Dennis Scanlon, Graduate Research Assistant, Howard B. Maidlow, Undergraduate Intern, and Andrew Nelson, Undergraduate Intern, these gentlemen have assisted me in the development of the DGPS programs and performed most of the data collection presented in this work.

Additional thanks go to Dr. Robert W. Lilley, Associate Director, and Mr. James D. Nickum, my co-engineer, for reviewing this document and Ms. Alicya Shade and Ms. Michele Nutter for the extra hours they put in for the production of this paper.

7.0 BIBLIOGRAPHY

[1] Kruh, P., Brady, W.F., and Schmitt, D.L., "A Strategy for Buildup to the Operational NAVSTAR GPS Constellation," Institute of Navigation National Aerospace Meeting, Arlington, Virginia; March 22-25, 1983.

[2] "Radionavigation System Characteristics," Federal Radionavigation Plan, DOD -4650.4-P-III and DOT-TSC-RSPA-81-12-III, Vol. 3; March, 1982.

[3] Campbell, Steven D., and LaFrey, Raymond R., "Flight Test Results for an Experimental GPS C/A-code Receiver in a General Aviation Aircraft," NAVIGATION, Journal of the Institute of Navigation, Vol. 30, No. 4, pp. 350-368; Winter 1983-1984.

[4] "Defense Department Boosts Civil NAVSTAR Precision," Aviation Week and Space Technology, p. 24; June 27, 1983.

[5] Beser, Jacques and Parkinson, Bradford W., "The Application of NAVSTAR Differential GPS in the Civilian Community," Institute of Navigation Thirty-Seventh Annual Meeting, Annapolis, MD.; June 9-11, 1981.

[6] Magnavox Advanced Products and Systems Company, "Civil Applications of Differential GPS Using a Single Channel Sequential Receiver," NASA Contractor Report 166168; May, 1981.

[7] Kalafus, Rudolph M., "Synopsis and Recommendations of the TSC Workshop on Differential Operation of NAVSTAR GPS," Transportation Systems Center, Cambridge, MA., (DOT-TSC-RSPA-83-10, October, 1983); June 9-10, 1983.

[8] Kruh, Pierre, "The NAVSTAR Global Positioning System Six-Plane 18-Satellite Constellation," The 1981 National Telecommnications Conference of the IEEE, pp. E9.3.1-E9.3.8; November, 1981.

[9] Shively, Curtis A., "A Real Time Simulation for Evaluating a Low-Cost GPS Navigation," MITRE/METREK, McLean, VA., Report MTR-80W00081; April, 1980.

[10] Noe, Philip S., and Myers, Kenneth A., "A Position Fixing Algorithm for the Low-Cost GPS Receiver," IEEE Trans. Aerospace and Electronics Systems, Vol. AES-12, No. 2, pp. 295-297; March 1976.

[11] Shively, Curtis A., op. cit., Appendix B.

[12] Martin, E.H., "GPS User Equipment Error Models," NAVIGATION, Journal of the Institute of Navigation, Vol. 25, No. 2, pp. 201-210; Summer, 1978.

[13] Klobuchar, J.A., "Ionospheric Time-Delay Corrections for Advanced Satellite Ranging Systems," AGARD Conference Proceedings No. 209 on Propagation Limitations of Navigation and Positioning Systems, Electromagnetic Wave Propagation Panel Specialists Meeting, Istanbul, pp.3-1 - 3-13; October 20-22, 1976.

[14] Altshuler, Edward E. and Kalaghan, Paul M., "Tropospheric Range Error Corrections for the NAVSTAR System," U.S. Air Force Cambridge Research Laboratories, L.G. Hanscom Field, Bedford, MA., Report No. AFCRL-TR-74-0198; April 16, 1974.

[15] Shively, Curtis A., op. cit., Appendix C.

[16] Kalafus, Rudolph M., "NAVSTAR GPS Accuracy Study," Proceedings of the Surface Transportation Navigation User's Conference, Washington, D.C.; November 16-17, 1982

[17] Kalafus, Rudolph M., "Synopsis...," op. cit.

1. Report No.	2. Government Accession No.	3. Recipient's Catalog No.
NASA CR 177326		

4. Title and Subtitle	5. Report Date
A Study of the Application of Differential Techniques to the Global Positioning System for a Helicopter Precision Approach	November 1984
	6. Performing Organization Code: FSN
7. Author(s): Daryl L. McCall	8. Performing Organization Report No.
	10. Work Unit No.: T3771
9. Performing Organization Name and Address: Avionics Engineering Center, Dept of Electrical & Computer Engineering, Ohio University, Athens, OH 45701	11. Contract or Grant No.: NAG2-231
	13. Type of Report and Period Covered: Contractor Report
12. Sponsoring Agency Name and Address: National Aeronautics & Space Administration, Washington, D.C. 20546	14. Sponsoring Agency Code: 532-01-11

15. Supplementary Notes: Point of Contact: Technical Monitor, Fred G. Edwards, M.S. 210-9, Ames Research Center, Moffett Field, CA 94035, 415-694-5437 or FTS 464-5437

16. Abstract

This report documents the results of a simulation study to define the functional characteristics of a airborne and ground reference GPS receiver for use in a Differential GPS system. The operations of a variety of receiver types (sequential-single channel, continuous multi-channel, etc.) are evaluated for a typical civil helicopter mission scenario. The math model of each receiver type incorporated representative system errors including intentional degradation. The results include the discussion of the receiver relative performance, the spatial correlative properties of individual range error sources, and the navigation algorithm used to smooth the position data.

17. Key Words (Suggested by Author(s))	18. Distribution Statement
NAVSTAR GPS Differential GPS Helicopter GPS GPS Simulation	Unclassified - Unlimited STAR Category 04

19. Security Classif. (of this report)	20. Security Classif. (of this page)	21. No. of Pages	22. Price*
Unclassified	Unclassified	80	

*For sale by the National Technical Information Service, Springfield, Virginia 22161